Critical phenomena in microgravity: Past, present, and future

M. Barmatz and Inseob Hahn

Jet Propulsion Laboratory, California Institute of Technology, Pasadena, California 91109, USA

J. A. Lipa

Physics Department, Stanford University, Stanford, California 94305, USA

R. V. Duncan

Physics and Astronomy, University of New Mexico, Albuquerque, New Mexico 87131, USA

(Published 2 January 2007)

This review provides an overview of the progress in using the low-gravity environment of space to explore critical phenomena and test modern theoretical predictions. Gravity-induced variations in the hydrostatic pressure and the resulting density gradients adversely affect ground-based measurements near fluid critical points. Performing measurements in a low-gravity environment can significantly reduce these difficulties. A number of significant experiments have been performed in low-Earth orbit. Experiments near the lambda transition in liquid helium explored the regime of large correlation lengths and tested the theoretical predictions to a level of precision that could not be obtained on Earth. Other studies have validated theoretical predictions for the divergence in the viscosity as well as the unexpected critical speeding up of the thermal equilibrium process in pure fluids near the liquid-gas critical point. We describe the scientific content of previously flown low-gravity investigations of critical phenomena as well as those in the development stage, and associated ground-based work.

PACS number(s): 05.70.Jk, 64.60.Fr, 64.60.Ht, 65.20.+w

CONTENTS

I. INTRODUCTION

The study of critical phenomena began over 180 years ago with observations of the supercritical phase (Cagniard de la Tour, 1822) and the critical point of CO_2 (Andrews, 1869). Shortly thereafter, Van der Waals (1873) developed his equation of state and applied it to the liquid-gas critical point. This was later extended to describe a wide range of other critical points observed in solid systems (Landau, 1937; Brout, 1965). The concept

of an order parameter was introduced by Landau (1937). This classical or mean-field approach made seemingly innocuous assumptions that the free energy in the critical region had an analytic expansion in the order parameter and that thermodynamic fluctuations could be neglected. The minimization of this free energy led to an equation of state and explicit predictions for the critical exponents that characterize the singular behavior of thermodynamic properties as the critical point is approached.

As more precise experimental techniques were developed, it became apparent that the behavior of real systems was inconsistent with the predictions of this model. Guggenheim (1945) demonstrated this difficulty by showing that the shape of the coexistence curve of a fluid system is not parabolic as predicted by the theory. On the theoretical side, Onsager (1944) obtained the exact solution of the two-dimensional (2D) Ising model which also shows significantly different singular behavior. This solution predicts that the specific heat in zero magnetic field will diverge logarithmically at the critical point, in contrast to the prediction of mean-field theory, which allows only a step discontinuity. In the following years, experiments (Buckingham and Fairbank, 1961; Voronel *et al.*, 1964; Moldover and Little, 1965) and numerical calculations (see Fisher, 1964, for a review) led to the *scaling* concept (Widom, 1965a, 1965b), which used a homogeneous functional form for the thermodynamic potential to define relationships between the critical exponents associated with various singular quantities. Also, the concept of *universality* was introduced, combining different critical-point systems into discrete classes having the same singular behavior (Kadanoff, 1966; Griffiths, 1970b; Griffiths and Wheeler, 1970).

A major breakthrough came with the application of the renormalization-group (RG) technique to the theory of critical phenomena by Wilson (1971a, 1971b) and co-workers (Wilson and Fisher, 1972; Wilson and Kogut, 1972). This approach established the theoretical foundation for the scaling and universality concepts using the ideas of phase-space flows and fixed points. By combining RG ideas with field theoretic methods, new computational tools were developed that confirmed earlier results and led to many further predictions. The RG approach avoids the analyticity assumption and replaces it with a model of the growing thermodynamic fluctuation effects as the critical point is approached. The theory was also extended to describe the behavior of dynamic properties such as thermal conductivity and viscosity near the critical point (Halperin *et al.*, 1976a, 1976b). Wilson (1971a) also noted that the RG method could be used to describe corrections to scaling. Wegner (1972) used this approach to determine the form of the corrections to the asymptotic scaling law behavior as one moves away from a critical point. More recently, detailed theoretical models have been developed to describe the crossover from the asymptotic behavior close to a critical point to the mean-field behavior farther away both in the case of static properties (Bagnuls and Bervillier, 1985; Dohm, 1985a, 1987; Bagnuls *et al.*, 1987;

Schloms and Dohm, 1989) and for dynamic properties (Dohm and Folk, 1980, 1981).

Modern experimental research on static critical phenomena aims to test the RG theory not only in the asymptotic regime but also in the crossover regime, where corrections to scaling and background contributions compete in a complex manner. Near the critical point, theory predicts that the free energy, which is usually a function of two independent variables, can be expressed as a universal scaling function of one scaled variable and a noncritical background. It is important to note that this simple property of two-scale-factor universality is valid for isotropic systems like fluids but not for anisotropic systems with noncubic symmetry (Chen and Dohm, 2004). Ideally, microgravity experiments aim to precisely determine critical exponents and critical amplitudes in the asymptotic region to test the most central theoretical predictions. Once the asymptotic values are known, the crossover behavior for a given fluid can be determined and compared with crossover theories.

More recently, the dynamics of phase change in bulk and finite-size systems have also been explored in well-controlled experiments near critical points (Weichman *et al.*, 2003). These results display far more complex behavior than is seen in the static properties, and while the results do not follow the simple predictions of scaling and universality, they are expected to obey generalizations of these concepts.

In more recent times, it has become clear that determining the limiting asymptotic behavior of various thermophysical properties requires precision measurements very close to second-order phase transitions where the ordered phase transforms in a continuous way into the disordered phase. Measurements in solids close to magnetic critical points are adversely affected by impurities and crystal imperfections, while gravity distorts the local density and hinders measurements in pure fluids (Voronel and Gitterman, 1965; Levelt Sengers *et al.*, 1977). In fluids, many ground-based measurements have been performed in samples of small vertical height to minimize gravity effects. However, if the sample height is too small, finite-size effects become important as the transition is approached. Thus, in both solid and fluid systems, measurements become significantly distorted close to a critical point. The interpretation of precision measurements farther away from the transition must also take nonasymptotic corrections into account. These problems have made it difficult to perform accurate experiments to test modern theoretical predictions of critical phenomena with high precision.

The effect of gravity near the gas-liquid critical point was reviewed by Moldover *et al.* (1979). These authors concluded that, in space, an improvement in temperature resolution of three to four orders of magnitude was achievable before gravity effects again became large, depending on the details of the experiment. Efforts to take advantage of a low-gravity environment began in the mid-1980s with sounding rockets that provided a very short period (~6 min) of reduced gravity. With the development of the Space Shuttle in 1981, more ambitious

reduced-gravity studies could be performed during flights of two-week duration. More recently, the Russian MIR Space Station has permitted longer-duration studies to be performed. Many government agencies have engaged in cooperative agreements to develop and use flight facilities because of the continuing need for more sophisticated and costly apparatus to perform studies in microgravity (Zappoli *et al.*, 2003). In a few years, the International Space Station (ISS) should be completed, allowing further long-duration studies. Many groups have been planning and developing facilities for future critical-phenomena studies on the ISS. In recent years, the U.S. National Aeronautics and Space Administration (NASA) provided funding for the development of the Low Temperature Microgravity Physics Facility (LTMPF) for operation on the ISS. Future investigations of the ^{4}He lambda transition, the ^{3}He liquid-gas critical point, and the ^{3}He-^{4}He tricritical point are planned for this facility to test various predictions of RG theory.

In this review, we focus on the work that has been performed in microgravity since publication of the review by Moldover *et al.* (1979). The main thrust of the present work is the investigation of the asymptotic region close to the transition where the correlation length becomes large, and its relationship to the crossover region. In Sec. II, we give a brief theoretical introduction to critical-phenomena concepts and describe how gravity can affect measurements close to fluid critical points. Past, present, and future flight facilities are described in Sec. III, and some special precautions required for performing experimental studies in a microgravity environment are emphasized. In Secs. IV–VI, we describe flight experiments that have been designed to investigate various aspects of bulk critical phenomena in the liquid-gas systems, at the ^{4}He lambda transition, and near the ^{3}He-^{4}He tricritical point. For completeness, in Sec. VII we cover finite-size studies previously performed in a space environment or planned for future space flights. It is not the intent of this review to cover all previous ground-based critical-phenomena studies. Instead, we provide a limited review of important theoretical and experimental milestones that are pertinent to studies in a microgravity environment. More complete guides to the literature on ground-based critical phenomena can be found in Stanley (1971), Anisimov (1991), Domb (1996), and Tobochnik (2001). Many reviews of specific aspects in this field can be found in the series *Phase Transitions and Critical Phenomena*, edited by C. Domb and M. S. Green (later replaced by J. L. Lebowitz) and published by Academic Press, London.

II. THEORETICAL BACKGROUND

In this section, we briefly review the theoretical background relevant to the experiments discussed below. The modern theory of critical phenomena was developed based on two main ideas. First, it was assumed that the asymptotic behavior as a critical point is approached is independent of the interatomic potential. Second, the singular behavior in the asymptotic region was assumed

to be due to the growth of fluctuations in the order parameter. These ideas led to the development of the scaling laws and the universality concept that were subsequently derived rigorously within the RG theory (Wilson, 1971a, 1971b). This theory also opened up the possibility of calculating the details of the universal critical behavior using analytical techniques.

A key feature of a critical phase transition is scale invariance in the fluctuations of the order parameter, which implies fractal-like self-similarity between large- and small-scale fluctuations. Scale invariance also occurs in many systems that are still not completely understood, such as the Universe at the onset of the "Big Bang" as currently envisioned by cosmologists (Guth and Pi, 1982), the clustering of galaxies (Peebles, 1980; Jones *et al.*, 2004), massless fields in elementary particle physics (Jackiw, 1972; Meyer-Ortmanns, 1996), the distribution of earthquakes (Gutenberg and Richter, 1954), and turbulence in fluids and plasmas (Kolmogorov, 1941; Batchelor, 1970). In each of these examples, there is a wide range of some relevant scale over which properties of interest vary as a power law of the scale. The RG theory is the most successful approach developed thus far to derive and explore the relations between the characteristics of a system on many different length scales.

Singular behavior near a critical point can occur in both static and dynamic properties. Static properties such as heat capacity, compressibility, and thermal expansion coefficient are determined by single-time correlation functions, while dynamic properties such as thermal conductivity and viscosity are determined by equilibrium multitime correlation functions, and hence depend more directly on the equations of motion (Hohenberg and Halperin, 1977). Both static and dynamic critical phenomena affected by gravity will be discussed in this review.

A. Critical exponents and scaling

Critical phenomena can be described at various levels of development (Widom, 1965b; Fisher, 1966; Kadanoff, 1966, 1971; Griffiths, 1967). Thermophysical quantities typically exhibit *power-law behavior* in the asymptotic region very close to a critical point, depending on the thermodynamic path by which it is approached. For example, near a liquid-gas critical point the isothermal susceptibility χ_T diverges as $\chi_T^+ = \Gamma_0^+ t^{-\gamma}$ [where the reduced temperature $t \equiv (T - T_c)/T_c$] along a path of constant critical density (critical isochore, $\rho = \rho_c$) above the transition, and as $\chi_T^- = \Gamma_0^- |t|^{-\gamma'}$ along either the liquid or gas side of the coexistence curve below the transition. $\Gamma_0^{\pm}$ are the leading asymptotic critical amplitudes, with the superscript $\pm$ defining the single- (+) or two-phase (−) region. Along the path of constant critical temperature (critical isotherm, $T = T_c$), the variation of pressure with density is given by $\Delta P = D \Delta \rho |\Delta \rho|^{\delta-1}$, where $\Delta P = (P - P_c)/P_c$ is the reduced pressure and $\Delta \rho = (\rho - \rho_c)/\rho_c$ is the reduced density. Here the quantities γ, γ', and δ are critical exponents, which are predicted to be invariant from system to system.

Many inequalities among different critical exponents were derived in the early stages of theoretical development of critical phenomena (Rushbrooke, 1963; Griffiths, 1965a, 1965b; Josephson, 1967; Coopersmith, 1968a, 1968b; Buckingham and Gunton, 1969; Fisher, 1969). Early experimental measurements, however, suggested that the inequalities might be equalities. While there has been no general rigorous proof that any of the inequalities are actually equalities, proofs for various exactly soluble models do exist and the exponent equalities do follow from the RG fixed-point picture. This equality conjecture has led to the *homogeneous function approach* (or *static scaling hypothesis*) to define the basic form of the thermodynamic potential (Widom, 1965a, 1965b; Kadanoff *et al.*, 1967). The static scaling hypothesis asserts that any thermodynamic potential can be written as a generalized homogeneous function of its arguments (Stanley, 1971). For a given property, the scaling hypothesis predicts that the critical exponents above and below the transition are equal ($\gamma = \gamma'$, etc.).

This approach leads to exact relations between critical exponents, called *scaling laws*, and to the prediction that there are only two independent critical exponents. A well-known example of a scaling law is the Rushbrooke (1963) relation

$$\alpha + 2\beta + \gamma = 2, \tag{1}$$

where α is the constant-volume specific-heat exponent and β describes the shape of the coexistence curve. This scaling law allows one to determine the critical exponent β, for example, once the values of α and γ are known. The homogeneity assumption also predicts that measurements of a given quantity along various thermodynamic paths can be scaled in such a way that all experimental data should overlap onto a single curve.

A further advancement occurred with the development of the *hyperscaling relations*, in which the critical exponents are predicted to depend in specified ways on the behavior of spatial correlations in the system and on the system's spatial dimensionality d. An example of a hyperscaling relation, developed by Buckingham and Gunton (1969), is

$$\delta = \frac{d + 2 - \eta}{d - 2 + \eta}. \tag{2}$$

The exponent η describes the power-law behavior of the two-point correlation function (a fluctuation-response relation) at the critical point. Another useful hyperscaling relation, developed by Josephson (1967), is given by

$$\alpha = 2 - d\nu, \tag{3}$$

where ν is the critical exponent for the correlation length, $\xi \propto t^{-\nu}$.

B. Universality

Early insights about the possible analogy between the liquid-gas critical point and the Ising model, magnetism, liquid ^{4}He, and order-disorder transitions in binary alloys were made by Onsager (1944), Tisza (1948), and Lee and Yang (1952). The resulting universality concept states that all phase transitions can be divided into several distinct classes, and within a given class all critical points have the same asymptotic behavior (Kadanoff, 1971).

The most widely used method of defining universality classes is the $O(n)$ classification scheme. The three main factors that determine to which $O(n)$ universality class a given system belongs are the dimensionality d, the order parameter symmetry index n, and the range of the interaction potential. The $n=1$ universality class corresponds to a scalar order parameter and includes the three-dimensional Ising model, liquid-gas critical points, and fluid mixture consolute points. The $n=2$ class corresponds to a complex two-component order parameter and includes the superfluid or lambda transition in ^{4}He, easy-plane ferromagnets, and some transitions in smectic liquid crystals (de Gennes and Prost, 1993). However, within a given universality class, it is necessary to distinguish isotropic systems (e.g., fluids) from anisotropic systems (e.g., magnets) with noncubic symmetry (Chen and Dohm, 2004). For isotropic systems, two-scale-factor universality is valid (i.e., only two nonuniversal amplitudes suffice to characterize the asymptotic critical behavior of a specific system) (Stauffer *et al.*, 1972; Aharony, 1974; Gerber, 1975; Hohenberg *et al.*, 1976; Wegner, 1976). This is not the case for anisotropic systems in which there are, in general, $1 + d(d+1)/2$ nonuniversal amplitudes that need to be known in order to characterize the asymptotic critical behavior of the bulk order parameter correlation function. The application of universality to dissimilar critical points is based on the *isomorphism principle* (Anisimov, 1991; Anisimov *et al.*, 1995a, 1995b), which formulates the conditions for expressing the theoretical scaling fields through physical field variables.

This universality approach is a very powerful and unifying concept. In this review, we will discuss the $O(1)$ and $O(2)$ universality classes, focusing on the liquid-gas critical point and on the ^{4}He lambda transition, respectively.

C. Renormalization-group theory

The RG approach to critical phenomena now provides the intellectual justification for the observed and conjectured relationships associated with power laws, scaling relations, and universality. In fact, the formulation of this theory confirmed the validity of the above advances in critical phenomena (Wilson, 1971a, 1971b; Wilson and Fisher, 1972; Wilson and Kogut, 1974; Fisher, 1974). Detailed information on RG theory can be obtained from textbooks and extensive reviews on the subject and references therein (Fisher, 1974, 1998; Ma, 1976; Parisi, 1988; Itzykson and DrouHe, 1989; Binney *et al.*, 1993; Cardy, 1996; Kleinert and Schulte-Frohlinde, 2001; Zinn-Justin, 2001, 2002; Pelissetto and Vicari, 2002). Here we give a brief introduction to RG theory to set the stage for later discussion.

The RG approach is used to calculate the behavior of physical quantities via a phenomenological field theory rather than a microscopic model. One averages over the microscopic discreteness of the system and defines an energy functional that can be expanded in terms of the order field. The most widely accepted form of this energy functional is the Landau-Ginzburg-Wilson functional (Wilson and Kogut, 1974) and the resulting field theory is called the ϕ^4 theory, or more loosely the RG theory. This approximation has been sufficient to provide precise predictions for critical behavior in many different $O(n)$ systems that are in close agreement with experiment. Approximate values for the critical exponents have been determined using the ϕ^4 theory by two approaches. One approach was based on a perturbation expansion at fixed dimension $d=3$ (Parisi, 1973) and the other used the Wilson and Fisher (1972) $\varepsilon=4-d$ expansion (Vladimirov *et al.*, 1979). Calculations were also made for the universal asymptotic amplitude ratios (Watson, 1969; Nicoll and Albright, 1985; Bervillier, 1986) and the equation of state (Avdeeva and Migdal, 1972; Wallace and Zia, 1974; Nicoll and Albright, 1985). With further perturbative extension of the series expansion for the free energy in the ϕ^4 theory, more accurate calculations of the critical exponents, asymptotic amplitude ratios, and equation of state have been made (Guida and Zinn-Justin, 1997, 1998; Jasch and Kleinert, 2001). Campostrini *et al.* (2001, 2002) have performed accurate calculations using high-temperature series expansions. Also, Halperin *et al.* (1976a, 1976b) developed a systematic set of energy density functionals and their associated Langevin equations that describe a wide set of phenomena in systems spanning a wide variety of universality classes.

The RG method has also been successfully applied to the calculation of dynamic critical properties. Halperin *et al.* (1972) applied the method to the time-dependent Ginzburg-Landau model and showed that the RG method is consistent with earlier mode-coupling theory and dynamic scaling when the order parameter is conserved. The method has been developed successfully and applied to both $O(1)$ and $O(2)$ systems. A detailed review of the early developments in this field has been given by Hohenberg and Halperin (1977). These authors point out that the definition of the universality classes is affected by dynamical factors other than those considered above, but for the purposes of this review the above $O(n)$ classification scheme suffices. A range of dynamic models was introduced, with liquid-gas systems represented by model H and superfluid helium by model F. For the former class, the primary links to experiment are through inelastic light scattering and transport coefficients. For the superfluid transition, the behavior of the thermal conductivity, the second-sound damping coefficient, and some inelastic light-scattering measurements are relevant. A major success of the RG approach to dynamics was predicting the detailed behavior of the thermal conductivity near the superfluid transition (Dohm, 1991). Asymptotic dynamic amplitude ratios have also been calculated (Hohenberg and Halperin,

1977; Dohm and Folk, 1980, 1981; Dohm, 1991). Another aspect of critical-point dynamics is nonlinear behavior. This has been studied extensively for the superfluid transition. Because of the unique ability of superfluid helium to support a heat flux with essentially no temperature gradient, several interesting nonlinear effects can be studied. These include nonlinear thermal conductivity, depression of the transition temperature in a heat flux, enhanced specific heat, and studies of interface phenomena. We refer the reader to Haussmann and Dohm (1994) and to Weichman *et al.* (2003) for more information on nonlinear heat transport effects. In the sections below, we give more details of the relevant theoretical background for the various dynamic critical-point experiments.

In addition to the predictions for the asymptotic behavior very near a critical point, the RG approach has also been used to make predictions in the crossover region farther away from a critical point where the correlation length no longer dominates the behavior of the system.[1] Three other fruitful areas discussed below are the application of RG techniques to finite-size systems, and scaling predictions for critical boiling studies and critical adsorption. These areas can be viewed as applications of critical-point theory to other systems of interest.

At present, the validity of the RG theory predictions for critical-point phenomena is widely accepted. However, as mentioned earlier, the asymptotic predictions in the case of fluids cannot be unambiguously confirmed in Earth-based experiments because of gravity effects. In solid systems, testing is limited by transition rounding due to crystal defects and impurities. Thus, without microgravity measurements, we are in a rather weak position when attempting to test the theory by refutation.

D. Gravity effects

In this review, we focus on experiments where a reduction of gravity effects on fluids near critical points has given, or is expected to give, significantly improved results. In most experiments, the primary effect of gravity is to introduce a vertical pressure gradient (taken along the z direction) given by

$$\frac{dP}{dz} = -\rho g, \qquad (4)$$

----

[1]See Chang and Houghton, 1980; Dohm and Folk, 1980, 1981; Bagnuls and Bervillier, 1984, 1985; Bagnuls *et al.*, 1984; Dohm, 1985a, 1985b, 1991; Albright *et al.*, 1986, 1987; Bagnuls *et al.*, 1987, 2002; Schloms and Dohm, 1989, 1990; Chen, Abbaci, *et al.*, 1990; Chen, Albright, *et al.*, 1990; Anisimov *et al.*, 1992; Larin *et al.*, 1998; Agayan *et al.*, 2001; Bagnuls and Bervillier, 2002a, 2002b; Garrabos *et al.*, 2002; Rudnick *et al.*, 2003; Strösser and Dohm, 2003.

TABLE I. Critical parameters for selected simple fluids (CO_2, Xe, SF_6, and ^3He).

	T_c (K)	P_c (M Pa)	ρ_c (kg m^{-3})	$H_0 \times 10^{-3}$ (m)
CO_2	304.14	7.375	467.8	1.608
Xe	289.74	5.840	1110	0.537
SF_6	318.68	3.761	730	0.525
^3He	3.3155	0.117	41.2	0.290

where ρ is the fluid density and g is the acceleration of gravity. The presence of this gradient is important for measurements very near the ^4He lambda point since the transition temperature is pressure dependent, i.e., $T_\lambda(P)$. In a constant-density cell of height h, $\Delta P = \rho g h$. Thus there will be a gravity-induced averaging of thermo-physical measurements very near the transition in a sample of finite height. In cells at constant temperature, there will be a region near T_λ where superfluid and normal fluid ^4He will coexist (Ahlers, 1968a, 1991, 1999). For example, even for a superfluid sample of only 0.5 mm in height in $1g$, this coexisting region will occur over a temperature range of 6.4×10^{-8} K. To the extent that local properties can be measured within a cell, of course, the above limitation does not apply. For example, in thermal conductivity measurements this effect is less restrictive because the thermal gradient stratifies the column of helium, permitting local measurements that are not rounded by the pressure gradient across the entire sample (Day *et al.*, 1998). But nonlinear effects in the thermal conductivity depend strongly on gravity, since the divergence of the correlation length is limited on Earth by hydrostatic pressure effects across the correlated volume, as discussed in Sec. V.D.

In the case of a liquid-gas critical point, where the isothermal compressibility β_T and related isothermal susceptibility χ_T [$\beta_T = \chi_T/\rho^2 = (1/\rho)(\partial\rho/\partial P)_T$], diverge, the pressure gradient induced by gravity leads to a density gradient $(\partial\rho/\partial h)_T = \rho^2 g \beta_T$ that also diverges as the critical point is approached. This was first pointed out by Gouy (1892). The first quantitative treatment of the gravity effect was an analysis of specific-heat measurements in xenon near the liquid-gas critical point (Edwards *et al.*, 1968). This treatment was later extended to derive $t_h = (mgh/2k_BT_c)^{1/\beta\delta}$ that is a measure of the gravity-affected region for a given experiment (Lipa *et al.*, 1970). Here m is the atomic mass of the fluid and k_B is Boltzmann's constant.

The magnitude of the gravity effect depends on the molecular weight and critical parameters of the fluid, the sample height, the strength of gravity, and the distance from the liquid-gas critical point (Moldover *et al.*, 1979). The effect can also be characterized by $H_0 = P_c/(\rho_c g)$, which represents a gravity scale height in a fluid (Levelt Sengers, 1975). Table I gives values for H_0 in the Earth's gravitational field ($g = 981$ cm s^{-2}) and critical parameters for fluids that have been investigated or are planned for future microgravity studies. The smaller H_0,

the larger is the gravity effect. Since many thermophysical quantities, such as the susceptibility and specific heat, are dependent on the density near the critical point, this gravity-induced density gradient causes significant rounding in the measurements. As an example, a ^3He sample of only 0.5 mm in height in $1g$ will have a density difference of ~6% across the sample at a temperature 3×10^{-5} K above the critical point. Thus, we see that gravity has a much more pronounced effect near liquid-gas critical points than for the ^4He lambda transition. Given an equation of state, the effects of gravity can be corrected by integrating the appropriate physical property over the height of the sample. Detailed calculations of the gravity effect have been done by Hohenberg and Barmatz (1972) and Moldover *et al.* (1979).

Clearly, smaller sample heights lead to less gravity rounding, but soon a limit is reached where the height is so small that finite-size effects begin to appear. Far from a critical point this would occur at the angstrom level; however, near a critical point the correlation length ξ controlling these effects diverges as $\xi = \xi_0 t^{-\nu}$, magnifying the effect enormously. This behavior is intrinsic to all cooperative transitions, being associated with the physics of the transition process in an essential way. The competition between gravity and finite-size effects will soon limit the resolution of many ground experiments on bulk fluids.

III. FLIGHT FACILITIES

A. Sounding rockets

Sounding rockets are relatively low cost in comparison with satellites, and a payload can usually be developed in a short time. The flight profile of a sounding rocket follows a parabolic trajectory with the peak altitude typically ranging from 35 to 300 km. Shortly after launch, the solid fuel rocket is separated from the payload and falls back to Earth. The science experiment payload continues into space after the separation and experiments are begun. A parachute is normally used to bring the payload gently back to Earth. The payload or parts of it can often be refurbished and flown again. A residual acceleration level of $10^{-4}g$ can be attained for durations of 5–6 min. Countries including the United States, Germany, Japan, France, and China have used sounding rockets for conducting microgravity experiments. The TEXUS (Technologische Experimente unter Schwerelosigkeit) sounding rocket program of ESA (European Space Agency) has been used many times to study fluids near the liquid-gas critical point. Many pioneering investigations of temperature equilibration near the critical point have been performed using this platform (Nitsche *et al.*, 1984; Nitsche and Straub, 1986, 1987; Klein *et al.*, 1991; Guenoun *et al.*, 1993). Phase separation in critical binary fluids was also studied (Houessou *et al.*, 1985; Beysens *et al.*, 1988).

B. Space Shuttle

The Space Shuttle, developed by NASA, went into service in 1981. Approximately two weeks of microgravity conditions are available, with the duration of a given flight mainly limited by the resources required to support the crew. Numerous critical phenomena experiments have been performed on this platform. The ESA-developed Spacelab was a reusable, pressurized laboratory mounted inside the cargo bay of the Shuttle and was flown on a number of missions between 1983 and 1997. A high-precision thermostat (HPT) was used to measure the specific heat of SF_6 near its critical point during the 1985 Spacelab D-1 mission (Straub *et al.*, 1993). Holographic interferometry measurements on SF_6 were also performed during this mission (Klein and Feuerbacher, 1987) using the Holographic Optics Laboratory (HOLOP). Later, a similar heat-capacity instrument was used to investigate the piston effect and specific heat of SF_6 near the critical point during the Spacelab D-2 mission (Straub *et al.*, 1993, 1995, 1995a; Haupt and Straub, 1999).

The Critical-Point Facility (CPF) was also built by ESA for research on critical-point phenomena aboard the Spacelab. The CPF was capable of supporting experiments of several researchers on any one mission. Interchangeable thermostats for controlling the temperature of an experimental sample were inserted into the CPF, where they were surrounded by an optical diagnostics system to monitor the phenomena of interest. Many critical-point experiments were performed using the CPF during the missions IML-1 and IML-2 including phase separation and equilibration phenomena in cyclohexane-methanol mixtures (Perrot *et al.*, 1994), transport of heat and mass near the critical point (Garrabos *et al.*, 1993), thermal equilibrium dynamics of SF_6 (Fröhlich *et al.*, 1996; Wilkinson *et al.*, 1998), the density equilibration time scale (Ikier *et al.*, 1996a), wetting phenomena near the critical point (Ikier *et al.*, 1996b), and electrostriction effects of SF_6 near the critical point (Zimmerli *et al.*, 1999a).

NASA has also developed several flight instruments for use aboard the Space Shuttle to study critical phenomena. These instruments were designed for a single experiment remotely controlled from the ground. The "Critical Light Scattering Experiment" in xenon (Zeno), located in the cargo bay of the Space Shuttle, was developed to measure the decay rates of density fluctuations in xenon near the critical point (Gammon, 1987). An experiment called "Critical Viscosity of Xenon" (CVX) measured the viscosity near the critical point using a thermostat also located in the cargo bay (Berg *et al.*, 1998, 1999a, 1999b). A low-temperature superfluid helium Dewar located in the bay was flown twice to measure the specific heat of ^4He near the lambda point in different sample geometries; the "Lambda Point Experiment" (LPE) (Lipa *et al.*, 1996, 2003) and the "Confined Helium Experiment" (CHeX) (Lipa *et al.*, 2000).

C. MIR

Launched in 1987, the Soviet Union's MIR (Peace) Space Station orbited the Earth (51.6° inclination, 300–400 km altitude) for over a decade. The French space agency Centre National D'Etudes Spatiales (CNES) sponsored the Analyse des Liquides Critiques dans I'Espace (ALICE) program onboard the MIR platform (Marcout *et al.*, 1995). The ALICE-2 facility was flown on MIR to study different fluid samples and different heating protocols during the 1996 joint French-Russian Cassiopée, 1998 Pegase, and 1999 Perseus missions, and the 1999 joint French-American GMSF mission. Many successful critical-phenomena experiments were performed near the SF_6 critical point under the ALICE program, including studies of piston effects (Garrabos *et al.*, 1998; Wunenburger *et al.* 2000, 2002; Garrabos, Dejoan, *et al.*, 2001; Bartscher and Straub, 2002), boiling phenomena (Garrabos, Lecoutre-Chabot, *et al.*, 2001), and wetting behavior (Hegseth *et al.* 2002, 2005).

D. International Space Station

The International Space Station (ISS) orbit has a nominal 450 km altitude and a 51.6° inclination. The inclination was chosen as a compromise to accommodate all international partners who will be launching from different latitudes. For comparison, early Space Shuttle flights had a typical inclination of 28.5° and an altitude of less than 300 km. Because of the higher inclination and altitude, the ISS encounters a worse particle radiation environment than the Space Shuttle. Over many years, NASA and its European partners have developed three main facilities aboard ISS that are suitable for the study of critical phenomena.

The Low Temperature Microgravity Physics Facility (LTMPF) was developed by NASA to perform low-temperature physics experiments aboard the ISS on the Japanese Experiment Module/External Facility (JEM/EF). The LTMPF facility design includes a cryogenic Dewar, telemetry-command systems, data acquisition electronics, and two separate vacuum spaces for multiple experiments (Liu *et al.*, 2000; Larson *et al.*, 2003). The facility would provide a low-temperature environment for several months with experimental stages capable of nanokelvin temperature stability. Several experiments on critical phenomena and relativistic physics have been planned for this facility (Barmatz, 1999; Ahlers, 2000; Duncan, 2000; Larson, 2000; Goodstein, 2002; Hahn, 2002; Lipa, 2003). The facility and experiments can be controlled remotely from the Earth.

ESA is building the Fluid Science Lab (FSL), which is a multiuser internal platform on board the pressurized Columbus Laboratory dedicated to room-temperature investigations in microgravity conditions. The facility, to be launched aboard the Space Shuttle, offers a broad range of optical diagnostic instruments with a field of view 80×80 mm^2 for use in a central experiment module into which experiment containers can be inserted

and operated. Possible FSL research areas include convection and heat transfer, drops and bubbles, and a variety of experiments near the liquid-gas critical point (Beysens and Garrabos, 2001).

CNES is developing the Dispositif pour l'Etude de la Croissance et des Liquides Critiques (DECLIC) facility to investigate critical phenomena, chemical reactivity in supercritical water, and directional solidification in transparent media near room temperature (Cambon *et al.*, 1997; Beysens and Garrabos, 2001). The facility is equipped with a phase-contrast microscope, an interferometer, and a high-speed video camera. The facility, which will be launched aboard the Space Shuttle, is a multiuser platform designed for control of the experiment from the ground.

E. Space environment

1. Microgravity

The term microgravity is used to describe the near-weightless environment of space. While the absolute acceleration can be made very small, a number of residual effects come into play to varying degrees in different spacecraft. For example, an orbiting spacecraft will experience atmospheric drag and solar radiation pressure. The resulting accelerations mimic the effect of gravity and cause internal objects to seem to be pushed about relative to the spacecraft. A rotating spacecraft, such as the ISS, which rotates once per orbit, can also produce a centrifugal force. Tidal forces, also called gravity gradient forces, are present in an orbiting spacecraft due to small differences in the force of gravity over an extended object. The small tidal force will slightly distort the shape of a spherical bubble in orbit and elongate it along the local vertical with respect to the Earth. In a low-Earth-orbiting spacecraft, these microgravity effects can be reduced to the level of $10^{-6}g$ at very low frequencies. Within a small region near the center of mass of the spacecraft, a level of $10^{-7}g$ can be achieved. Levels of $10^{-8}g$ and below can be achieved at somewhat higher altitudes where atmospheric drag is reduced. For extreme needs, drag compensation can be used to reduce the local acceleration to the $10^{-12}g$ range (Lange, 1964).

2. Vibration environment

The vibration environment of a spacecraft can be divided into three main regimes: quasisteady, vibratory, and transient. For instance, the ISS definition of quasisteady vibrations refers to disturbances at frequencies below 0.01 Hz. The primary sources of these disturbances are atmospheric drag, gravity gradient, and rotational effects. The quasisteady acceleration environment of ISS is ~1 μg rms averaged over the frequency range from dc to 0.01 Hz. The vibratory regime covers the frequency range from 0.01 to 300 Hz. Typical disturbance sources are crew activity, thruster firings, fans, and pumps. The ISS requirements on the vibratory acceleration limits are defined over a set of frequency intervals. In the low-frequency regime ($f < 0.1$ Hz), the limit is

< 1.6 μg. In the frequency range $0.1 < f < 100$ Hz, the limit is below $16 \times f$ μg. The acceleration limit is less than 1600 μg in the frequency range between 100 and 300 Hz. The ISS requirements also specify minimum time intervals of 30 continuous days of the "microgravity mode" operation specified above, with a cumulative time of not less than 180 days per year. The transient regime covers relatively short-duration disturbances that are typically caused by identifiable events such as docking, operation of airlock valves, and routine maintenance. The transient acceleration limits of ISS are an instantaneous limit of 1000 μg and an integrated impulse limit of 10 μg s per axis over any 10-s interval. It is important to point out that the ISS vibration level is much worse than can easily be achieved in a laboratory on the ground. Extra care has to be taken when one designs a space experiment with stringent vibration requirements.

3. Particle radiation environment

There are three major sources of charged particles in the space environment: galactic cosmic rays, solar particles, and trapped particles in the Van Allen belts. The galactic cosmic ray flux is approximately isotropic in the hemisphere away from the Earth, with energies up to hundreds of GeV. Trapped particles relevant to the ISS orbit are about 83% protons. The main problems encountered are electrostatic charging and errors caused by single-event phenomena in electronic devices. In the case of critical-phenomena experiments, typical impacts of charged particles on experiments are noise in data acquisition electronics (Berg *et al.*, 1999b) and direct heating effects in high-resolution specific-heat measurements (Lipa *et al.*, 1996, 2003). In the case of the heating effect, the placement of extra shielding material near the instrument may not help because of secondary shower effects of the charged particles. Low-Earth-orbiting spacecraft typically pass through a region called the South Atlantic anomaly (SAA), which contains a large flux of protons trapped close to the top of the atmosphere due to the tilted, off-center magnetic field of the Earth. About 50% of the ISS orbits pass through the SAA. Here the proton dose rates exceed 10 protons $cm^{-2} s^{-1}$ for approximately 10 min per orbit. Away from the SAA, the heating effect is due to galactic cosmic rays. Critical-phenomena experiments near room temperature are relatively immune from cosmic ray heating due to the large heat capacity of the experimental cells. However, care has to be taken with cosmic ray heating issues in low-temperature critical-phenomena experiments using ^{3}He and ^{4}He (Barmatz, 1999; Ahlers, 2000; Duncan, 2000; Larson, 2000; Goodstein, 2002; Hahn, 2002; Lipa, 2003). In some circumstances the neutron flux from the atmosphere also needs to be considered.

IV. $O(1)$ UNIVERSALITY CLASS—LIQUID-GAS CRITICAL POINT

The $O(1)$ universality class in three dimensions (d $=3$) consists of systems having short-range forces and a scalar order parameter ($n=1$) (Kadanoff, 1971, 1976). This class includes the three-dimensional (3D) Ising model, liquid-gas critical points, binary fluid mixtures, uniaxial ferromagnets, polymer-solvent systems, and protein solutions. Each of these systems is predicted to have the same critical exponents and critical amplitude ratios. Long-range van der Waals interactions of fluids do not change the critical exponents but they do cause a nonuniversal change of the asymptotic scaling function of the bulk order parameter correlation function on length scales $\gg \xi$, even arbitrarily close to T_c. This effect has implications for finite-size scaling (Widom, 1964; Chen and Dohm, 2000, 2002; Dantchev, 2001; Dantchev and Rudnick, 2001).

The singular behavior theory of dynamic properties was reviewed by Hohenberg and Halperin (1977). Dynamic properties such as the thermal conductivity and viscosity have been studied extensively on the ground. However, only viscosity has been studied in microgravity and the background for those experiments is discussed in Sec. IV.F. In the remainder of this introduction to the $O(1)$ universality class, we will emphasize static properties.

In the case of $O(1)$ systems, substantial difficulties exist in obtaining details of the asymptotic behavior for static properties. An exact determination of the asymptotic region extent cannot be made theoretically because the leading asymptotic critical amplitudes and critical temperature are system dependent, and there are additional correction-to-scaling confluent singularities that also contain system-dependent amplitudes. Furthermore, most experimental measurements performed on the ground extend outside the asymptotic region. The development of the confluent singularity approach to corrections to asymptotic behavior has alleviated this problem significantly (Wegner, 1972; George and Rehr, 1984; Le Guillou and Zinn-Justin, 1987; Zinn-Justin and Fisher, 1996). Taking into account the range of correction-to-scaling terms leads to the following ex-

pressions for measurements along the critical isochore and coexistence curve near a liquid-gas critical point:

$$\chi_T^{\pm *} \equiv (P_c/\rho_c^2)\chi_T^{\pm} = \Gamma_0^{\pm}|t|^{-\gamma}[1 + \Gamma_1^{\pm}|t|^{\Delta} + \Gamma_2^{\pm}|t|^{2\Delta} + \cdots], \tag{5}$$

$$C_V^{\pm *} \equiv (T_c\rho_c/P_c)C_V^{\pm}$$
$$= A_0^{\pm}|t|^{-\alpha}[1 + A_1^{\pm}|t|^{\Delta} + A_2^{\pm}|t|^{2\Delta} + \cdots] + B_{\mathrm{cr}} + C_B, \tag{6}$$

$$\Delta\rho_{L,V} \equiv \rho_{L,V}/\rho_c - 1$$
$$= \pm B_0|t|^{\beta}(1 + B_1|t|^{\Delta} + B_2|t|^{2\Delta} + \cdots), \tag{7}$$

$$\xi^{\pm *} \equiv (k_B T_c/P_c)^{-1/3}\xi^{\pm}$$
$$= \xi_0^{\pm}|t|^{-\nu}[1 + \xi_1^{\pm}|t|^{\Delta} + \xi_2^{\pm}|t|^{2\Delta} + \cdots]. \tag{8}$$

Here α, β, γ, ν, and Δ are universal critical exponents that can be estimated (currently to about three or four decimal places) from theory. The susceptibility expression applies along the critical isochore ($+$) above T_c, and along the coexistence curve ($-$) below T_c, while the specific-heat and correlation-length expressions apply both above ($+$) and below ($-$) the critical point along the critical isochore. In the specific-heat expression, B_{cr} and C_B are the critical and analytical background contributions, respectively. These background terms cannot be distinguished experimentally. Because of the weak divergence in C_V, a constant analytic background term must be included even for measurements near the critical point. The system-dependent leading asymptotic critical amplitudes are given by $\Gamma_0^{\pm}$, $A_0^{\pm}$, B_0, and $\xi_0^{\pm}$, and the first-order Wegner expansion amplitudes are given by $\Gamma_1^{\pm}$, $A_1^{\pm}$, B_1, and $\xi_1^{\pm}$. The complete Wegner expansion includes not only the series indicated, but additional terms such as $D_C^{\pm}|t|$ and $E_{Ci}^{\pm}|t|_i^{\Delta}$, where D_c and E_{Ci} are constants and Δ_i are higher-order exponents related to irrelevant operators (Wegner, 1972). Since the terms $E_{Ci}^{\pm}|t|_i^{\Delta}$ involve extensions beyond the basic ϕ^4 theory, we will not consider them in this review. Other important paths through the critical point include the critical isotherm and critical isobar. In real fluids, other nonasymptotic corrections

TABLE II. Theoretical estimates of the leading asymptotic critical exponents for the $O(1)$ universality class.

α	β	γ	ν	Reference
		1.2385 (15)		Chen *et al.* (1982)[a]
0.109 (4)	0.3258 (14)	1.2396 (13)	0.62304 (13)	Guida and Zinn-Justin (1998);[b] Zinn-Justin (2001)[b]
0.1109 (15)	0.3262 (4)	1.2366 (15)	0.6297 (5)	Hasenbusch (2001)[c]
0.1091 (24)	0.3257 (5)	1.2403 (8)	0.6303 (8)	Jasch and Kleinert (2001)[b]
0.1096 (5)	0.32653 (10)	1.2373 (2)	0.63012 (16)	Campostrini *et al.* (2002)[a]

[a]High-temperature expansion.
[b]Field theoretical analysis.
[c]Monte Carlo simulation.

TABLE III. Theoretical estimates of important universal asymptotic amplitude ratios for $O(1)$ systems.

A_0^+/A_0^-	Γ_0^+/Γ_0^-	$\alpha A_0^+ \Gamma_0^+/B_0^2$	Reference
0.523 (9)	4.95 (15)	0.0581 (10)	Fisher and Zinn (1998)[a]
0.527 (37)	4.73 (16)	0.0569 (35)	Guida and Zinn-Justin (1998);[a] Zinn-Justin (2001)[a]
0.537 (19)	4.79 (10)	0.0574 (20)	Guida and Zinn-Justin (1998);[b] Zinn-Justin (2001)[b]
0.541 (15)	4.758 (29)	0.0593 (8)	Bagnuls and Bervillier (2002a)[c]
0.537 (19)	4.789 (102)	0.0574 (20)	Bagnuls and Bervillier (2002b)[d]
0.535	4.94	0.0580	Schloms and Dohm (1990);[a] Zhong *et al.* (2003)[a]

[a]ε expansion.
[b]Field theoretical analysis.
[c]Improved six-loop scheme.
[d]Seven-loop scheme.

due to liquid-gas asymmetry in the coexistence curve (Patashinskii and Pokroviskii, 1979) and higher-order analytic background terms also come into play.

Recent predictions for the asymptotic critical exponents in this class for static properties are given in Table II. In addition, the RG approach can be used to calculate values for a number of universal asymptotic amplitude ratios. Examples of asymptotic amplitude ratios are given in Table III. The calculations by Bagnuls and Berviller (2002a, 2002b) used a massive renormalization scheme while Zhong *et al.* (2003) used the minimal subtraction renormalization scheme of Schloms and Dohm (1989). The first accurate experimental determination of the asymptotic amplitude ratio for the specific heat was made by Lipa *et al.* (1977), who obtained $A_0^+/A_0^-=0.54$ near the critical point of CO_2, consistent with theory. The only direct experimental determination of an asymptotic critical exponent and amplitude ratio independent of confluent singularities is the SF_6 microgravity experiment of Haupt and Straub (1999), which gave the results $\alpha=0.1105^{+0.025}_{-0.027}$ and $A_0^+/A_0^-=0.521^{+0.085}_{-0.057}$.

Theoretical studies have also provided estimates of universal correction-to-scaling, crossover exponents, and amplitude ratios. The leading crossover exponent associated with the Wegner expansion is estimated to have the value $\Delta=0.52\pm0.02$ (Zinn-Justin and Fisher, 1996; Guida and Zinn-Justin, 1998). Table IV gives recent theoretical estimates of universal crossover amplitude ratios.

In testing theoretical predictions, experimentalists use samples of small vertical height to minimize gravity effects. However, as mentioned in Sec. II.D, finite-size effects limit the sample height at which bulk measurements can still be performed. In recent years, finite-size effects near the liquid-gas critical point have been studied theoretically (Chen and Dohm, 1999a, 1999b; Dantchev, 2001; Dantchev and Rudnick, 2001), and future experiments on the ground and in space will be required to test these theoretical predictions. In addition, experimental studies of the liquid-gas critical point have been hindered not only by gravity effects but also by the long equilibration times associated with the singular approach of the thermal diffusivity to zero.

The dramatic effect of gravity near the ^{3}He critical point is illustrated in Fig. 1, which shows the calculated variation of density as a function of height for different levels of the gravitational field. The restricted cubic model equation of state (Ho and Litster, 1970) was used for these calculations (Moldover *et al.*, 1979). Reducing gravity to the $3\times10^{-6}g$ level expected on the ISS in the microgravity mode leads to a significant reduction of the density inhomogeneity in a 4-cm-high sample. The temperature region around the ^{3}He critical point, where the density variation in such a sample will be more than 1%,

TABLE IV. Theoretical values of the first universal crossover amplitude ratios for $O(1)$ systems.

A_1^+/A_1^-	Γ_1^+/Γ_1^-	B_1/Γ_1^+	Reference
0.99 (19)	0.317 (14)	0.91 (21)	Bagnuls and Bervillier (2002a)[a]
1.36 (47)	0.215 (29)	0.40 (35)	Bagnuls and Bervillier (2002b)[b]
1.07	0.228	0.76	Schloms and Dohm (1990); Zhong *et al.* (2003)

[a]Improved six-loop scheme.
[b]Seven-loop scheme.
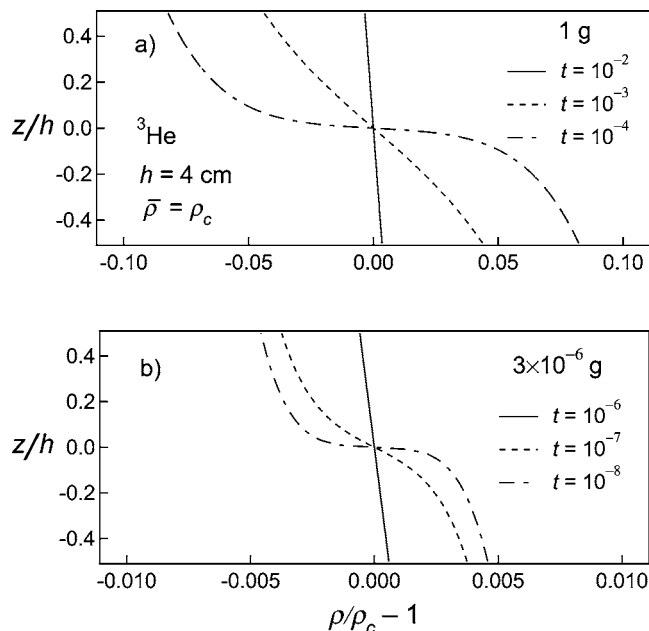
FIG. 1. Density as a function of height in the single-phase region of ^{3}He near the critical temperature. (a) Calculated density inhomogeneity in a 4-cm-high sample in $1g$; (b) calculated density inhomogeneity in a $3 \times 10^{-6}g$ environment.

is shown in Fig. 2. It can be seen that in a $3 \times 10^{-6}g$ environment, gravity effects in ^{3}He will become important only for reduced temperatures $t \lesssim 2.5 \times 10^{-7}$ even for this 4-cm-high sample.

A. Equilibration processes

A detailed understanding of relaxation rates near a liquid-gas critical point is very important for designing
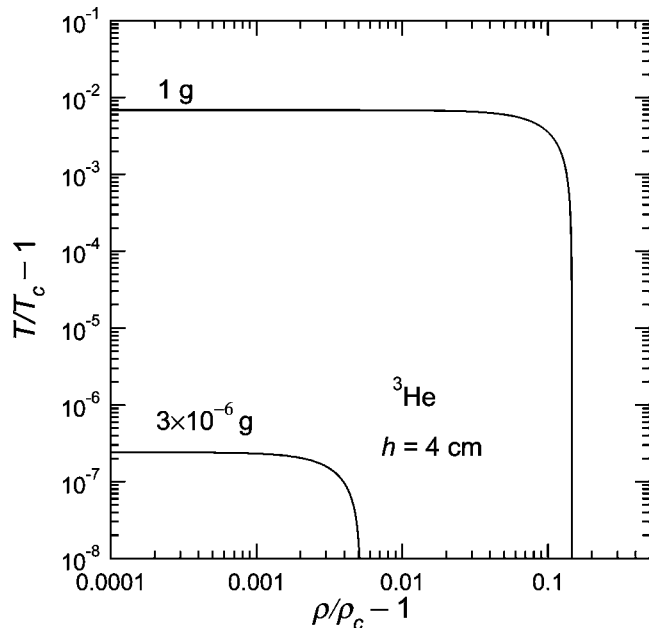
FIG. 2. Region of temperature and densities near the ^{3}He critical point where the local density varies by more than 1% over a height of 4 cm. Even for a large 4-cm sample, measurements in a near-microgravity environment can be made much closer to the transition with minimal gravity effects.

microgravity experiments where the measurement time is limited. Far from the critical point, a disturbed fluid system will equilibrate with a diffusive relaxation time τ inversely proportional to the thermal diffusivity $D_T = \kappa / \rho C_P$, where κ is the thermal conductivity and C_P is the specific heat at constant pressure. Near a liquid-gas critical point, C_P and κ vary approximately as ξ^2 and ξ, respectively; thus $\tau \propto D_T^{-1} \propto \xi$. This result implies that a diverging relaxation time will be observed for a fluid near the critical point. This conclusion was assumed to be correct for all experimental situations. However, more precise ground-based experiments near critical points performed on a constant-volume sample found a very fast relaxation time as the critical point was approached (Dahl and Moldover, 1972; Pittman *et al.*, 1982). This unexpected behavior was initially assumed to be due to gravity-induced buoyancy convection. Early low-gravity, critical-point experiments on TEXUS sounding rockets (Nitsche *et al.*, 1984; Nitsche and Straub, 1986) and the Space Shuttle (Klein and Feuerbacher, 1987) also observed faster-than-expected relaxation times near the critical point.

This unusual relaxation behavior was later understood when it was recognized that the divergences in the isothermal compressibility and isobaric thermal expansion near the critical point could lead to a critical speeding-up phenomenon. For a fixed volume sample, a sharp change in the boundary temperature leads to a boundary diffusion layer that acts like a piston to produce an adiabatic volume change within the sample interior. This adiabatic process came to be known as the piston effect. It is interesting to note that this effect was also alluded to by Gitterman and Steinberg (1970) and by Schmidt *et al.* (1988). This phenomenon was explained in more detail by a purely thermodynamic approach that neglected any initial variations in the pressure on the acoustic time scale (Boukari, Briggs, *et al.*, 1990a; Boukari, Shaumeyer, *et al.*, 1990b; Onuki and Ferrell, 1990; Onuki *et al.*, 1990), and by a direct simulation of the nonlinear Navier-Stokes equation using the van der Waals equation of state (Zappoli *et al.*, 1990). Analytical 1D solutions of the Navier-Stoke–van der Waals system were produced later for acoustic (Zappoli, 1992) and piston-effect time scales (Zappoli and Durand-Daubin, 1994). Space experiments were performed that provided a better understanding of the piston effect (Klein *et al.*, 1991; Guenoun *et al.*, 1993; Straub *et al.*, 1995a; Fröhlich *et al.*, 1996; de Bruijn *et al.*, 1997; Wunenburger *et al.*, 2000, 2002; Bartscher and Straub, 2002).

Theoretical models were also developed further to describe the time evolution of temperature and density inhomogeneities in a microgravity and $1g$ environment (Behringer *et al.*, 1990; Zappoli, 1992; Ferrell and Hao, 1993; Boukari *et al.*, 1995; Zhong and Meyer, 1995, 1996; Straub and Eicher, 1995; Zappoli and Carlès, 1995; Amiroudine *et al.*, 1997; Bailly and Zappoli, 2000; Garrabos, Lecoutre-Chabot, *et al.*, 2001; Nikolayev *et al.*, 2003). The first controlled temperature equilibration measurements after a temperature jump were per-

formed by Boukari, Briggs, *et al.* (1990a) and Boukari, Shoameyer, *et al.* (1990b). The first experimental demonstration of density relaxation governed by the piston effect was obtained by Zhong and Meyer (1993). In 1993, the basic features of the piston effect were also demonstrated with interferometric measurements of heat transport in supercritical CO_2 in the ALICE instrument during the ANTARES MIR mission (Bonetti *et al.*, 1994; Garrabos *et al.*, 1998). The late-stage diffusive behavior was validated on a Space Shuttle experiment performed in the Critical-Point Facility (Wilkinson *et al.*, 1998). This experiment used interferometry to measure changes in density during the late stage of thermal equilibration near the SF_6 liquid-gas critical point. The piston effect can play an important role in the design and successful completion of liquid-gas critical-point experiments both on the ground and in space (Berg, 1993; Carlès *et al.*, 2005). It can also influence the onset of convection and turbulence (Carlès, 2000; El Khouri and Carlès, 2002; Furukawa and Onuki, 2002; Amiroudine and Zappoli, 2003). More details regarding the piston effect can be found in recent reviews by Zappoli (2003) on the hydrodynamics of near-critical fluids, and by Meyer and Zhong (2004) on a comparison of ^{3}He and SF_6 experimental results with numerical calculations.

A few questions still remain regarding the piston effect. The simplifying assumption of a homogeneous pressure distribution in the early stages of the piston effect may fail close to the critical point due to bulk viscosity effects (Carlès, 1998; Carlès and Dadzie, 2005). Also, very near the critical point, the thermal equilibration time is predicted to become shorter than the typical acoustic time (sound wave period). This situation has been analyzed theoretically (Zappoli and Carlès, 1996), but never fully tested experimentally. Also, the boundary layer thickness becomes less than the diverging correlation length near the critical point. The behavior in this situation is not well understood. Recently, the Japan Aerospace Exploration Agency has been conducting ground-based investigations (Miura *et al.*, 2004) in preparation for a rocket flight experiment (Kobayashi *et al.*, 2004) to study the elementary process of the piston effect in the microsecond regime.

B. Specific heat

Specific heat is one of the most fundamental quantities for determining the thermodynamic behavior of a real system. Earlier mean-field theories predicted only a jump in C_V at the critical point (Stanley, 1971). However, this conclusion was questioned once the behavior of C_V in the 2D Ising model was shown to have a logarithmic divergence as T_c was approached (Onsager, 1994). The first experimental measurements that indicated a divergence in C_V were made by Michels and Strijland (1952). Later, Bagatskii *et al.* (1962) made more precise measurements along the critical isochore of argon. Their measurements were consistent with a logarithmic singularity at the transition. This surprising result was further verified in oxygen (Voronel *et al.*, 1964), in new measurements in argon (Voronel *et al.*, 1965), in nitrogen (Voronel *et al.*, 1966), and in ^{3}He and ^{4}He (Moldover and Little, 1965; Moldover, 1969).

In the case of the liquid-gas critical point, the RG theory predicts that specific heat at constant volume will have a weak divergence ($\alpha=0.109$), in contrast to the prediction of a strong divergence in the isothermal susceptibility ($\gamma=1.239$) and in the specific heat at constant pressure. Furthermore, because of this weak divergence in C_V, analytic background terms cannot be neglected. In practical ground-based experiments, correction terms to power-law behavior generally become important for reduced temperatures $|t|\geq10^{-4}$, and gravity effects become important for $|t|\leq10^{-4}$. The first experimental evidence that divergent behavior might not be logarithmic was obtained by Edwards *et al.* (1968). They found that after applying gravity corrections the behavior of xenon was better represented by a small positive exponent than a logarithmic singularity, especially if a symmetric logarithmic form ($A_0^+=A_0^-$) was imposed. Higher-precision ground-based specific-heat measurements were performed on CO_2 (Lipa *et al.*, 1970). These measurements were also corrected for gravity at $|t|\geq4\times10^{-5}$. A simple power-law analysis of these measurements in the limited asymptotic range $4\times10^{-5}\leq|t|\leq5\times10^{-3}$ gave $\alpha=0.125\pm0.005$. Brown and Meyer (1972) also performed high-precision measurements in ^{3}He and analyzed those data for $|t|\leq0.1$ including a confluent singular term. They obtained a value of $\alpha=0.105\pm0.015$, which is close to the latest theoretically predicted value. Moldover (1982) extended the fit of the Lipa *et al.* (1970) CO_2 measurements to $|t|\leq3\times10^{-2}$ by adding a confluent singular term and also obtained $\alpha=0.105$. However, in general, experimental measurements in the asymptotic power-law region are very limited and accurate analyses must take into account correction-to-scaling terms and/or gravity effects (Hocken and Moldover, 1976).

From these early studies, it became clear that specific-heat measurements in microgravity were needed to obtain a wider asymptotic temperature range for a more accurate test of theoretical predictions (Moldover *et al.*, 1976). Measurements of the specific heat near the ^{3}He critical point (Zhong *et al.*, 2003) shown in Fig. 3 illustrate the effects of gravity close to the transition and corrections to scaling farther away. These measurements were carried out on a sample 0.5 mm high. The temperature changes from heat pulse measurements close to the transition were obtained using a custom-built high-resolution thermometer (HRT) while measurements farther away used a germanium resistance thermometer. The HRT used for these experiments was based on the same principle as that developed for ^{4}He experiments (Lipa *et al.*, 1981), which are discussed in Sec. V.A The ^{3}He HRT contained a $GdCl_3$ paramagnetic salt (Adriaans *et al.*, 1991; Welander *et al.*, 2000; Welander and Hahn, 2001) in contrast to other materials developed for ^{4}He investigations. By using a 1-Hz low-pass filter in the
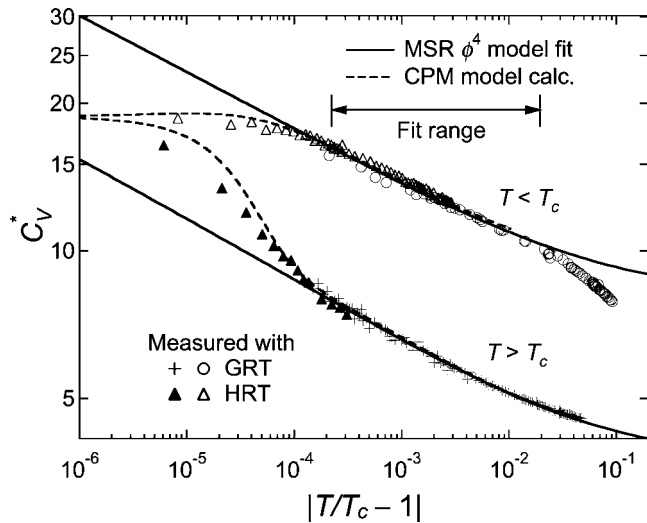
FIG. 3. Specific-heat measurements along the critical isochore in ^{3}He including the gravity-affected region. Solid curves correspond to a MSR best fit to measurements in the gravity-free region (adapted from Zhong *et al.*, 2003). The dashed curves correspond to a CPM best fit extended into the gravity-affected region (adapted from Zhong and Barmatz, 2004).

superconducting quantum interference device (SQUID) readout electronics, the temperature resolution was typically 1 nK near the ^{3}He critical point ($T_c \sim 3.31$ K). The best fit of the minimal subtraction renormalization (MSR) crossover model (Zhong *et al.*, 2003) to the specific-heat measurements in the gravity-free region ($2 \times 10^{-4} < |t| < 2 \times 10^{-2}$) is shown in Fig. 3 by solid curves. Also, the optimum parameters obtained from a fit to the equation-of-state crossover parametric model (CPM) (Agayan *et al.*, 2001) of the same gravity-free data (Zhong and Barmatz, 2004) were used to calculate the behavior of the specific heat in the gravity-affected region, as shown by dashed curves. This calculation required integrating the temperature derivative of the entropy over the height of the sample.

The first measurement of C_V in a low-gravity environment was performed on SF$_6$ using a high precision thermostat (HPT) during the 1985 German Spacelab D1 mission (Nitsche and Straub, 1987). The results of these heating measurements along the critical isochore showed only a gentle rise and smooth drop in C_V rather than the expected sharp peak at T_c. After an extensive investigation (Straub and Nitsche, 1993), it was concluded that the long relaxation time for the density was responsible for this result, with the design of the experimental cell (Haupt, 1997) leading to a much longer diffusion-length scale in microgravity. Even the slowest microgravity warming ramp rate, starting in the two-phase region, led to a large density inhomogeneity that smeared out the sharp divergence expected in the specific heat. The heating temperature ramp rates starting from the two-phase region required to eliminate these relaxation time effects were considered to be impractical during a space flight. It was decided that a uniform critical state could be obtained during future microgravity

measurements by slowly cooling the sample from above T_c into the two-phase region.

A reflight of the SF$_6$ specific-heat experiment, renamed HPT-HYDRA, was performed on the second German Spacelab D-2 mission in 1993. A scanning ratio calorimeter (Buckingham *et al.*, 1973; Straub *et al.*, 1993) was employed to measure C_V during both heating and cooling runs through the transition along the critical isochore. Analysis of these heating and cooling runs confirmed the presence of the piston effect (Straub *et al.*, 1995b) in both the one- and two-phase regions. Specific-heat measurements covered a wide temperature range $3 \times 10^{-6} < |t| < 1 \times 10^{-2}$. A range-shrinking analysis was employed where a data point from above and below T_c was discarded after each fit (Haupt and Straub, 1999). Analyzing the superposition of several cooling runs using this approach indicated that a simple power law was valid only in the range $|t| < 1.6 \times 10^{-4}$. The values obtained for the critical exponent $\alpha = 0.1105^{+0.025}_{-0.027}$ and asymptotic amplitude ratio $A_0^+/A_0^- = 0.521^{+0.085}_{-0.057}$ were consistent with theoretical predictions. The attempt of Haupt and Straub to include higher-order correction terms in the fit was only partially successful.

Recently, these measurements were reanalyzed (Barmatz *et al.*, 2004, 2005) using both a simple power law and the MSR crossover model (Zhong *et al.*, 2003). In this reanalysis, application of the same range-shrinking analysis failed to find any significant variation from a simple power law over the entire experimental data range ($|t| < 1 \times 10^{-2}$) in contrast to the previous Haupt and Straub analysis. To further test the surprising conclusion found in the simple power-law reanalysis, the SF$_6$ measurements were analyzed using the MSR crossover model. The results of the MSR analysis, shown in Fig. 4, also confirmed that all data were actually within the asymptotic region. For this MSR analysis, the critical exponent α was fixed at the theoretical value (Guida and Zinn-Justin, 1998) $\alpha = 0.109$. The MSR model has three system-dependent parameters $\{u, \mu, a\}$. However, only two of these are independent. In this analysis, the model parameters $\{\mu, a\}$ were chosen as fitting parameters (Barmatz *et al.*, 2004, 2005). In Fig. 4(a), the lines represent the theoretical fit. The difference between experiment and theory is also shown in the upper part of the figure. Figure 4(b) shows the fit to the scaled specific heat, which by dividing out the divergent term enhances the crossover behavior. The horizontal solid lines represent the asymptotic critical amplitudes obtained from the fit. Theoretical models predict a universal amplitude ratio between the Wegner first-order heat capacity and susceptibility, $A_1^+/\Gamma_1^+ \simeq 0.9$. Garrabos (1986) reanalyzed earlier SF$_6$ susceptibility measurements (Cannell, 1975) to obtain $\Gamma_1^+ = 1.14$. This result implies $A_1^+ \simeq 1$, which is inconsistent with the value $A_1^+ = (1.7 \pm 0.06) \times 10^{-4}$ obtained from the specific-heat reanalysis. The reason for this inconsistency in SF$_6$ is not yet understood.

The "Microgravity Scaling Theory Experiment" (MISTE) was developed to perform a set of thermodynamic measurements to within 10^{-6} K of the liquid-gas
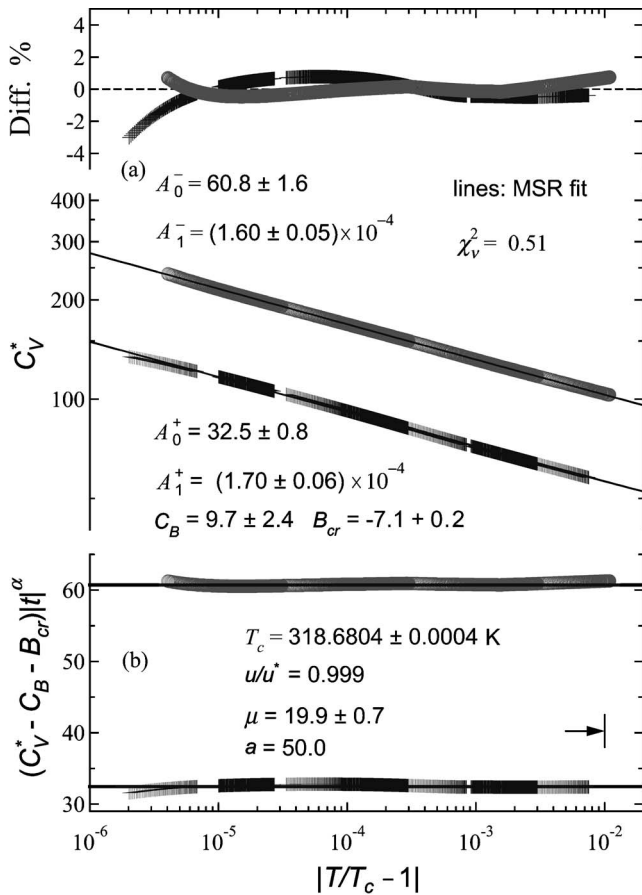
FIG. 4. Fit of the MSR model to the SF_6 microgravity specific-heat measurements. (a) Comparison of specific-heat measurements of Haupt and Straub (1999) in both the single-phase region (dark plus symbols) and two-phase region (gray circle symbols). The difference between experiment and theory is also shown. (b) Scaled critical part of the specific heat versus reduced temperature. Horizontal lines represent the asymptotic critical amplitudes obtained from the fit. Adapted from Barmatz *et al.*, 2004, 2005.

critical point of ^{3}He. An additional experiment called the "Coexistence Boundary Experiment" (COEX) was developed to share the MISTE apparatus. These experiments were designed to perform measurements of C_V, χ_T, the coexistence curve, and the equation of state in a single experimental cell of 4 cm height. The MISTE and COEX experiments were designed to obtain gravity-free measurements at least two decades in reduced temperature closer to the critical point (to $|t| \sim 1 \times 10^{-6}$) than can be obtained on the ground. Together they would provide a rather complete set of thermodynamic measurements throughout the ^{3}He critical region. These microgravity measurements would allow a more accurate determination of the leading asymptotic exponents α, β, γ, and δ as well as the amplitude ratios A_0^+/A_0^-, Γ_0^+/Γ_0^-, and $\alpha A_0^+ \Gamma_0^+/B_0^2$. More accurate values of the leading asymptotic amplitudes would also permit a stringent test of recent crossover equation-of-state models. Extensive ground-based experimental and theoretical studies were
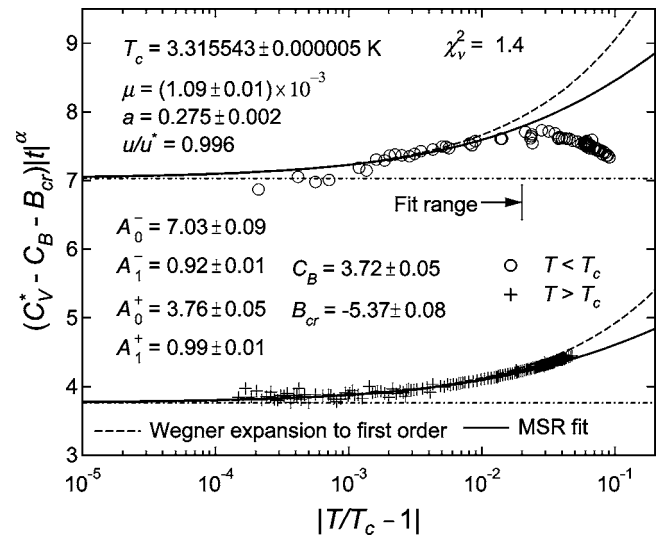
FIG. 5. Fit of specific-heat ground-based measurements in ^{3}He to the MSR model. The MSR model parameters $\{\mu, a\}$ were obtained from a joint fit of susceptibility, specific-heat, and co-existence curve measurements. The crossover region is clearly observed. Solid curves correspond to the best fit. The Wegner expansion to first order is shown as dashed lines using the critical amplitudes A_0^+ and A_0^- obtained from the fit to the MSR model. Adapted from Zhong and Barmatz, 2004.

performed in preparation for flight.[2] Figure 5 shows a fit of the MISTE ground-based scaled ^{3}He specific-heat data to the MSR crossover model. In this figure, which is similar to Fig. 4(b) the solid curves and MSR model parameters $\{\mu, a\}$ were obtained from a joint fit of susceptibility, specific-heat, and coexistence curve measurements (Zhong and Barmatz, 2004). The critical exponents used in this MSR joint fit were fixed at the theoretical values (Guida and Zinn-Justin, 1998) $\gamma = 1.2396$, $\alpha = 0.109$, $\beta = 0.3258$, and $\Delta = 0.504$. The horizontal dot-dashed lines represent the asymptotic critical amplitudes obtained from the fit. The dashed curves correspond to a fit to Eq. (6) including only the first Wegner crossover term. These ^{3}He measurements clearly show the crossover region for measurements $|t| > 1 \times 10^{-4}$ in contrast to the fit to the SF_6 measurements shown in Fig. 4.

C. Susceptibility

One of the most important response functions of a fluid system is the isothermal susceptibility $\chi_T = \rho (\partial \rho / \partial P)_T$. The divergence of this quantity leads to the strong gravity-induced density gradient seen in ground-based experiments. The most precise susceptibility measurements have generally been performed using light-scattering techniques. Susceptibility measurements of

[2]See Cowan *et al.*, 1996; Barmatz *et al.*, 1998, 2001; Barmatz, Hahn, *et al.*, 2000; Barmatz, Zhong, *et al.*, 2000, 2003; Hahn *et al.*, 2001; Weilert *et al.*, 2002; Zhong *et al.*, 2003; Rudnick *et al.*, 2003; Zhong and Barmatz, 2004.
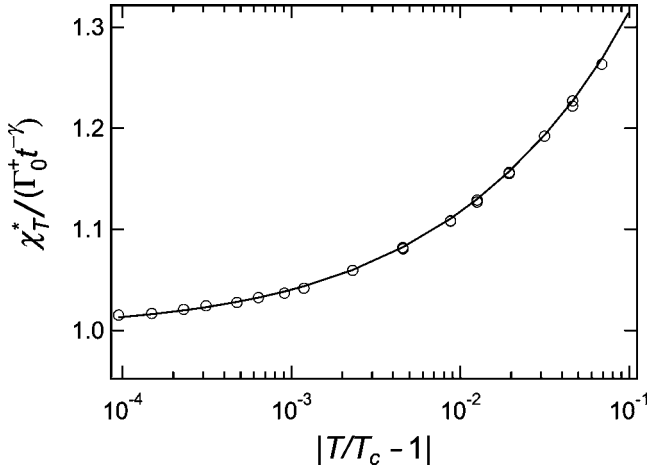
FIG. 6. Normalized susceptibility measurements in the gravity-free region near the xenon critical point. Solid curve is the best fit by Güttinger and Cannell (1981) to a theoretical expression that includes Wegner crossover terms to the third order assuming $\gamma = 1.241$ and $\Delta = 0.496$.

xenon in the region unaffected by gravity (Güttinger and Cannell, 1981) are shown in Fig. 6. These precision measurements above the critical point were fitted over the reduced temperature range $9.6 \times 10^{-5} \le t \le 10^{-1}$ with the extended crossover expression

$$\chi_T^* \equiv (P_c/\rho_c^2)\chi_T = \Gamma_0^+ t^{-\gamma}(1 + \Gamma_1^+ t^\Delta + \Gamma_2^+ t^{2\Delta} + \Gamma_3^+ t^{3\Delta}), \quad (9)$$

which includes Wegner terms to third order. The best fit of this expression to the data is shown by the solid curve, which corresponds to $\gamma = 1.241$, $\Gamma_0^+ = 0.0577$, $\Gamma_1^+ = 1.29$, $\Gamma_2^+ = 1.55$, and $\Gamma_3^+ = 1.9$. Background terms and the correction term t^{Δ_2} arising from the asymmetric ϕ^5 term of field theory that are not shown in Eq. (9) may be just as important as the third-order Wegner term.

In Fig. 7, we show susceptibility measurements of ^{3}He where the effect of gravity can be seen. The solid curves and MSR model parameters $\{\mu, a\}$ were obtained from a joint fit of susceptibility, specific-heat, and coexistence curve measurements (Zhong and Barmatz, 2004). The horizontal dot-dashed lines represent the asymptotic critical amplitudes obtained from the best fit. The dashed curves correspond to a fit to Eq. (9) including only the first Wegner crossover term. The figure also shows gravity-affected measurements along the coexistence curve in the range $|t| < 2 \times 10^{-4}$. It is important to note that earlier susceptibility measurements by Pittman *et al.* (1979) are comparable in quality with the measurements shown, and agree with them if a small shift in T_c is made (Meyer, 2001).

The MISTE experiment was designed to measure the susceptibility near the critical point of ^{3}He in a microgravity environment using two approaches. For $|t| \ge 6 \times 10^{-4}$, a *PVT* approach was planned where the pressure and density are measured as fluid is slowly removed from the sample chamber at constant temperature. The sample density is determined by measuring the dielectric constant using a capacitive sensor while the pressure is
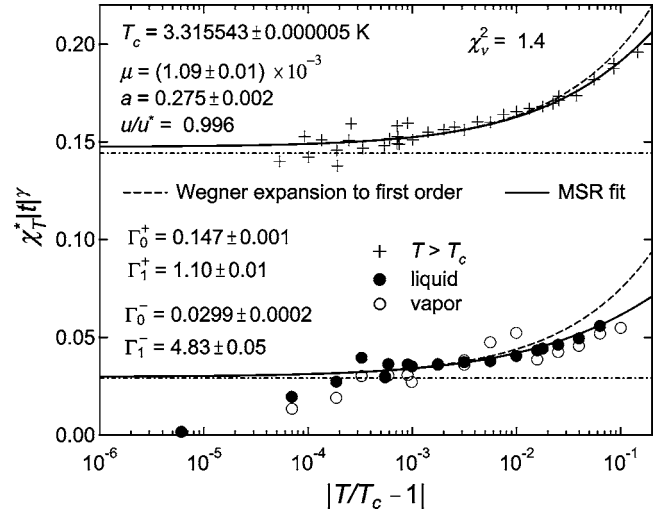
FIG. 7. Fit of susceptibility measurements in ^{3}He to the MSR model. The upper part shows measurements above the transition, and the lower part shows measurements along the coexistence curve. The MSR model parameters $\{\mu, a\}$ were obtained from a joint fit of susceptibility, specific-heat, and coexistence curve measurements. Solid curve is the best fit while the dashed curve corresponds to a Wegner expansion to first order. Gravity-affected measurements along the coexistence curve are shown in the range $|t| < 2 \times 10^{-4}$. Only the gravity-free measurements were fitted with the MSR model. Adapted from Zhong and Barmatz, 2004.

obtained using a capacitive sensor in vacuum where one of the capacitor plates is attached to a flexible part of the chamber wall. The susceptibility above the transition is obtained by differentiating the P-ρ curve. Below the transition, the susceptibility along the coexistence curve is determined from the slope of the P-ρ curve in the one-phase region just as the sample enters or leaves the two-phase region. The shape of the coexistence curve could also be determined from the discontinuity in the P-ρ measurements upon entering or leaving the two-phase region.

For $|t| < 4 \times 10^{-3}$, an electrostriction method of measuring the susceptibility was planned for MISTE. The electrostriction effect was previously demonstrated in a microgravity experiment using the Critical-Point Facility that flew on the Second International Microgravity Laboratory IML-2 mission. That experiment (Zimmerli *et al.*, 1999a, 1999b) measured a density change in SF_6 consistent with the predictions of the electrostriction effect. This electrostriction method takes advantage of the fact that an electric field gradient can produce an equivalent pressure gradient within a dielectric fluid (Panofsky and Phillips, 1955). A dc voltage across a capacitor immersed in the fluid induces an electric field E and associated pressure ($\delta P \propto E^2$) within the capacitor gap. The pressure difference between the inside and outside of the capacitor causes fluid to flow into the gap. Assuming that the ambient density outside the capacitor does not change when an additional small amount of fluid enters the gap, the susceptibility can be measured

to a first approximation using $\chi_T \propto \Delta\rho/E^2 \propto \Delta C/E^2$, where ΔC is the capacitance change. This measurement approach was successfully demonstrated in ground-based measurements near the ^{3}He critical point (Barmatz *et al.*, 1998; Barmatz, 1999; Barmatz, Zhong, *et al.*, 2000).

D. Coexistence curve

Upon cooling a liquid-gas system through the critical point along the critical isochore, the growth of the order parameter is determined by the shape of the coexistence curve, described by Eq. (7). The modern understanding of critical phenomena, that is, the concept of universality and scaling, was initiated by the Guggenheim (1945) plot of coexistence curve measurements. That plot showed the approximately universal nature of coexistence curves near the critical point of various fluids using T/T_c and ρ/ρ_c coordinates and demonstrated a significant deviation from the shape predicted by classical theory. Historically, gravity effects on fluids near the critical point were also demonstrated by measurements of the coexistence curve in different height samples using optical methods (Lorentzen, 1953) and the *PVT* method (Habgood and Schneider, 1954). There have been numerous measurements of the coexistence curve in various fluids performed on the ground to determine the critical exponent β and critical amplitudes. For a general review of results, see, for example, Sengers (1974), Anisimov (1991), and Privman *et al.* (1991). Many of the early experimental results have been summarized by Heller (1967). While gravity effects distort the shape of the coexistence curve near the critical point, ground-based measurements are consistent with current theoretical predictions. Perhaps the best result to date is for N$_2$ and Ne (Pestak and Chan, 1984), which gave $\beta = 0.327 \pm 0.002$. Despite the existence of numerous ground-based studies, no high-resolution coexistence curve measurements have yet been attempted under microgravity conditions.

The COEX experiment was designed to measure the coexistence curve of ^{3}He very near the liquid-gas critical point. As mentioned earlier, this experiment will share the MISTE apparatus. Figure 8 shows recent ground-based results of the ^{3}He coexistence curve in preparation for the COEX flight experiment (Hahn *et al.*, 2004). The liquid-gas coexistence curve shape of ^{3}He near the critical temperature T_c was measured in the range $-5 \times 10^{-3} < T/T_c - 1 < -1.5 \times 10^{-6}$ using a quasistatic thermogram technique. This technique was chosen because data can be obtained using the specific-heat measurement cell developed for the MISTE flight experiment. This ground-based study was performed using two cells of very different heights (0.5 and 48 mm). Figure 8 shows coexistence curve measurements scaled by the leading power-law behavior with the critical exponent β fixed at 0.3258. In this scaled plot, the horizontal dashed line corresponds to the asymptotic critical amplitude B_0 in Eq. (7). The upward curvature of the measurements
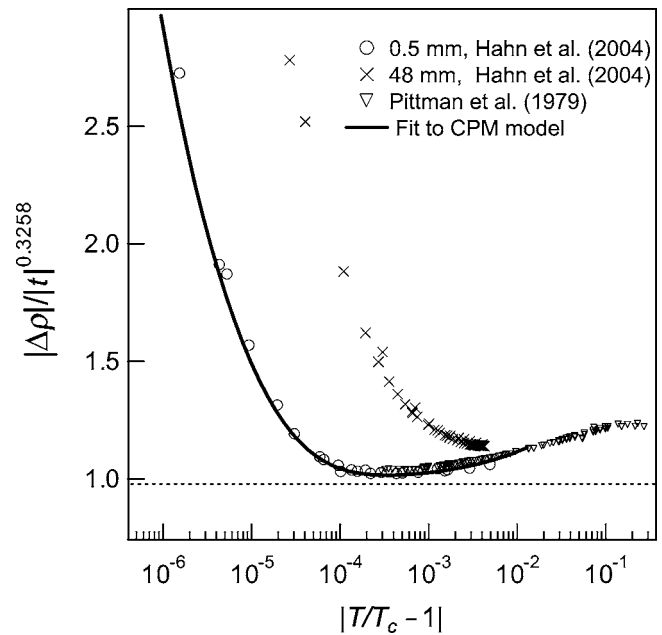
FIG. 8. Normalized plot of ^{3}He coexistence curve measurements emphasizing the gravity-affected region. The density is scaled by the leading power-law term $|t|^\beta$ to expose nonasymptotic behavior and gravity effects. This plot includes both liquid- and gas-side data. The dashed horizontal line corresponds to the predicted asymptotic critical amplitude B_0. The solid curve shows a fit of the 0.5-mm gravity-affected measurements to the CPM equation of state model. The gravity-free measurements are consistent with the earlier measurements of Pittman *et al.* (1979) farther away from the transition. Adapted from Hahn *et al.*, 2004.

from this horizontal line close to the transition is due to the effect of gravity. The measured coexistence curves are also very different for the two cells and clearly show the effect of gravity. Even in the measurements with the 0.5-mm-high cell, the predicted asymptotic behavior is not observed in this ground-based experiment. Furthermore, the onset of the gravity effect in these data overlaps the temperature range where nonasymptotic correction terms begin to come into play. These recent measurements are consistent with the earlier data of Pittman *et al.* (1979) farther away from the transition. The overlap of gravity effects and nonasymptotic correction terms makes it difficult to accurately obtain B_0 and B_1 by fitting data to the Wegner expansion [see Eq. (7)].

The shape of the coexistence curve ($\Delta\bar{\rho}$ vs t) measured in a finite height sample container in the presence of gravity can be calculated using an equation-of-state model. Recently, Agayan *et al.* (2001) developed the crossover parametric model (CPM) equation of state for the critical region of 3D Ising-like systems. The coexistence curve calculated including the gravity effect using the CPM model is in quantitative agreement with experimental measurements close to the transition (Hahn *et al.*, 2004) as shown in Fig. 8 by the solid curve for 0.5-mm measurements. Earlier data sets of the ^{3}He coexistence curve over a wide gravity-free temperature range, compiled by Luijten and Meyer (2000), have also
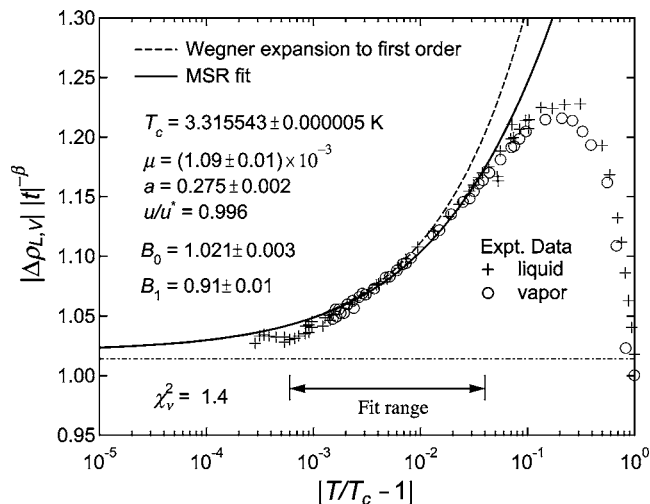
FIG. 9. Fit of coexistence curve measurements in ^{3}He to the MSR model. Data sets of gravity-free measurements farther away from the critical point, compiled by Luijten and Meyer (2000), were used in the fit. The MSR model parameters $\{\mu,a\}$ were obtained from a joint fit of susceptibility, specific-heat, and coexistence curve measurements. The solid line corresponds to the best fit and the dashed curve corresponds to a Wegner expansion to first order. The dot-dashed straight line represents the asymptotic prediction from the fit. Adapted from Zhong and Barmatz, 2004.

been compared to the MSR crossover model (Zhong *et al.*, 2003; Zhong and Barmatz, 2004). That comparison is shown in Fig. 9. The fit was limited to the range $6 \times 10^{-4} \le |t| \le 2 \times 10^{-2}$. The solid curves and MSR model parameters $\{\mu,a\}$ were obtained from a joint fit of susceptibility, specific-heat, and coexistence curve measurements (Zhong and Barmatz, 2004). The dashed curve corresponds to a Wegner expansion to first order. A background contribution associated with the order parameter approaching absolute zero temperature (Zhong *et al.*, 2003) significantly affects measurements farther away from T_c.

E. Correlation length

The correlation length is a direct measurement of the spatial fluctuation range for the order parameter. Precision measurements of the correlation length have been performed on the ground where gravity effects are small. Figure 10 shows the results of light-scattering measurements along the critical isochore in SF$_6$ above the critical temperature (Cannell, 1975). Measurements farther away from the transition, shown by circles, were obtained using a differential intensity method. Measurements close to the transition, shown by crosses, were determined from turbidity and compressibility measurements. Measurements unaffected by gravity could be obtained over the wide temperature ranged $4 \times 10^{-6} \le t \le 3.1 \times 10^{-2}$ because of the narrow optical beam diameter used. Cannell (1975) obtained $\nu = 0.621$, which compares well with the theoretical value $\nu = 0.630$ (Guida and Zinn-Justin, 1998).
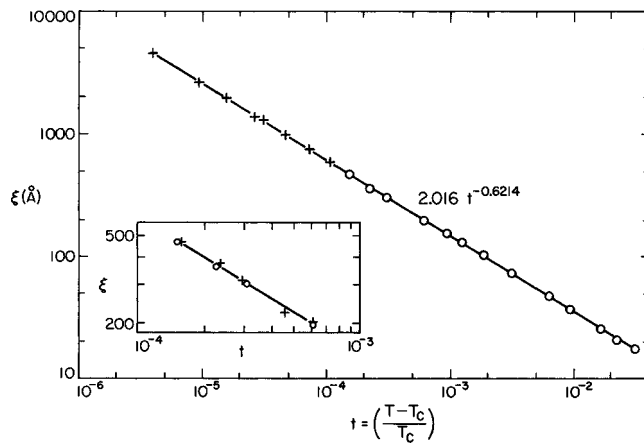
FIG. 10. Long-range correlation length of SF$_6$ as a function of temperature on the critical isochore. Circles are the results of differential intensity measurements, and crosses are values determined from turbidity measurements. The inset compares the results in the temperature range where both methods could be used. From Cannell, 1975.

The Zeno microgravity experiment was designed to measure the temperature dependence of two fundamental dynamic properties of critical fluctuations: their spatial extent given by the correlation length and their lifetime given by the decay rate. Light-scattering spectroscopy was used to measure these quantities near the critical point of xenon. The Zeno experiment was flown twice aboard the Space Shuttle, first during the USMP-2 mission in 1994 (Gammon *et al.*, 1996) and later during the USMP-3 mission in 1996. Measurements obtained from both of these microgravity investigations were compromised by local heating of the sample at the cell windows induced by the laser beam. This local heating effect led to a long-lasting density inhomogeneity during the flight experiments. The equilibration time for these density inhomogeneities was much longer than observed on the ground since gravity-induced convection was no longer present. The resulting long equilibration times were not anticipated in flight time sequences between temperature changes and limited the comparison of measurements to theoretical predictions (Gammon, 1998). These early microgravity studies clearly demonstrated the importance of designing the experimental apparatus to minimize density inhomogeneities associated with temperature gradients.

F. Viscosity

The theory of dynamic critical phenomena predicts that, along the critical isochore in the limit of zero frequency, the viscosity η diverges as ξ^{z_η} with the correlation length ξ, diverging as $t^{-\nu}$, i.e., $\eta \propto t^{-\nu z_\eta}$ (Hohenberg and Halperin, 1977; Sengers, 1985). The viscosity exponent z_η is very small and is difficult to determine on the ground because of a large background contribution. As with other measurements, gravity limits the uniformity of a sample near the critical point. The CVX experiment was performed on the Space Shuttle mission STS-85 in

1997 to better determine the divergent behavior of the viscosity. This experiment used a viscometer consisting of a nickel screen torsion oscillator that vibrated between two pairs of paddlelike electrodes while immersed in xenon at the critical density (Berg, 1995; Berg *et al.*, 1999b). The thermostat designed for CVX (Berg *et al.*, 1998) could achieve temperature differences within the sample of less than 0.2 μK (Berg *et al.*, 1998). The temperature program constrained the density to be sufficiently close to equilibrium based on an understanding of the temperature and density dynamics near the liquid-vapor critical point including the piston effect (Berg *et al.*, 1999b). The viscosity was determined from the ratio of the screen's motion to the applied force. The analysis of the CVX measurements required a theoretical model that included a scaling function for near-critical viscoelasticity (Bhattacharjee and Ferrell, 1983), a crossover function (Bhattacharjee *et al.*, 1981), and a background viscosity (Berg and Moldover, 1990).

The characteristic lifetime τ of density fluctuations also diverges as the critical point is approached. This quantity is given by

$$\tau = \frac{6\pi\eta\xi^3}{k_B T_C} = \tau_0 t^{-\nu(z_\eta+3)}, \tag{10}$$

where τ_0 is the fluctuation decay-time amplitude (Hohenberg and Halperin, 1977). This characteristic lifetime increases much faster than the viscosity as the critical point is approached. When the viscometer's oscillation frequency is higher than the characteristic fluctuation frequency $1/\tau$, the slow fluctuations remember the previous oscillations and the fluid exhibits viscoelasticity (frequency-dependent viscosity, or the ability of a fluid to stretch as well as flow). This phenomenon was also studied near the critical point as a function of the viscometer's oscillation frequency.

Using low frequencies and small amplitudes, the temperature dependence of the viscosity was determined to $t=3\times10^{-7}$. Figure 11 shows the results of this experiment (Berg *et al.*, 1999b). The best-fit value of z_η $=0.0690\pm0.0006$ obtained from these results is consistent with the value $z_\eta=0.067\pm0.002$ obtained from a two-loop perturbation expansion calculation (Hao *et al.*, 2005). The results of this viscosity study near the xenon liquid-gas critical point were recently shown to obey the predictions of rheological models (Berg, 2004). Viscoelastic behavior was observed in the range $t<10^{-5}$, as can be seen in Fig. 12. The CVX experiment resulted in a few surprises. The viscoelastic response time in xenon was a factor of 2 slower than predicted (Bhattacharjee and Ferrell, 1983) and the sample density reached equilibrium faster than expected, suggesting convection driven by microgravity and by electric fields. The viscoelastic results were recently shown to be consistent with the Cox-Merz rule, which relates viscoelasticity to shear thinning (Berg, 2004).

A second flight experiment, CVX-2, was performed on the Space Shuttle mission STS-107 in 2003. The CVX-2 experiment used the same apparatus and sample
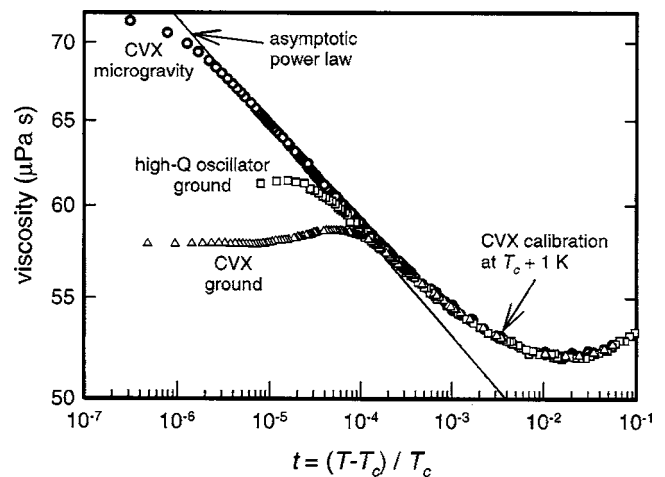
FIG. 11. Log-log plot of xenon's viscosity measured along the critical isochore near the critical point. The asymptotic line has the slope $v z_\eta$=0.0435 deduced from the present microgravity data. Near T_c, the CVX microgravity data depart from the asymptotic line because of viscoelasticity. The two sets of ground data depart from the asymptotic line further from T_c because the xenon stratified in Earth's gravity. From Berg *et al.*, 1999b.

as CVX but operated the viscometer at larger amplitudes to study shear thinning, the decrease of viscosity predicted at large shear rates (Oxtoby, 1975). For pure fluids composed of small molecules, the relaxation time τ is too short for shear thinning to be observed except near the critical point, where microgravity is necessary to achieve density homogeneity. Attempting to observe shear thinning far from the critical point would have required a shear rate so large that the associated viscous heating would have ruined the temperature and density homogeneity of the sample.

For the CVX-2 study, the viscometer screen was vibrated with amplitudes up to 30 times larger than in CVX. At these large amplitudes, the shear rate exceeded the frequency $1/\tau$, causing fluctuations to become distorted and the fluid to show shear thinning. The tragic disintegration of Space Shuttle Columbia upon reentry into the Earth's atmosphere in 2003 delayed the recovery of the microgravity data. The CVX-2 data are currently being analyzed.

G. Two-phase phenomena

The behavior of fluids in the two-phase region below the critical point is more complicated than in the single-phase region because of heat and mass transfer between the liquid and gas phases. Microgravity experiments provide a unique opportunity to investigate these processes without the effects of convection and stratification. Near the critical point, phase separation and the decay of the resulting density inhomogeneities can be studied over a longer time period due to critical slowing down. When a fluid is heated or cooled within the two-phase region near the critical point, its nonequilibrium behavior is complicated because the piston effect is different in the
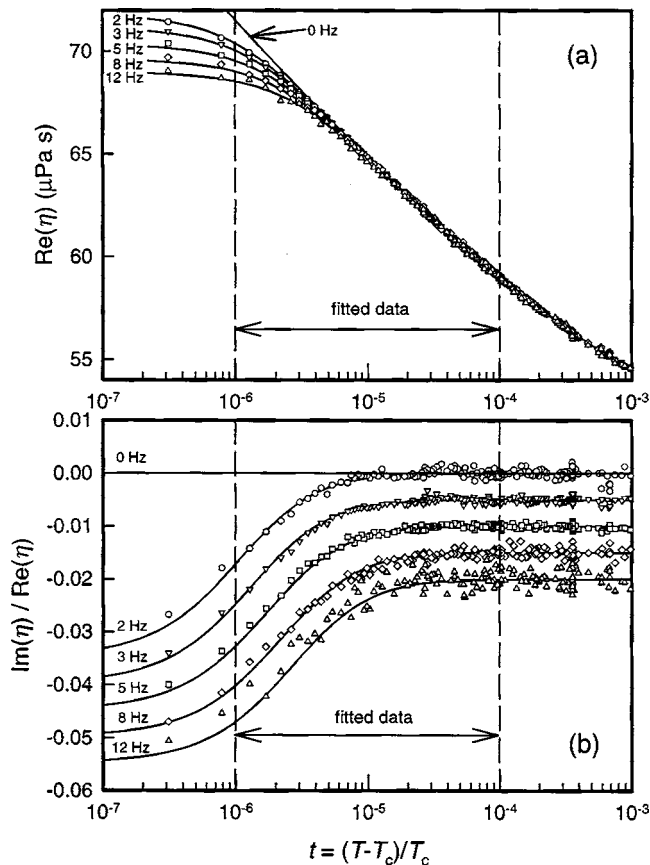
FIG. 12. Xenon's viscosity at critical density measured at frequencies from 2 to 12 Hz. The solid curves resulted from fitting the data in the range $10^{-6} < t < 10^{-4}$ to theory. (a) The real viscosity $\mathrm{Re}(\eta)$. Near $t = 10^{-5}$, the data depart from the 0 Hz curve because of viscoelasticity. (b) The ratio $\mathrm{Im}(\eta)/\mathrm{Re}(\eta)$. For clarity, the ratio data at frequencies above 2 Hz are displaced downward by integer multiples of 0.005; otherwise they would coincide at $t > 2 \times 10^{-5}$. From Berg *et al.*, 1999b.

liquid and gas phases. In addition, boiling can be studied in the absence of buoyancy, which causes gas bubbles to rise within a liquid on Earth.

1. Phase separation

Phase separation presents a rich phenomenology in the case of liquids where hydrodynamic flows occur simultaneously with nonequilibrium processes. In particular, during phase separation the system splits into many domains characterized by different densities, growth rates, and coalescence behavior. On Earth these processes are affected by gravity, which induces domain sedimentation and convection. Gravity effects come into play when the size of the growing domains becomes comparable to the capillary length $l_c = \sqrt{\sigma/\rho g}$, where σ is the surface tension. The characteristic evolution time scale of the domains is identical to the time scale τ_ξ of the relaxation of order parameter size fluctuations. This implies that phase separation is very rapid away from the critical point but slows down dramatically as the critical point is approached. Thus, near-critical systems (both pure fluids and binary liquid mixtures) are useful

in studying the kinetics of phase separation. However, since l_c vanishes at the critical point, gravity effects govern the domain growth shortly after the onset of separation. Therefore, buoyancy effects have to be completely suppressed in order to study the intrinsic kinetics of phase separation.

For phase separation experiments, it is more advantageous to use pure fluids rather than binary mixtures because during a thermal quench the piston effect induces a homogeneous and rapid temperature change in the entire bulk of a pure sample, whereas a temperature change propagates diffusively in a binary mixture. In a pure fluid, phase separation studies near the critical point are usually performed by applying a temperature quench from the one-phase region through the coexistence curve into the two-phase region. The coexistence and spinodal curves are very close near the critical point, and are in contact at the critical point. The spinodal curve separates the region of instability from the metastability region closer to the coexistence curve. Near the critical point, the spinodal curve is not sharply defined, but is replaced by a narrow crossover region in which the nucleation time becomes comparable to the time scale of the experiment. When the final quenched state is below the spinodal curve, any fluctuation of the order parameter becomes unstable (Beysens *et al.*, 1988) and *spinodal decomposition* occurs. If the final quenched state is below the coexistence curve but above the spinodal curve, the one-phase state is metastable, and only sufficiently large domains can nucleate and grow. In this case, phase separation is triggered by *nucleation*. After nucleation, further growth of the domains occurs by *Ostwald ripening*, evaporation and/or condensation through species diffusion (Lifshitz and Slyosov, 1961). Near the critical point, fluctuations broaden the spinodal curve, making the distinction between the coexistence and spinodal curves difficult to observe (Dahl and Moldover, 1972; Beysens *et al.*, 1988). After penetrating the coexistence curve, a near-critical system rapidly phase-separates into domains of droplets and bubbles, and local thermodynamic equilibrium is reached where the volume fractions and compositions of the phases stabilize. Then phase coalescence begins, in which only the number of domains diminishes. Experiments performed in low gravity on near-critical systems are designed primarily to observe this phase coalescence.

In preparation for microgravity experiments, ground-based studies were performed on phase separation in density-matched binary mixtures using isotopes of carbon to minimize the effects of gravity (Houessou *et al.*, 1985; Guenoun *et al.*, 1987). These studies observed new microscopic spinodal decomposition patterns and thin wetting layers. The first low-gravity experiments on phase separation in liquid binary mixtures and pure fluids were performed during 6-min flights on ESA TEXUS-11 and 13 sounding rockets (Beysens *et al.*, 1988). Low-gravity studies of the heat transport process near the CO_2 critical point were also performed in 1990 on the TEXUS-25 rocket (Guenoun *et al.*, 1993). In that study, a sample was quenched into the two-phase region
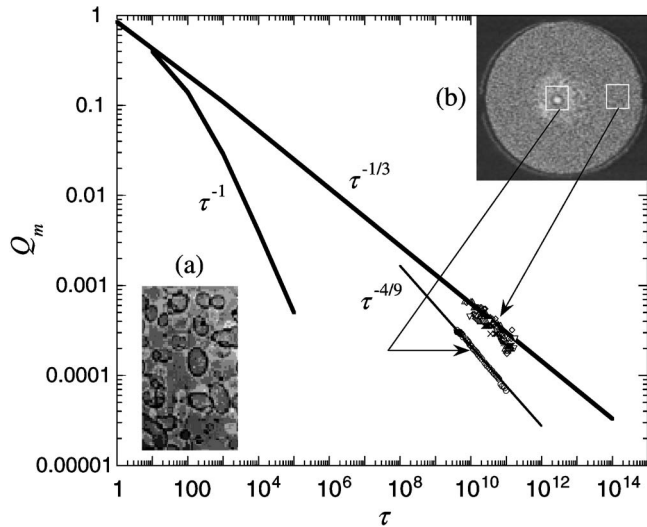
FIG. 13. Growth laws of phase-separating fluid close to the critical point for the reduced coordinate $Q_m = 2\pi/L_m$, where L_m is the average spacing between drops. The experimental points illustrate the growth of the central CO_2 single bubble for temperature quenches of 85, 90, and 100 mK with the exponent close to −0.5 while the $Q_m(\tau) \sim \tau^{-1/3}$ behavior is recovered far from the illuminated area. The fit using the theoretical $-4/9 \approx -0.44$ exponent is also shown. Inset (a) shows growth of interconnected domains when volume fraction $\varphi > 30\%$ $[Q_m(\tau) \approx \tau^{-1}]$; inset (b) shows growth of isolated droplets when $\varphi < 30\%$. From Beysens, Garrabos, Nikolayev, *et al.*, 2002.

and spinodal decomposition, growth of gas and liquid domains, and the piston effect were observed (Garrabos *et al.*, 1992). Nucleation and growth studies in a binary liquid and in SF_6 were performed in the CPF facility during the Space Shuttle mission STS-42 in 1992. A new kinetic region of phase separation, the $\tau^{1/3}$ time regime, was discovered (Perrot *et al.*, 1994). Thermal quenches were used to demonstrate that the growth of tightly packed droplets could be explained over seven decades in τ by a single power law. The morphology and kinetics of phase coalescence near the critical point in the late stages of growth were analyzed in some detail using the results from these experiments (Perrot *et al.*, 1999). It was unambiguously demonstrated that the kinetics of phase coalescence depends on the volume fraction φ of the minority, nonwetting phase (Perrot *et al.*, 1999). For $\varphi > 0.3$, the domains are interconnected and grow rapidly from frequent coalescence events activated by hydrodynamic interactions (Nikolayev *et al.*, 1996), and the size of the domains (gas bubbles in the case of pure fluids) grows linearly with time. For $\varphi < 0.3$, the domains are well separated and grow by Brownian-motion-induced coalescence rather than by Ostwald ripening (Perrot *et al.*, 1994); their size grows slowly in time as $\tau^{1/3}$. This description is universal in the sense that it is valid for both binary mixtures and pure fluids. Later, it was also shown that laser beam heating could accelerate domain growth in microgravity by thermocapillary migration (Garrabos, Nikoloyev, *et al.*, 2002a). Figure 13 shows the various growth laws for a phase-separating fluid near the critical point for interconnected domains and isolated droplets.

Another interesting area related to phase separation and finite-size effects is critical adsorption. Thommes *et al.* (1994) studied the excess adsorption of SF_6 in graphite pores along the critical isochore. For $|t| > 10^{-2}$, they found the power-law behavior predicted by Fisher and de Gennes (1978), but closer to the transition an unexpected decrease in the adsorption was observed. Thommes and Findenegg (1995) later performed similar measurements in microgravity during the EURECA-I free-flyer mission. A similar result was obtained, implying that the phenomenon is an intrinsic property of the system. These authors have also performed a Monte Carlo simulation, which indicates that the effect is due to density depletion in the core region of the pores as $T \to T_c$. Results on other substrates have confirmed the existence of the effect (Thommes *et al.*, 1995).

2. Equilibration

In a microgravity environment, in the absence of any gravity-induced phase stratification, the distribution of phases within a sample and the shape of the liquid-gas interface are determined by the complete wetting of the liquid, the thermal history of the sample, and the geometry of the experimental cell, since surface tension is very weak. As a consequence, it is very difficult to predict the phase distribution within a cell.

As initially pointed out by Brown and Meyer (1972) and Dahl and Moldover (1972), and later discussed in more detail by Behringer *et al.* (1990), thermal equilibration in the two-phase region near the critical point of pure fluids is much slower than in the one-phase region. This phenomenon is commonly known as the *interface bottleneck*. Onuki and Ferrell (1990) showed theoretically that the energy exchange between liquid and gas (latent heat) becomes more important during a temperature quench as the critical point is approached, and that different temperature gradients are expected to form in the liquid and gas during adiabatic heating. Zhong and Meyer (1996) observed this interface bottleneck in their experiments and numerical simulations. On the other hand, Straub and co-workers did not observe it on the ground or in space (Straub *et al.*, 1995a). It is speculated that the temperature sensor dedicated to the gas phase in the microgravity experiment actually measured the interface temperature. A possible explanation for the differences between ground-based studies is that the sample cells used by Brown and Meyer (1972) and Zhong and Meyer (1996) were very thin (having a small Rayleigh number with no convection) and that the liquid wetting layers efficiently isolated the gas from the thermostat walls, whereas the large spherical cell of Straub and co-workers supported strong convection that restored rapid thermal equilibration of the two-phase sample.

An experimental study of the thermal response to a positive temperature step in the two-phase fluid SF_6 was performed in low gravity using the ALICE-2 facility on-
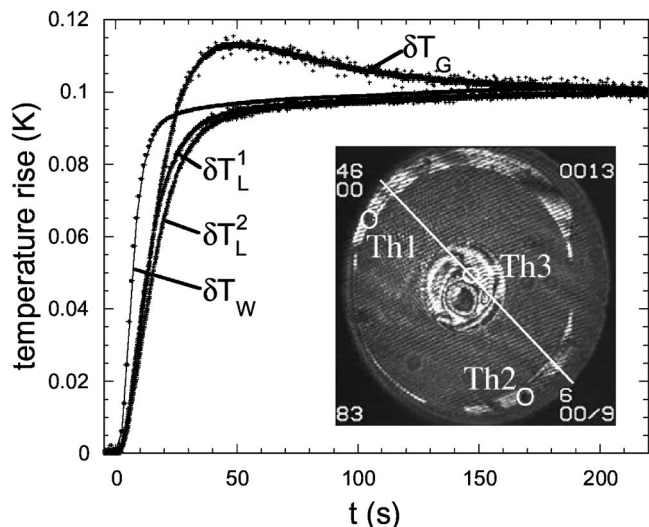
FIG. 14. Thermal response to a temperature quench in the two-phase region of SF_6. A temperature rise of 100 mK was set at the cell wall. Evolution of the temperature at the wall (δT_W), in the gas (δT_G) at the thermistor position Th3, and in the liquid ($\delta T_L^{1,2}$) at the thermistor positions Th1 and Th2, respectively, are shown. Overheating of 23% was observed in the gas phase at 10 K below the critical temperature (Wunenburger *et al.*, 2000). The inset picture is an interferometric cell image of the sample during the quench with the thermistors (Th1–Th3) marked by open circles. From Zappoli, 2003.

board the MIR station in 1999. An unusual thermal response was observed during the step. The gas temperature exceeded the temperature of the heated cell walls, leading to an overshoot of 23% (Wunenburger *et al.*, 2000). This overheating phenomenon, shown in Fig. 14, was caused by differences in the liquid and gas in converting the piston effect into a temperature change (Beysens, Garrabos, Wunenberger, *et al.* 2002b; Wunenburger *et al.*, 2002). This difference led to a more efficient heat transfer in the gas than in the liquid. This heating effect was accentuated in microgravity where the vapor bubble was thermally isolated from the cell walls by the liquid. The thermally isolated gas phase was initially overheated leading to late-stage heat transfer from the hot gas phase to the cooler liquid phase as the system diffusively approached thermal equilibrium.

3. Critical boiling

Microgravity has been used to study the boiling crisis that occurs in large-flux heat exchangers (e.g., those of power plants) where the heated walls can be dried by a layer of gas formed by boiling that thermally isolates the walls from the fluid. This overall drying leads to a drop of the heat flux through the walls and ultimately to their destruction through overheating. The value of using near-critical two-phase fluids to study the boiling crisis relies on the fact that a large gas production rate can be obtained using a small heat flux, since latent heat goes to zero at the critical point. Also, the mechanical effect on the interface of the vapor production (vapor recoil force) due to the momentum variation of the fluid un-

dergoing phase change at the interface is large compared to surface tension effects. Thus, large shape variations of a gas plume undergoing rapid heating near the critical point can be observed. The singular behavior of both latent heat and surface tension in near-critical pure fluids can thus be used to mimic the situation occurring in large-scale heat exchangers with noncritical fluids.

Boiling studies in SF_6 and CO_2 were carried out on several Cassiopée and Pegase French-Russian and GMSF French-American missions on the MIR Space Station using the ALICE-2 instrument. Observations of bubble images for various cell aspect ratios and during various ramping rates and quenches demonstrated large liquid contact angles and unexpected wetting of a gas at a solid surface (Garrabos *et al.*, 1999; Garrabos, Lecoutre-Chabot, *et al.*, 2001b). It was speculated that these phenomena may be caused by both a surface-tension gradient due to a temperature gradient along the interface and a vapor recoil force due to evaporation (Hegseth *et al.* 2002, 2005). This recoil force, which expands bubbles, could explain the boiling crisis since the associated area increase of the solid-vapor surface isolates the solid from the liquid and increases the temperature gradients and consequently the gas production. A theoretical model was also developed to explain the growth of gas bubbles after a rapid sample quench from the one-phase to the two-phase region in pure CO_2 (Beysens, Garrabos, Nikolayer, *et al.*, 2002a). Further studies of critical boiling phenomena are planned for the ISS using the DECLIC facility (Cambon *et al.*, 2004).

V. $O(2)$ UNIVERSALITY CLASS—LAMBDA TRANSITION IN ^{4}He

The lambda transition of helium is the primary example of the $O(2)$ universality class. While magnetic critical phenomena in XY ferromagnets also fall within this class, demagnetization effects and sample uniformity problems limit the approach to the critical point to $t \approx 10^{-4}$. Of primary interest for static phenomena near the superfluid transition is the behavior of C_P and the superfluid density ρ_s measured along constant pressure paths. As for the $O(1)$ universality class, in a quantitative analysis of the temperature dependence of these parameters it is necessary to deal with nonasymptotic representations because data are obtained a finite distance from the superfluid transition temperature $T_\lambda(P)$. In this region, the RG theory predicts (Wegner, 1972)

$$C_P = \frac{A^\pm}{\alpha}|t|^{-\alpha}(1 + a_C^\pm|t|^\Delta + b_C^\pm|t|^{2\Delta} + \cdots) + B, \qquad (11)$$

where the + and − signs refer to $T > T_\lambda$ and $T < T_\lambda$, respectively, and

$$\rho_s = \rho_{s0}|t|^\nu(1 + a_{\rho_s}|t|^\Delta + b_{\rho_s}|t|^{2\Delta} + \cdots), \quad T < T_\lambda. \quad (12)$$

Equation (11) is essentially the same as Eq. (6) shown for the $O(1)$ case, and Eq. (12) is similar to Eq. (8) due to the hyperscaling relationship mentioned earlier. The critical and background contributions to B are typically

TABLE V. Theoretical estimates of the leading exponents for the $O(2)$ class.

ν	α	Reference
0.67168 (3)	−0.01504 (9)	Williams (1993)
0.6703 (15)	−0.011 (4)	Guida and Zinn-Justin (1998)
0.671	−0.013	Yukalov and Gluzman (1998)
0.6723 (8)	−0.0169 (24)	Hasenbusch and Török (1999)
0.67098 (20)	−0.01294 (60)	Kleinert (1999)
0.6704 (7)	−0.0112 (21)	Jasch and Kleinert (2001)
0.67155 (27)	−0.0146 (8)	Campostrini *et al.* (2001)
9/13 [=0.69231]	−1/13 [=−0.07692]	Kaupuzs (2001)

combined for the $O(2)$ case, as for α small and negative, the critical contribution is very large. Higher-order corrections and other background terms are discussed below. In parallel with the $O(1)$ case, the quantities $A^\pm$, B, and ρ_{s0} as well as the correction amplitudes $a_C^\pm$, $b_C^\pm$, a_{ρ_s}, and b_{ρ_s} depend on system-dependent parameters of the statistical distribution of the order parameter, while the critical exponents ν, α and the confluent singularity exponent Δ are independent of these parameters, i.e., universal. Certain ratios of the nonuniversal amplitudes are also predicted to be universal (Privman *et al.*, 1991), for example, A^+/A^-, a_C^+/a_C^-, a_C^-/a_{ρ_s}, and $P_A=(1-A^+/A^-)/\alpha$, a combination less sensitive to the exact value of α when it is small (Barmatz *et al.*, 1975). As before, the complete Wegner expansion includes not only the series indicated, but additional terms such as $d_C^\pm|t|$ and $e_{Ci}^\pm|t|^{\Delta_i}$, where d_C and e_{Ci} are constants and the Δ_i are higher-order exponents related to irrelevant operators (Wegner, 1972; Eyal *et al.*, 1996). Since the terms $e_{Ci}^\pm|t|^{\Delta_i}$ involve extensions beyond the basic ϕ^4 theory, we neglect them. Also, over the temperature range of interest, the term $d_C^\pm|t|$ behaves like $b_C^\pm|t|^{2\Delta}$ since $\Delta \approx 0.529$. Thus it can be neglected in most experiments to date.

Using advanced analytical and numerical techniques, it has been possible to derive estimates for many of the $O(2)$ universal quantities, in particular, the exponents ν and α. These are linked by the hyperscaling relation in Eq. (3), which is an integral part of all calculations to date. In Table V, we list the estimates that have been published in the past decade or so. It can be seen that there are a number of precise estimates allowing high-quality tests of the theory. Most of the estimates have been obtained with advanced RG techniques using various expansion and resummation methods. In general, it is quite difficult to obtain quantitative estimates of the uncertainties involved, so the bounds given in this table should be treated with caution. This point has been emphasized by Kleinert and Schulte-Frohlinde (2001) and by Zinn-Justin (2003). The most recent value of α obtained by standard methods that we are aware of is 0.0146 ± 0.0008 obtained by Campostrini *et al.* (2001). Related earlier work by Hasenbusch and Török (1999) using Monte Carlo techniques with suppression of corrections to scaling is also listed in this table. Jasch and

Kleinert (2001) obtained $\alpha=0.0112\pm0.0021$ using a fast convergent resummation algorithm and a seven-loop expansion series. Some of the results in this table were obtained by techniques significantly removed from the more mainstream RG methods. The result of Kaupuzs (2001) involves a special regrouping of Feynman diagrams to obtain an array of exact predictions with integers then selected to fit Monte Carlo results for finite XY systems. To avoid conflict with experiment, he argued that the asymptotic region might be much closer to the transition than has been appreciated. The possibility of logarithmic corrections to Eq. (11) has also been proposed, allowing a reasonable fit over a wider range of t (Kaupuzs, 2005). Williams (1993) used vortex ring theory to derive exponent estimates that are in good agreement with the results of Campostrini *et al.* (2001). Yukalov and Gluzman (1998) obtained their results from self-similar approximation theory. This approach has now been combined with that of Kleinert (1999) and may well lead to even higher-precision results (Kleinert and Yukalov, 2005). The leading crossover exponent has been estimated by Guida and Zinn-Justin (1998), who obtained $\Delta=0.529\pm0.009$.

The $O(2)$ amplitude ratios can be calculated from the RG theory with varying degrees of accuracy. The most recent predictions for the amplitude ratio A^+/A^- are based on three- and four-loop RG calculations and Borel resummations. Strösser and co-workers (Strösser *et al.*, 1999, 2000; Strösser and Dohm, 2003) obtained $A^-/A^-=1.056\pm0.004$ and $P_A=4.433\pm0.077$ if $\alpha=-0.0126$. Campostrini *et al.* (2001) obtained $A^+/A^-=1.062\pm0.004$ based on their value for α. For this case we estimate $P_A=4.247\pm0.5$, where the error bar is very conservative. Kleinert and Van den Bossche (2001) obtained $A^+/A^-=1.045\,16\pm0.004$ from a three-loop calculation, assuming $\alpha=-0.010\,56$. This implies $P_A=4.28\pm0.4$ where again the error bar is conservative. Earlier calculations by Bervillier (1986) gave $A^+/A^-=1.029\pm0.013$ and $P_A=4.455\pm0.04$, with $\alpha=-0.007$. Schultka and Manousakis (1995a) obtained $A^+/A^-=1.044\pm0.038$ using Monte Carlo techniques. It is important to remember that estimates of A^+/A^- are typically correlated with α, which had a range of values for the numbers given above. To improve the comparison be-

TABLE VI. Theoretical estimates of the universal leading specific-heat ratio for the $O(2)$ class. The normalized ratio refers to the computation of A^+/A^- for fixed $\alpha=-0.0127$. For the case with no P_A entry, the value is not normalized.

P_A	Normalized A^+/A^-	Reference
4.433 (77)	1.0563 (40)	Strösser *et al.* (1999, 2000, 2003)
4.247 (500)	1.0539 (40)	Campostrini *et al.* (2001)
4.455 (40)	1.0566 (130)	Bervillier (1986)
	1.044 (38)	Schultka and Manousakis (1995a)
4.28 (40)	1.0544	Kleinert and Van den Bossche (2001)

tween the results, we have recomputed the values of A^+/A^- in Table VI assuming $\alpha=-0.0127$, the most recent experimental value (Lipa *et al.*, 1996, 2003). Unfortunately there is not always enough information to compute P_A. The only estimates we know of for a_C^+/a_C^- are those of Chang and Houghton (1980), who obtained ~ 1.17 using an ε-expansion approach, and Schloms and Dohm (1990), who obtained ~ 1.6 using a field-theoretical approach.

Universality tests can be performed by measuring the predicted universal quantities along the lines of transitions obtained by increasing the pressure in the helium or the concentration of the ^{3}He isotope. Both these perturbations affect the ^{4}He-^{4}He atomic interaction, modifying the statistical distribution function and depressing the transition temperature. Various measurements of the specific heat and superfluid density singularities are described in the sections below.

In the case of transport properties, the theoretical situation is more complex due to the existence of slowly convergent terms, at least in the case of the thermal conductivity. Here, even at the highest experimental resolution, only an effective exponent is predicted to be observed. Dohm's flow-parameter model based on two-loop RG equations (Dohm, 1991) appears to give an excellent representation of experiment results to date (Tam and Ahlers, 1985; Dingus *et al.*, 1986; Lipa *et al.*, 2003), as discussed further below. Isothermal heat transport in superfluid helium, under a heat flux Q, fails suddenly at a temperature designated $T_c(Q)$, where $T_c(Q) < T_\lambda$. Transport measurements made close to $T_c(Q)$ have been predicted (Haussmann and Dohm, 1994) and observed (Day *et al.*, 1998) to become dependent on Q itself, in what is called the nonlinear region. Slightly below $T_c(Q)$, the superfluid density is predicted to be depressed by the superfluid counterflow velocity, resulting in a dynamical enhancement in the superfluid heat capacity just before the isothermal heat transport fails at $T_c(Q)$ (Haussmann and Dohm, 1994; Chui *et al.*, 1996). Initial measurements of this heat-capacity enhancement have been made on Earth (Harter *et al.*, 2000), but a detailed study of this and other nonlinear heat-transport effects will require a microgravity laboratory. Nonlinear heat-transport measurements that have been performed as precursors for future space flights are described below, along with a brief review of the emerging theory of nonlinear transport phenomena.

The lambda transition is currently the fluid transition that is least susceptible to the effects of gravity since the compressibility is only weakly divergent at the transition. Nevertheless, due to the availability of high-resolution thermometry at low temperatures, the gravitational rounding of the transition can easily be seen. The ultrahigh homogeneity of liquid helium together with these high-resolution techniques make it possible to observe effects associated with the divergent correlation length exceptionally close to the transition temperature. As discussed in Sec. II.D, on Earth the transition is severely rounded over a temperature interval of about 1.3 μK per centimeter of hydrostatic head in a sample, due to the slope of the lambda line, $(\partial T/\partial P)_\lambda$. For a sample of constant cross section, the effect on an equilibrium property, for example, the specific heat, can be visualized as a convolution of a gravity-induced temperature window $\Delta T_h = \rho g h(\partial T/\partial P)_\lambda$ with the gravity-free function in Eq. (11). This approximation is valid because, over the relatively small hydrostatic pressure heads encountered in typical experimental cells, the pressure dependence of thermodynamic properties can be neglected. This hydrostatic pressure effect was first reported by Ahlers (1968a) and has been observed in numerous experiments. As mentioned in Sec. II.D, finite-size effects set a lower limit on the sample height at which bulk measurements can be performed. In a finite system, the first-order departure from the bulk specific heat can be characterized as a surface specific-heat term that has been measured for lower-dimensional geometries. Since the magnitude of this effect is proportional to the surface area of a sample, the observed specific heat per unit volume can be written approximately as $C_{\mathrm{expt}} = C_P + (A/V)C_{\mathrm{surf}}$, where A/V is the surface area to volume ratio and C_{surf} is the surface specific heat per unit area. In first order, the surface specific heat can be characterized as a negative constant multiplied by the thickness of the affected surface layer, on the order of one correlation length. For precise tests of second-order phase transition theory, only small departures from bulk behavior are allowable, so such a model is appropriate. Figure 15 shows the percent change in the specific heat due to the surface layer in a spherical cell as a function of diameter and reduced temperature. It can be seen
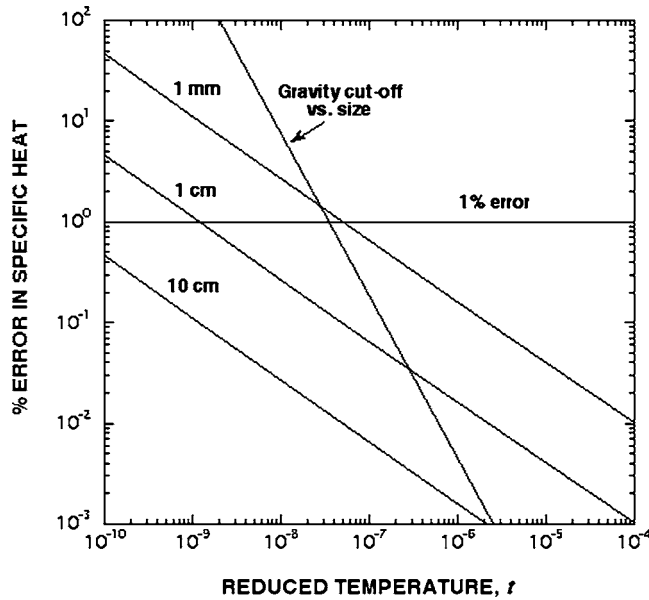
FIG. 15. Comparison of gravity and finite-size effects for the specific heat near the lambda point. Curves marked 1 mm, 1 cm, and 10 cm show the magnitude of the finite-size correction to the specific heat as a function of reduced temperature and spherical calorimeter diameter. Curve marked gravity cutoff indicates the closest approach possible on Earth before entering the gravitationally induced two-phase region due to the height of the cell. The horizontal line shows an arbitrary cutoff set at 1% finite-size correction. The useful region is below this curve to the right of the gravitational cutoff.

that the perturbation grows rapidly as the transition is approached. Also shown in the figure by the line marked "gravity cutoff" is the location of the gravitationally induced two-phase region for each cell diameter on Earth. Beyond this line, the gravitational perturbation grows very rapidly. The horizontal line marks a limit on the maximum finite-size effect tolerable, in this case arbitrarily set at 1%. The parameter space then available to the experimenter is below this line and to the right of the gravity cutoff. These considerations set the limits on what is possible at the lambda transition on Earth. Avoiding these limits is the primary motivation for performing experiments on relatively large samples in the microgravity environment of Earth orbit.

The possibility of approaching the lambda transition exceptionally closely in space has a significant implication for testing the theory of second-order phase transitions. Typically, for $O(1)$ systems, exponents are evaluated over 2–3 decades of temperature extending, say, from $t=10^{-2}$ to 10^{-4} or 10^{-5}. This means that the extraction of exponent values is complicated by the existence of the Wegner series to the extent that only effective values are obtained. In space, the range might be extended to $t \sim 3 \times 10^{-7}$, alleviating the problem to some degree. When proper allowance for the series is made, the uncertainties in the exponent estimates increase, diminishing the value of the exercise as a test of the basic theory. At the lambda transition, this problem can be further alleviated by extending the fitting region much

closer to the transition. For example, if the inner bound of the fitting region is $t=10^{-9}$, one could perform a test of the theory extending out to $t=10^{-5}$. When compared to the more typical fitting range above, it can be seen that the effect of the leading-order term in the Wegner series is reduced by a factor of about 30. Thus the presence of the series has much less of an impact on the exponent values obtained in a fit, resulting in a better test of the asymptotic predictions. Alternatively, one can increase the fitting range and fit the series as before but with less of an impact on the uncertainties of the parameter values obtained. Indeed, the experimental uncertainties in the exponent values obtained at the lambda transition routinely fall below the corresponding theoretical uncertainties, even in some ground-based experiments. This in turn provides an incentive for the theory community to devise yet more sophisticated computation schemes for estimating exponents and other quantities of experimental interest.

Since the lambda transition provides a unique opportunity to accurately determine the values of two asymptotic exponents as opposed to effective exponents, we examine the issues in more quantitative detail. From an inspection of Eq. (11) it can be seen that the value obtained for α is likely to be more reliable the smaller the value of t at which the curve fitting is done. However, as mentioned earlier for $O(1)$ systems, technical difficulties increase in this region, due to both measurement techniques and sample imperfections. On the other hand, as one includes data further from the transition, the curve-fitting procedure becomes more difficult since more terms must be carried in the function to obtain an accurate representation of the specific heat. Neglect of these terms leads to systematic bias in the remaining parameters that are evaluated. The extent to which it is reasonable to truncate the expansion series in Eq. (11) depends on the desired degree of fidelity in the parameter values obtained from the curve-fitting procedure. As noted already for the $O(1)$ universality class after Eqs. (5)–(8), the complete Wegner expansion includes additional terms related to irrelevant operators that are being neglected. This is well justified for the superfluid transition where, by symmetry, the subleading terms of the ϕ^4 theory are of $O(\phi^6)$ and not of $O(\phi^5)$.

To get a feel for what is possible, we now consider the hypothetical case of a specific-heat experiment limited only by currently available thermometry. In this case it can be shown by simple numerical modeling that we have the potential for obtaining a statistical uncertainty $\sigma_\alpha \approx 0.0001$ for the specific-heat exponent with data in the range $10^{-9} < |t| < 10^{-2}$, so it is of interest to consider potential sources of systematic error that could lead to this level of bias. First we consider the effect of neglecting a fourth-order term in Eq. (11), $c_C^{\pm}|t|^{3\Delta}$. Assuming for estimating purposes that $c_C^{\pm}=1$ and comparing fits to model data sets with and without the term, we find the bias from its neglect is $\Delta \alpha \sim 3 \times 10^{-4}$. This shows the importance of an appropriate functional form, especially in high-precision experiments over very wide temperature

ranges. Alternatively one can restrict the range of the fit to reduce the importance of the neglected terms, a tradeoff that sets the practical outer limit of the curve-fitting region. For example, if the fit to the model data is restricted to $|t| < 3 \times 10^{-3}$, the bias falls to $\Delta\alpha \sim 6.5 \times 10^{-5}$, less than the statistical uncertainty σ_α. Also, the experimental situation is actually slightly more complex than indicated so far, due to the possibility of regular background terms in the full representation of C_P. A more complete representation of the measured specific heat is $C_{\mathrm{expt}} = C_P + C_B$, where

$$C_B = c_0 + c_1 t + c_2 t^2 + \cdots, \tag{13}$$

in which the coefficients c_i are constants. Clearly, the constant background contribution c_0 can be absorbed into B in Eq. (11), but the effects of the other terms need to be considered. From the wide range behavior of the specific heat (Buckingham and Fairbank, 1961) where fluctuation effects are small, we obtain $c_1 \approx 2$ J/mol K. Thus for $t = 10^{-2}$ this term contributes $\sim 0.07\%$ to the specific heat, a small but detectable amount. To study this, we again made a set of simulated data in which the term $c_1 t$ was included in the generating function, but then ignored in the fitting procedure. We found a bias $\Delta\alpha \sim 2 \times 10^{-6}$, which is negligible at present. The value of c_2 is harder to determine, but it would appear to be similar to c_1. Even at $|t| = 10^{-2}$, such a term contributes $\ll 0.01\%$ to the specific heat and therefore can be neglected. Thus for the present a sufficiently good fitting function can be obtained by absorbing c_0 into Eq. (11) and ignoring the other terms. The small price paid for doing this is that the experimentally determined third-order coefficients no longer represent quantities of theoretical interest, and other coefficients may be slightly perturbed.

We now consider the effect of the term $b_c^\pm |t|^{2\Delta}$. This has a similar behavior to the term $c_1 t$ above, but now the potential effect is much larger due to the multiplicative effect of the leading singularity. Assuming $b_c = 0.1$, we find a shift $\Delta\alpha \sim 1 \times 10^{-3}$ from its neglect, implying that the term should be carried for high-accuracy curve fitting. On the other hand, reducing the outer limit of the data to $|t| = 10^{-3}$ would reduce this effect to $\Delta\alpha \sim 1.4 \times 10^{-4}$, close to the statistical uncertainty σ_α. This is an incentive for moving the fitting region closer to the transition as improved testing of the theory is attempted and would probably be necessary if further improvements in measurement precision are made. In a fit to data obtained in microgravity, it was found that $b_c^- \approx 0.33$ (Lipa *et al.*, 2003).

Near the transition we need to consider the intrinsic rounding effects described earlier, which could also perturb the exponent value. These perturbations depend on the details of the experiment. For example, for a microgravity experiment at $10^{-4} g$ steady residual acceleration, say, with a spherical sample of diameter 3.5 cm, we find the effect of neglecting the hydrostatic distortion of the singularity would lead to a bias $\Delta\alpha \sim 6 \times 10^{-5}$. The effect of the surface specific heat on the value obtained for α

can also be estimated. For the same sample and fitting over a range $10^{-9} < |t| < 10^{-2}$, we obtain a perturbation $\Delta\alpha \approx 3.4 \times 10^{-5}$, using the results of Lipa *et al.* (2000) to estimate C_{surf}. As one might expect, this perturbation becomes more important if the fitting range is further restricted.

A. Specific heat

The specific heat exhibits a weak, nearly logarithmic singularity at the lambda point. Close to the transition, RG theory predicts the functional form for C_P given in Eq. (11). Ground experiments have shown that the exponent α is slightly negative. Along the lambda lines, the experimental situation is somewhat complex because of the differing conditions with the various measurements. A number of experiments are in approximate agreement, but indicate a possible difference between the value of α at the saturated vapor pressure (SVP) and that along the lambda lines of pressure and ^{3}He concentration. The measurements up to 1976 have been reviewed extensively by Ahlers (1976). Here we touch on some of these measurements, focusing on the more accurate exponent determinations. Except for the most recent measurement in microgravity, the term $b_C^\pm |t|^{2\Delta}$ in Eq. (11) has been neglected in the curve fitting. This is probably acceptable given the precision of the various results.

The first indication that the specific-heat divergence at the lambda point may not be logarithmic was obtained by Ahlers (1971). Additional measurements of C_ν along the lambda line as a function of temperature and pressure supported this conclusion (Ahlers, 1973). To test universality, Mueller *et al.* (1976) performed measurements of the expansion coefficient at constant pressure, which has the same asymptotic behavior as C_P, along the lambda line as a function of pressure. When the data were fitted with Eq. (11), the values of α obtained were consistent with no pressure dependence within a scatter of about ± 0.006, and the best-fit exponent was -0.026 ± 0.004. These authors also refitted the data of Ahlers (1971) and obtained $\alpha = -0.016 \pm 0.002$. Gasparini and Moldover (1975) performed measurements of the specific heat along the ^{3}He-^{4}He lambda line at constant ^{3}He concentration. Gasparini and Gaeta (1978) fitted those measurements by Eq. (11) with $b_C^\pm = 0$. Excluding the measurements for pure ^{4}He, they obtained $\alpha = -0.025$ (± 0.006, our estimate), in very good agreement with the expansion coefficient result. On the other hand, their pure ^{4}He results gave $\alpha = -0.0198 \pm 0.0037$. When these results were combined with those along the lambda line, the optimum exponent was found to be -0.022. An experiment performed with the aid of high-resolution thermometry gave $\alpha = -0.0127 \pm 0.0026$ at the SVP (Lipa and Chui, 1983). While the differences are not large in absolute terms, the exponent results along the lambda lines do not appear to be entirely compatible with the SVP measurements. In Table VII, we have indicated an approximate range of α obtained from the

TABLE VII. Experimental results for the specific-heat exponent and leading amplitude ratio for the lambda point. Measurements at the vapor pressure are labeled with an asterisk.

α	A^+/A^-	Reference
−0.016 (2)*	1.068 (10)	Mueller *et al.* (1976)
−0.026 (4)	1.11 (2)	Mueller *et al.* (1976)
−0.0198 (37)*	1.081 (16)	Gasparini and Gaeta (1978)
−0.022 (4)	1.088 (20)	Gasparini and Gaeta (1978)
−0.023	1.090	Takada and Watanabe (1980)
−0.0127 (26)*	1.05 (2)	Lipa and Chui (1983)
−0.0127 (3)*	1.053 (2)	Lipa *et al.* (1996, 2003)

various groups. On a statistical basis there appears to be a noticeable discrepancy between the vapor pressure data and that along the lambda lines. The results for A^+/A^- are also listed in this table.

A value of P_A can be derived from the data of Lipa and Chui (1983). From their analysis, which did not constrain $B^+=B^-$, we obtain $P_A=4.57\pm0.4$, where the uncertainty was estimated by the present authors. We note that the value of P_A and its uncertainty are significantly affected by the fitting constraint $B^+=B^-$. This appears to be a result of the strong correlations between A^+ and B^+ and A^- and B^- in the curve fitting procedure. If this constraint is added to the analysis of Lipa and Chui, we obtain $P_A=3.98\pm0.02$. This result is somewhat outside the range of theoretical estimates listed in Table VI.

1. Microgravity measurements

By the early 1980s, the resolution obtainable on the ground was limited by the competition of gravity and finite-size effects described earlier. In 1992, the "Lambda Point Experiment" (LPE) was performed on the Space Shuttle mission STS-52 to measure the specific heat on the low-temperature side of the transition and obtain improved information on the form of the divergence (Lipa *et al.*, 1996, 2003). Some measurements were also made above the transition, but the accuracy was expected to be lower due to thermal relaxation effects. The sample consisted of a 3.5-cm-diam sphere of helium with a small gas bubble to allow measurements at the SVP. It was isolated from the surroundings by a four-stage thermal control system enclosed in a liquid-helium Dewar operating at about 1.75 K. Specific-heat measurements were made to within 10^{-9} K of the transition temperature. Two significant technology developments were needed to perform the experiment. The most significant was the development of reliable high-resolution thermometry capable of resolving to the limit imposed by thermodynamic fluctuations. Paramagnetic salt thermometry with a SQUID readout was developed to the desired level in the late 1970s (Lipa *et al.*, 1981). A noise performance in the 10^{-10} K range was later demonstrated and the noise power spectrum was shown to be consistent with the fluctuation-dissipation theorem (Chui *et al.*, 1992). Also important was the development
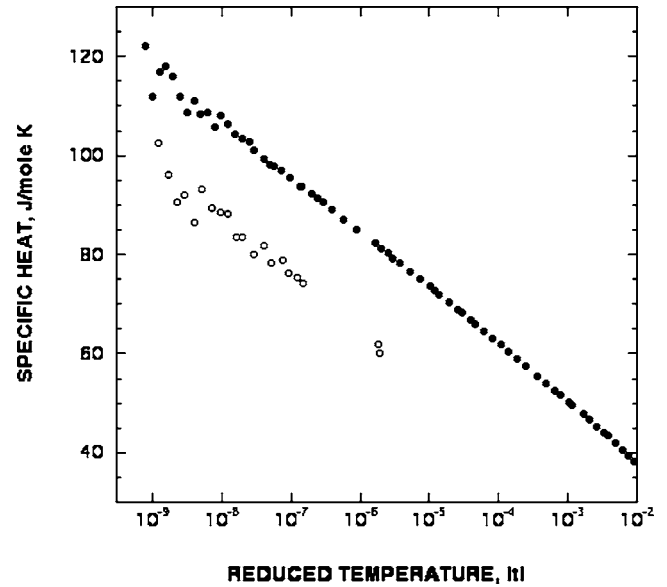
FIG. 16. Specific-heat results near the ^{4}He lambda transition obtained in microgravity on a log-linear scale. Filled circles are below the transition, open circles, above. From Lipa *et al.*, 2003.

of a thermal isolation system capable of high stability. A multistage thermal isolation system was developed for ground specific-heat measurements (Lipa and Chui, 1983; Lipa *et al.*, 1992). This system used the new thermometry on the fourth stage of control and was capable of controlling heat inputs to a calorimeter to $<10^{-12}$ W. Details of the experiment and hardware can be found in Lipa *et al.* (2003), and references therein.

Specific-heat results from the mission are shown in Fig. 16 on a semilogarithmic scale. These were fitted over the whole range measured with the trial function,

$$C_P = \frac{A^-}{\alpha}|t|^{-\alpha}(1 + a_C^-|t|^\Delta + b_C^-|t|^{2\Delta}) + B, \quad T < T_\lambda,$$

$$C_P = \frac{A^+}{\alpha}|t|^{-\alpha} + B, \quad T > T_\lambda. \tag{14}$$

The simpler form was used above T_λ because the data only extended to $t \sim 10^{-6}$, where additional terms would still be negligible. All parameters were allowed to vary except for Δ, which was fixed at the value 0.529 (Guida and Zinn-Justin, 1998), and T_λ, which was determined independently. The best-fit values for the parameters below the transition are listed in Table VIII along with the ratio A^+/A^-. The corresponding uncertainties are listed below the values and refer to the standard statistical error evaluated from the curve-fitting routine.

A number of variations were made in the fitting procedure to determine the sensitivity of the main results to the process. Taking into account the systematic effects of the various constraints, it was estimated that the results indicate $\alpha=-0.0127\pm0.0003$ and $A^+/A^-=1.053\pm0.002$ with a high degree of confidence. These values can be compared with the theoretical estimates given in Tables

TABLE VIII. Results from curve fitting to the microgravity specific-heat data using Eq. (14) over the range $5 \times 10^{-10} < t < 10^{-2}$. Statistical uncertainties are given in parentheses beneath values. Units of A and B are J/mol K.

Parameter	α	A^+/A^-	A^-	B	a_C^-	b_C^-	P_A
Best-fit value	−0.01264	1.05251	5.6537	460.19	−0.0157	0.3311	4.154
Uncertainty (1σ)	(0.00024)	(0.0011)	(0.015)	(7.3)	(0.0015)	(0.011)	(0.022)

V and VI. It can be seen that the result for α falls between the estimates by Campostrini *et al.* (2001) and Jasch and Kleinert (2001), giving increased confidence in the overall correctness of the RG approach. If the discrepancy between the two estimates can be resolved, a very high-quality test of the theory would result. It is interesting to note that the result falls very close to the theoretical value of $-0.012\,94 \pm 0.0006$ obtained earlier by Kleinert (1999). The value obtained for the ratio A^+/A^- can be compared with the calculation of Strösser, Mönnigmann, and Dohm (2000), whose result for P_A implies $A^+/A^- = 1.056 \pm 0.003$ if $\alpha = -0.0127$. The measured value of P_A was 4.154 ± 0.022 where the uncertainty is the 1σ statistical value including the effects of correlations of the parameters. This compares well with the result of 4.39 ± 0.26. Recently, Strösser and Dohm (2003) have obtained an improved result $P_A = 4.433 \pm 0.077$ from a four-loop analytic calculation, somewhat above the experimental value.

In Fig. 17, we show the residual deviations of the LPE flight data and those of earlier experiments at the SVP
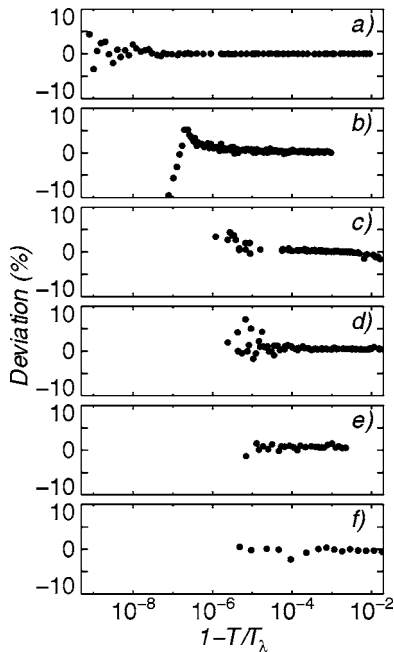
FIG. 17. Deviation plots of specific-heat data below T_λ obtained in various experiments: (a) Lipa *et al.* (2003); (b) Lipa and Chui (1983); (c) Ahlers (1971); (d) Gasparini and Moldover (1975); (e) Takada and Watanabe (1980); (f) Buckingham and Fairbank (1961). Reference function in all cases is Eq. (14) with the parameters listed in Table VIII.

from Eq. (14) using the parameter values in Table VIII. In general it can be seen that there is good agreement between the various measurements. The deviations close to the transition seen in some of the data sets are due to the effect of gravity. Further developments in high-resolution thermometry (Qin *et al.*, 1996; Klemme *et al.*, 1999) demonstrated in the microgravity finite-size specific-heat experiment CHeX (Lipa *et al.*, 2000) should in principle allow approximately a factor of 5 decrease in the uncertainty of the specific-heat exponent relative to the LPE result.

B. Enhanced specific heat under a heat flux

The theory of static critical phenomena, as discussed above, predicts that certain aspects of the aggregate behavior with critical systems are independent of the details of the microscopic interactions of the system under study, and that the resulting emergent behavior depends mainly on the number of order parameters, the dimensionality of the system, and the range of the forces involved. For dynamic critical phenomena, this is not completely true since new experimental parameters are introduced that influence the correlation length and display specific aspects of the microscopic structure of the system. This behavior may be studied in a system driven out of equilibrium in a well-controlled manner, with the equilibrium state displaying the universal static behavior, permitting the dynamics to be characterized by generalizations of static concepts and quantities, such as temperature, correlation length, and specific heat. Formally, however, these quantities are not precisely defined in the out-of-equilibrium situation. See Dohm and Haussmann (1994) and Weichman *et al.* (2003) for a comprehensive overview of dynamic critical phenomena near the superfluid transition in ^{4}He.

Detailed nonequilibrium studies near the superfluid transition in ^{4}He may be performed using a sufficiently small heat flux to maintain the system below its convective threshold, exciting only heat diffusion, steady superfluid counterflow, or second-sound modes. All other methods of measuring dynamical properties near this transition, such as acoustic resonance and sound attenuation studies, particle scattering, and bulk and shear flow measurements, induce bulk flow, and hence impart far more momentum to the helium liquid. Generally, this drives the system farther from equilibrium than does a small heat flux. In order to simplify the geometry in ground-based experiments, it is convenient to heat helium with the steady heat flux oriented either directly

along or against gravity. This makes the problem quasi-one-dimensional, since in this system the variation of temperature across the column is in the same direction as the hydrostatically induced pressure variation in the superfluid transition temperature. With this pragmatic restriction in mind, the two possible orientations of the heat flux are referred to as heat from above (HfA), in which the top of a cell is heated, and heat from below (HfB), with the bottom heated.

A dynamical enhancement of the static specific heat by a heat flux through a column of superfluid helium has been measured in the HfB geometry (Harter *et al.*, 2000). The measured enhancement was about a factor of 10 larger than predictions from theory (Haussmann and Dohm, 1994; Chui *et al.*, 1996). This enhancement results from the abrupt failure of superfluid counterflow to transport heat when a critical value of the counterflow velocity is exceeded, which is a particular microscopic feature of this system, and hence not universal. These measurements depend upon the dynamic depression of the order parameter (the superfluid density, in this case), which becomes observable only very close to $T_c(Q)$, where the isothermal heat transport breaks down, and where this effect is predicted to diverge.

The two-fluid model assumes that only the normal fluid component transports entropy in the superfluid phase, so the heat flux through a column of helium is $Q = \rho S T V_n$, where S is the entropy per unit mass and V_n is the normal fluid velocity. If there is no bulk flow, then $\rho V = \rho_s V_s + \rho_n V_n = 0$, where V is the bulk velocity, ρ_n is the normal fluid density, and V_s is the superfluid velocity. Hence $Q = -(\rho \rho_s / \rho_n) S T V_s \approx -S_\lambda T_\lambda \rho_s V_s$ near the superfluid transition, where $\rho \approx \rho_n$. If ρ_s is independent of flow velocities, then this equation predicts that the magnitude of heat flux carried by counterflow would increase indefinitely as V_s increases. But it has been shown that ρ_s decreases as V_s increases over a wide temperature range (Hess, 1978) and in the range near the superfluid transition (Duncan *et al.*, 1988; Harter *et al.*, 2000). This effect can become sufficiently strong that a point is reached where $dQ/dV_s = 0$, which occurs at $T_c(Q) < T_\lambda$ (Mikeska, 1969). At $T_c(Q)$, the near-perfect heat transport through the superfluid will begin to fail, since any increase in flow velocities will result in less normal fluid heat transport, destabilizing the counterflow heat transport. Hence for $T > T_c(Q)$ the heat will be transported, at least in part, by some form of diffusion, resulting in a thermal gradient. Alternatively, if the temperature of the superfluid is held constant as the heat flux is increased, then above some heat flux Q_c such that $T(Q_c) = T_c(Q)$ helium will suddenly become thermally resistive. This is somewhat like the depression of the superconducting transition temperature in a metal as the current through the metal is increased, except in this case superfluid helium is uncharged, so increase in the superfluid free energy with increasing Q comes only from the kinetic energy increase within the flow, and not from the magnetic-field-induced increase in free energy that results from

the charge flow associated with superconducting electrons.

At $T_c(Q)$, the specific heat of superfluid helium is expected to be singular, based upon model-independent, thermodynamic arguments (Chui *et al.*, 1996) and RG modeling (Dohm and Haussmann, 1994). This is a remarkable prediction that can only be explored near the superfluid transition of helium, since the steady-state heat transport of a heat flux Q with no resulting thermal gradient is possible only within a superfluid. Such a heat flux would produce a temperature gradient in any other system, and this temperature gradient would push the system away from the critical point, and hence out of the region where such dynamical effects on the specific heat can be observed. Indeed, for $Q > 3 ~\mu\text{W cm}^{-2}$, a temperature gradient with heat applied from below becomes large enough to be observable with high-resolution thermometry near T_λ in the superfluid state. This superfluid thermal gradient is presumably due to a dissipative interaction between the normal fluid component of counterflow and flow created by a superfluid vortex tangle, which is generally referred to as a Gorter-Mellink mutual friction gradient (Gorter and Mellink, 1949). Such a gradient in the critical region near the superfluid transition has been measured by Baddar *et al.* (2000). Remarkably, much larger superfluid thermal gradient is observed under nominally identical conditions when the superfluid helium column is heated from above, suggesting that the hydrostatic pressure variation across the cell may produce a component of the resulting superfluid temperature gradient that does not reverse when the direction of the heat flux is reversed (Melnikovsky, 2005). The onset of this mutual friction gradient has been observed experimentally to depress the overall specific heat of a superfluid column in HfA measurements, thus masking the specific heat of the superfluid state (Lee *et al.*, 2004). So enhancement of the specific heat may be observed only under low heat flux ($Q \leq 5 ~\mu\text{W cm}^{-2}$) when heated from below on Earth. Typically, the cell height is greater than about 2 mm to avoid substantial finite-size effects in the direction of the heat flux (Ahlers and Duncan, 1988). Hence the weightless laboratory is essential to measure these bulk dynamical enhancements free from the perturbations of gravitational rounding and finite-size effects. It is difficult to predict the size of the superfluid thermal gradient in the microgravity environment from measurements of the superfluid thermal gradient on Earth. If the heat flux across the cell is not uniform, then the superfluid breakdown will occur at $T_c(Q_{max})$, where Q_{max} is the maximum heat flux within the cell. Such an abrupt increase in the specific heat of superfluid helium as $T_c(Q)$ is approached from the low-temperature side has been measured by Harter *et al.* (2000), but their measurements are about a factor of 10 larger than the theoretically predicted effect (Dohm and Haussmann, 1994; Haussmann and Dohm, 1996; Chui *et al.*, 1996). The likely level of heat flux nonuniformity within the experimental cell of Harter *et al.* (2000) may have increased the size of the observed specific-heat enhancement effect by about this factor

over the result that would have been obtained if the heat flux Q were uniform across their cell. For this reason, a new type of cell endplate was developed for measurements in space. It uses layers of high-thermal-conductivity pure aluminum separated by layers of low-conductivity aluminum alloy in order to make the effective radial thermal conductivity much greater than the longitudinal thermal conductivity of the structure. This spreads the applied heat out radially over a much shorter length of the endplate than can be achieved by a single layer of high-purity aluminum.

In the HfA geometry, liquid helium can form a self-organized critical (SOC) state between the superfluid and normal fluid states. The temperature gradient within this SOC state equals the gradient in the superfluid transition temperature, even as the heat flux was varied by about four orders of magnitude experimentally (Moeur *et al.*, 1997; Lee *et al.*, 2004; Sergatskov *et al.*, 2004). The temperature of the SOC state $T_{\mathrm{SOC}}(Q)$ self-adjusts so that the thermal conductivity of the SOC state is given by $\kappa_{\mathrm{SOC}}(T_{\mathrm{SOC}}(Q)) = Q/\nabla T_\lambda$, assuring that the temperature gradient equals the gradient in T_λ at the applied Q. This implies that the SOC state exists only on a single path in the Q vs T plane. The mechanism that permits this self-organization to occur and the stability of the resulting SOC state is discussed in detail by Haussmann (1999b) and by Weichman and Miller (2000). The former author has predicted that the SOC state heat capacity will be the same as the equilibrium heat capacity over a wide temperature range, deviating from this equilibrium value only within about 100 nK of T_λ due to the limit to the diverging correlation length imposed by the hydrostatic pressure gradient. The SOC state provides a remarkable opportunity to measure heat transport at a constant distance from the critical line on Earth, but the temperature of the measurement, which is $T_{\mathrm{SOC}}(Q)$, is set by the heat flux on the SOC state, so the temperature and heat flux cannot be independently varied as they can be in a microgravity experiment.

It appears that enhancing the specific heat of superfluid helium by a uniform heat flux can just barely be observed on Earth, due to the rounding of the specific heat by the pressure gradient across the sample. Figure 18 shows the region over which the dynamical specific-heat enhancement should be observable in a microgravity environment. An experiment called "Enhanced Heat Capacity in Superfluid Helium by a Heat Flux" (CQ) (Goodstein, 2002) was added to the "Critical Dynamics in Microgravity" (DYNAMX) Flight Experiment discussed in Sec. V.D, to make these dynamical enhanced specific-heat measurements in a weightless laboratory. The CQ experiment is designed to provide measurements unaffected by gravity in the entire region below the curve marked $t_{\mathrm{DAS}}(Q)$, where $t_{\mathrm{DAS}}(Q) = [T_\lambda - T_{\mathrm{DAS}}(Q)]/T_\lambda$ and $T_{\mathrm{DAS}}(Q)$ are the data reported in Duncan *et al.* (1988). The heat-capacity divergence occurs at $T_{\mathrm{DAS}}(Q)$ on Earth, but it is predicted to diverge at $T_c(Q)$, which may be observed in orbit. If so, then the region below the $t_c(Q)$ curve will be measured in orbit.
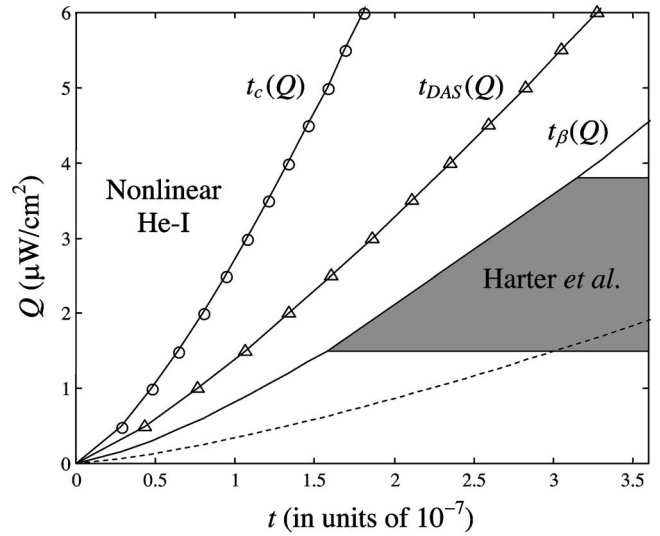
FIG. 18. The Q-t plane. The CQ experiment will yield measurements unaffected by gravity in the entire region below the curve marked $t_{\mathrm{DAS}}(Q)$, where $t_{\mathrm{DAS}}(Q) = [T_\lambda - T_{\mathrm{DAS}}(Q)]/T_\lambda$ and $T_{\mathrm{DAS}}(Q)$ are the data reported in Duncan *et al.* (1988). The heat-capacity divergence occurs at $T_{\mathrm{DAS}}(Q)$ on Earth, but it is predicted to diverge at $T_c(Q)$, which may be observed in orbit. If so, then the region below the $t_c(Q)$ curve will be measured in orbit. The related ground-based measurements of Harter *et al.* (2000) used endplate thermometers, limiting ground-based measurements to the shaded region below the $t_\beta(Q)$ curve, due to singular Kapitza resistance effects. The dotted line shows where the heat-capacity enhancement rises, above 1% according to a fit to the data of Harter *et al.* (2000). From Lee *et al.*, 2002.

In either case, the experimentally accessible region for measurement of this dynamical increase in specific heat is greatly expanded in a weightless laboratory, permitting this to be explored over a much larger parameter range than on the ground.

C. Superfluid density

The best available technique for measuring the temperature dependence of the bulk superfluid density close to the lambda point is to measure the velocity of second sound U_2. This is related to ρ_s by

$$U_2^2 = \frac{\rho_s T S^2}{\rho_n C_P} + O\left(\frac{U_2}{U_1}\right)^2, \qquad (15)$$

where U_1 is the first-sound velocity. Due to the high quality factors obtainable in second-sound resonators, U_2 can be measured accurately over a wide temperature range. In experiments to date it has been a reasonable approximation to neglect the second-order term in Eq. (15). Note that Eq. (15) also involves the specific heat C_P, so the two types of bulk static measurements discussed here are linked. The most extensive set of measurements designed to test the universality predictions for ρ_s was performed by Greywall and Ahlers (1973). They used a resonance technique to measure U_2 from

the SVP to 29 bars over the temperature range from
about 0.1 to 10^{-4} K from the transition. Velocity data
were converted to ρ_s using the specific-heat function of
Ahlers (1973). When the results were fitted with Eq.
(12), Greywall and Ahlers found that the exponent ν was
approximately constant, while the Wegner amplitude a_{ρ_s}
increased substantially with pressure. Their best-fit re-
sults gave $\nu=0.67\pm0.01$ independent of pressure. Addi-
tional analysis was performed by Singsaas and Ahlers
(1984), extending the range of the data included in the fit
and leading to a new vapor pressure result: ν
$=0.6717\pm0.0004$. However, the pressure dependence of
ν was not reevaluated. Ikushima and Terui (1973) have
also reported second-sound measurements over a wide
range of pressures, but their analysis did not include the
confluent singularity term, limiting its value. Schloms
and Dohm (1987) published a new analysis of the
Greywall-Ahlers data using an improved expression for
the Wegner correction series based on the RG tech-
nique. The number of parameters used in the fit was
reduced by this approach, and it was extremely encour-
aging to see that the general behavior of the corrections
as a function of pressure was well represented. No new
results for the exponent versus pressure were derived
from this analysis, although departures from universality
would show up as differences in the curvatures of the
data and the model, especially close to the transition.
More recent values of ν obtained from second-sound
data at the SVP are 0.6708 ± 0.0004 by Swanson *et al.*
(1992), 0.6705 ± 0.0006 by Goldner *et al.* (1993), and
$0.670\,16\pm0.000\,08$ by Adriaans *et al.* (1994). In the latter
case, the error quoted included only the statistical uncer-
tainty from velocity measurements. We also note that
the analyses to date neglect any uncertainty in the
specific-heat exponent when using Eq. (15).

   The above results can be combined with the micro-
gravity result for α to perform an improved test of the
Josephson (1967) hyperscaling relation Eq. (3). For ex-
ample, using the result of Goldner *et al.* (1993) for ν we
obtain $3\nu+\alpha=1.9989\pm0.0019$, where the uncertainties
have been combined in quadrature. The agreement with
the prediction is very good. Somewhat worse agreement
is obtained if we use the result of Adriaans *et al.* (1994)
which leads to $3\nu+\alpha=1.9979\pm0.0004$. We note that in
both these second-sound experiments, plots of measure-
ment deviations from the fits show systematic behavior,
indicating that the error bars quoted may be optimistic.
The result of Swanson *et al.* (1992), which shows a less
systematic effect in the residuals of the fit, gives $3\nu+\alpha$
$=1.9997\pm0.0012$. The level of agreement indicates that
the exponents obtained from the two independent types
of measurement are unlikely to be significantly mislead-
ing. Kaupuzs (2005) has argued that the results of Gold-
ner *et al.* (1993) fit his model better, but he has not yet
addressed the other two sets of data. Also, it should be
noted that his model of the specific heat will perturb the
conversion of the second-sound data to superfluid den-
sity slightly, affecting the resulting exponent. This effect
has not yet been included.
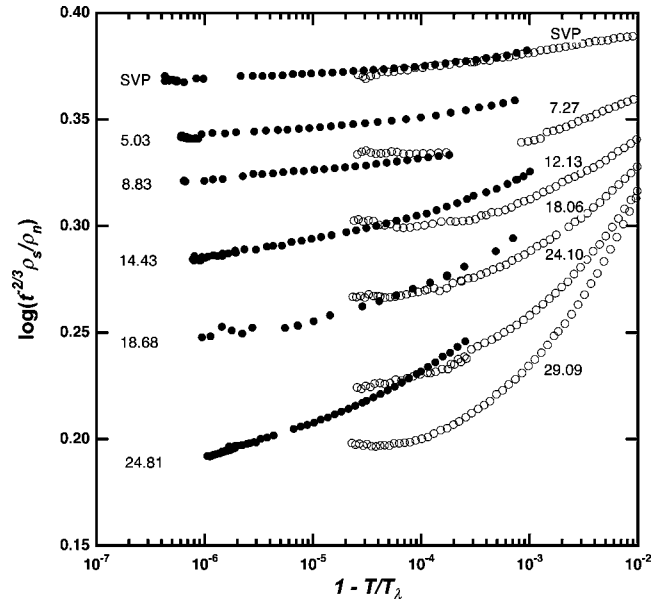
FIG. 19. Scaled superfluid density results derived from second-
sound velocity measurements as a function of reduced tem-
perature over a range of pressures from SVP to 25 bars. Filled
circles, high-resolution measurements corrected for gravity
(Nissen *et al.*, 2000; Lipa *et al.*, 2005); open circles, from Grey-
wall and Ahlers (1973).

   Second-sound measurements extending closer to the
transition along isobars at pressures up to 25 bars have
been reported (Nissen *et al.*, 2000). The apparatus for
the experiment consisted of a cylindrical sample cham-
ber of about 0.5 cm in diameter and 1.4 cm long at-
tached to a very high-resolution pressure controller and
filled with liquid helium. The sample chamber formed a
second-sound resonator with a quality factor typically
around 500. The detector was a single crystal of para-
magnetic salt, having an extremely high sensitivity, and
the generator was a resistive heater. The minimum de-
tectable signal corresponded to a thermal wave ampli-
tude of $\sim10^{-10}$ K. Pressure control was implemented us-
ing a variable-temperature ^{3}He tank separated from the
second-sound cell by a flexible diaphragm. A supercon-
ducting pressure gauge (Edwards *et al.*, 1996) attached to
the cell was used to generate a servo error signal, which
controlled the temperature of the tank. A model of the
specific heat as a function of temperature and pressure
developed by Ahlers (1973) was used to extract the su-
perfluid density from measurements. Preliminary results
for this quantity are shown in Fig. 19. They were found
to be consistent with $\nu=0.672\pm0.003$ over the entire
range $0.05<P<25$ bars when fitted with Eq. (12) (Lipa
et al., 2005). Improved specific-heat measurements are
being made to reduce uncertainties in the exponent re-
sults. Also shown further from the transition are the re-
sults of Greywall and Ahlers. It can be seen that above
the SVP there are some systematic differences between
the two sets of results. These are still under investiga-
tion.

A concept for a microgravity experiment called the superfluid universality experiment (SUE) was developed to perform very high-resolution measurements of the superfluid density using the technology described above (Lammerzahl *et al.*, 2004). The apparatus would be capable of making observations within 10^{-9} K from the transition and of making simultaneous specific-heat measurements at constant pressure. Observations would be made at pressures from 0.05 to 29 bars along the lambda line, resulting in a significantly improved test of universality.

D. Thermal conductivity

Well above the lambda point, liquid helium is an excellent thermal insulator, with a thermal conductivity of about 10^{-4} W cm^{-1} K^{-1}, comparable to that of plastics at low temperatures. In contrast, below the transition, superfluid counterflow creates an effectively infinite thermal conductivity at low heat flux. The thermal conductivity of ^{4}He diverges as the superfluid transition is approached from above due to critical fluctuations of the order parameter, matching the radically different effective thermal conductivities of the two phases. This divergence of the thermal conductivity was predicted by Ferrell *et al.* (1967, 1968a, 1968b) and observed by Kerrisk and Keller (1967, 1969) and studied systematically by Ahlers (1968b). Halperin *et al.* (1974, 1976a, 1976b) developed a generalization of the ϕ^4 equilibrium model called "model F" to describe the universal aspects of the near-critical superfluid dynamics. This theory predicts that the thermal conductivity of normal liquid ^{4}He should vary as $\kappa = R_\lambda g_0 \sqrt{k_B \xi C_P}$, where g_0 is the dynamic coupling constant with units of frequency. The factor R_λ is the dimensionless renormalization amplitude of the thermal conductivity, which may be calculated to any given order in perturbation theory. Although a detailed calculation of R_λ is a difficult task, once it has been obtained this theory claims to provide an exact prediction for the strongly divergent thermal conductivity near T_λ, based only on parameters that have been determined from measurements of static critical properties. A calculation of R_λ, renormalized to two-loop order, has been performed by Dohm and Folk (1981) using field theoretic techniques (Dohm, 1991). This prediction was later tested by Dingus *et al.* (1986), by Tam and Ahlers (1986), and by Lipa *et al.* (2003), and the agreement between theory and experiment was found to be very good. Thermal relaxation measurements on the spherical LPE calorimeter implied a similar singular behavior for the thermal conductivity, extending these measurements to $t < 3 \times 10^{-9}$. The general agreement with the theory is good, as displayed in Fig. 20. A comparison with results further from the transition was recently made by Dohm (2006). This ability to accurately predict the nonasymptotic behavior of heat transport near the lambda point in ^{4}He over at least six decades of reduced temperature represents one of the great successes in the development of renormalization-group methods in condensed-matter
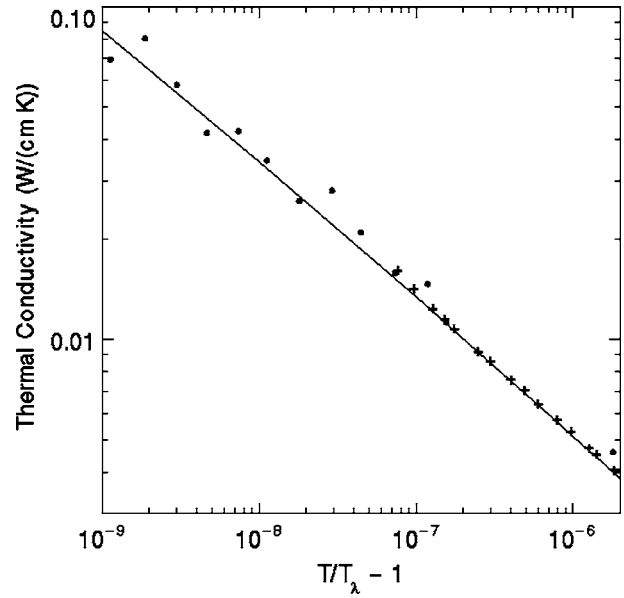
FIG. 20. Thermal conductivity data close to the lambda transition. The crosses are derived from ground-based data of Lipa and Li (1996). The filled circles are inferred from the thermal relaxation time of the LPE calorimeter taken in Earth orbit (Lipa *et al.*, 2003). These data extend about two orders of magnitude closer to the critical point than Earth-based data, and gravitational limits to the divergence of the correlation length have been avoided in this weightless environment. The curve is from the model of Dohm (1991). From Lipa *et al.*, 2003.

physics. In these measurements, the heat flux was adequately low, and the system was adequately far from criticality, so that the system was not driven too far from equilibrium by the heat flux used in the measurements. This condition is not maintained as one gets very close to the superfluid transition even with very small values of the heat flux Q.

1. Nonlinear thermal conductivity

The thermal conductivity measurements discussed above were taken in the linear regime, meaning that κ (and its reciprocal the thermal resistivity R) did not depend appreciably on the value of Q. Clearly R depends on temperature in a nonlinear way, but at any given temperature the value of this transport coefficient is essentially independent of Q in the measurements discussed above. Dohm and Haussmann (1994) extended the renormalization of model F to the nonlinear regime, where this coefficient becomes strongly Q dependent. This regime begins when the temperature drop across a correlation volume becomes comparable to $T - T_\lambda$, thereby substantially perturbing the critical dynamics away from local equilibrium (Weichman *et al.*, 1998).

In the static limit, the superfluid transition is continuous, meaning that there exists no discontinuity of the order parameter at the interface between the normal phase (He I) and superfluid phase (He II). There is instead a continuous variation of the superfluid order parameter across this interface, with a spatial taper of the
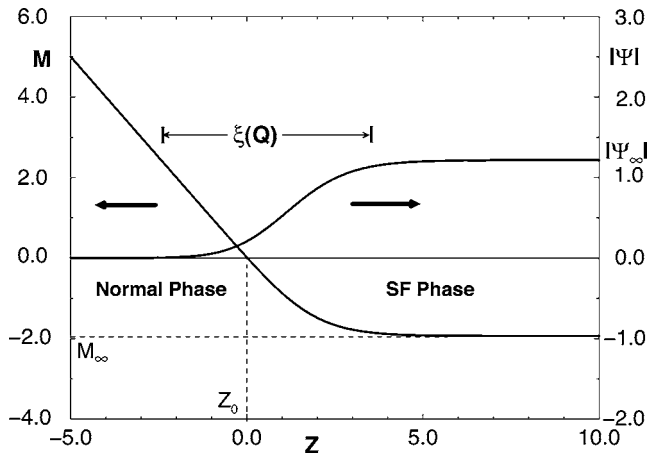
FIG. 21. Spatial variation of the order parameter $\Psi(z)$ at the He I/He II interface in a heat flux. Since this is a continuous phase transition, $\Psi(z)$ varies smoothly with the spatial coordinate over the interfacial region, which scales with the correlation length $\xi(Q)$. M is the local steady-state mean-field temperature. The dimensionless spatial coordinate z has been defined by Weichman *et al.* (1998). From Weichman *et al.*, 1998.

order parameter from its value deep in the superfluid to zero over a few correlation lengths, as predicted (Weichman *et al.*, 1998) and displayed in Fig. 21. Temperature profiles within the nonlinear region are within the interface between He I and He II. The thickness of this interface is greatly decreased by Earth's gravity, and it also decreases rapidly as Q increases. Hence a space-based measurement with precise stray heat control is necessary to carefully measure these effects, and to compare with theory. The measurement of this nonlinear thermal conductance is a major experimental challenge, since stray heat leaks to the cell have to be controlled to within a few picowatts, and temperature measurements have to be resolved to about 1 part in 10^{10} of the absolute temperature. The planned microgravity experiment (DYNAMX) must maintain stray heat control from all sources to within 20 pW over a 10-min measurement interval. This requires that the mass of the entire cell assembly, including the attached high-resolution thermometers, must be below 30 g in order to avoid unacceptable stray heat variations from the change in charged particle heat deposition as a function of the experiment's position in low-Earth orbit (Duncan, 2000). This mandated the development of a new miniature cryogenic valve with mass less than 2 g, and a new paramagnetic material that utilizes dilute Mn ions in Pd as the thermometric element to achieve a thermometer mass of less than 3 g (Duncan *et al.*, 2001). This new thermometer design (Klemme *et al.*, 1999) permitted much better thermal contact between the thermometric element and the stage to be measured than was possible in earlier paramagnetic susceptibility thermometers, resulting in lower thermal fluctuation noise. This metallic thermometric element has been sputtered for thin-film applications such as bolometry (Nelson *et al.*, 2002), and used in applications where the entire helium cell was constructed from
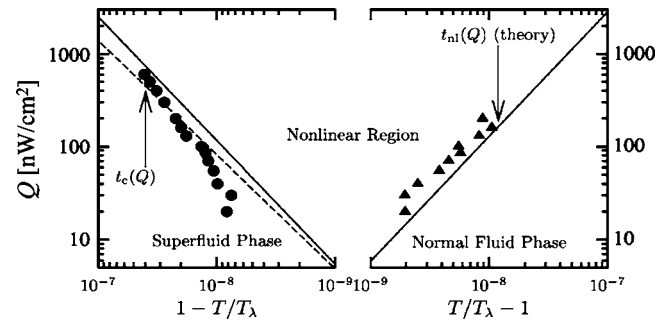
FIG. 22. Temperature dependence of the lambda transition as a function of heat flux. As Q is increased through the helium, the simple critical point at T_λ (corresponding to the branch cut in the middle of the figure) evolves into a nonlinear region, as shown in this dynamic phase diagram. The theoretical boundaries of this nonlinear region are displayed as the $t_c(Q)$ and $t_{nl}(Q)$ curves (Haussmann and Dohm, 1991, 1992a). The experimental determination of this phase boundary is described in Fig. 23. From Day *et al.*, 1998.

this PdMn metal (Green *et al.*, 2005). The use of a metallic thermometric element may prove useful in many future flight experiments.

The first measurements of temperature profiles within the nonlinear region were reported by Day *et al.* (1998). The boundary of the nonlinear region that was determined from these results, along with the predicted nonlinear regime (Haussmann and Dohm, 1991, 1992a) are displayed in Fig. 22. These boundaries of the nonlinear region may be thought of as an extension of the helium phase diagram, with reduced temperature along the horizontal axis, and the heat flux through helium along the vertical. Here the heat flux acts like an effective field that modifies the nature of this critical transition, but there is no conclusive experimental evidence that Q destroys the critical behavior at $T_c(Q)$, as does the magnetic field in magnetic critical phenomena studies, for example (Stanley, 1971). The heat flux is not the thermodynamic conjugate of the order parameter, so finite Q is not predicted to destroy the phase transition. The only true static critical point exists at T_λ in the $Q \to 0$ limit (Haussmann, 1999b), but the nature of the transition at $T_c(Q)$ will not be known until measurements are made without the masking influence of gravity. Notice that the distance from the point of inflection in the resistivity data displayed in Fig. 23 (where the temperature variation of R goes from concave down, which is indicative of a critical phase transition, to concave up, which is indicative of rounding) occurs about 15 nK above the highest temperature where R is zero (to within experimental resolution). The width of this rounded region does not increase steadily with Q, as it would if Q destroyed this phase transition. This implies that something other than the heat flux rounds the transition at this exceptionally fine scale. This rounding may be related to gravitational limits to the divergence of the correlation length, as discussed below.
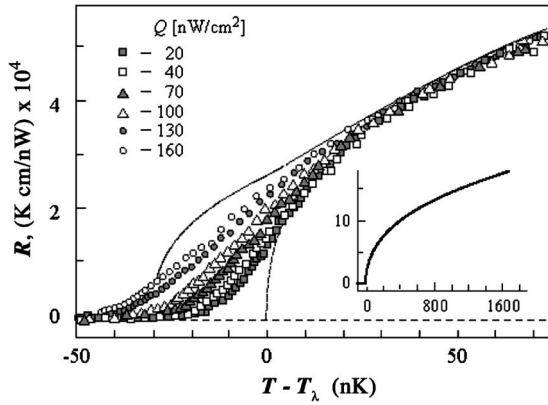
FIG. 23. Thermal resistivity measurements in the nonlinear region for different values of Q. The lower line is a simple power-law fit to the data in the linear region. The upper line is the prediction of Haussmann and Dohm (1991, 1992a) at $Q = 160$ nW cm^{-2} and $T > T_\lambda$. The short-dashed line is a plausible guide for the eye for $T < T_\lambda$, where the Haussmann-Dohm theory makes no prediction. The inset shows the same data over a wider temperature interval. These data were used to construct the phase diagram in Fig. 22, where $T_{nl}(Q)$ is defined as the temperature above which the thermal resistivity is within 5% of the linear resistivity, and $T_c(Q)$ is defined as the temperature at which no thermal resistance can be measured to within the experimental resolution. Adapted from Day *et al.*, 1998.

2. Hysteresis in the superfluid transition in ^{4}He

There is no predicted latent heat or thermal hysteresis associated with the superfluid transition in ^{4}He under static conditions, since this is a continuous phase transition. But when the helium is subjected to out-of-equilibrium conditions by imposing a heat flux Q through the fluid, hysteresis is predicted (Onuki, 1983, 1984; Haussmann, 1999a; Weichman and Miller, 2000). The temperature at which the system is predicted to develop thermal resistance abruptly as the liquid is heated from the ordered phase, designated $T_c(Q)$, is predicted to be higher than the temperature, designated $T_\infty(Q)$, of the superfluid phase well away from the interface in microgravity conditions, where pressure-induced gradients in T_λ have been ignored. Weichman and Miller (2000) predicted that this interface will form at the heated endplate and advance into the cell smoothly, but they also predicted that the transition may become hysteretic, exhibiting an abrupt interface formation beyond the heated endplate, when helium is heated at a nonzero rate. The theories of Onuki (1983, 1984) and of Weichman and Miller (2000) are made in the mean-field approximation, so the effects of fluctuations have not been estimated systematically. Hence the difference between $T_c(Q)$ and $T_\infty(Q)$ cannot be predicted accurately by these theories, but future microgravity measurements may determine this difference. Since this is a fluctuation-dominated effect, the difference between these two temperatures may depend on the time scale of the measurements.

No hysteresis in the superfluid transition under a heat flux has been observed to date. Measurements have been made by Liu and Ahlers (1994) that would have detected such hysteresis had it been as small as 3% of the theoretically predicted value (Onuki, 1983, 1984).

The reason for this lack of observed hysteresis is unclear, but three possible explanations have been discussed. First, it is possible that the critical fluctuations, which are large for low values of Q near the superfluid transition, may be so large that they swamp the difference in free energy of the helium at temperatures between $T_c(Q)$ and $T_\infty(Q)$. A second hypothesis is based on the pressure-induced variation in the superfluid transition temperature on Earth, which creates a chemical potential variation within the helium near the heated endplate that would oppose any discontinuous formation of the interface at that location. If this is the reason why hysteresis has not been observed at the predicted level, then such hysteresis in the superfluid transition under a heat flux may be observed in a microgravity laboratory. The third hypothesis is that the temperature variation in liquid helium near the heated endplate, which exists over the scale of the correlation length due to the singular Kapitza resistance (Duncan *et al.*, 1987; Murphy and Meyer, 1996; Kuehn *et al.*, 2002), is large compared to $T_c(Q) - T_\infty(Q)$, and hence always nucleates the transition to $T_\infty(Q)$. This hypothesis is compelling, since Weichman and Miller (2000) had to remove this singular boundary effect from their simulations in order to see the hysteresis effect.

3. Dynamical and gravitational effects on the correlation length

As discussed above, the thermal conductivity diverges near the superfluid transition due to the onset of local superfluid order on the scale of the diverging correlation length as the transition is approached from the high-temperature side. This divergent correlation length also determines the width of the He I/He II interface, and it grows from atomic dimensions far from the superfluid transition to macroscopic length scales as the transition is approached (Stanley, 1971). Ideally this correlation length ξ should diverge from the high-temperature side of the transition as $\xi = \xi_0 t^{-\nu}$, where $\xi_0 = 3.4 \times 10^{-8}$ cm (Singsaas and Ahlers, 1984) and hence can only be limited by the size of the helium container as $T \to T_\lambda$, since the ^{4}He sample is both chemically and physically free of imperfections. But on Earth the hydrostatic pressure variation across the sample of ^{4}He that is aligned along the direction of Q establishes a quasi-one-dimensional system in a cylindrical cell. This creates a hydrostatic pressure variation across the cell height that limits the divergence of the correlation length to some maximum ξ_g in all Earth-based experiments (Ahlers, 1976; Duncan *et al.*, 1998, 2000). The corresponding variation of the reduced temperature across this maximum correlation length is $\delta t = [\xi_0 (dT_\lambda/dz)/T_\lambda]^{1/1+\nu} = (15 \text{ nK}) T_\lambda^{-1} = 6.9 \times 10^{-9}$, where dT_λ/dz is the slope of the lambda line (Ahlers, 1968a), implying $\xi_g \approx 100$ μm. Hence on Earth
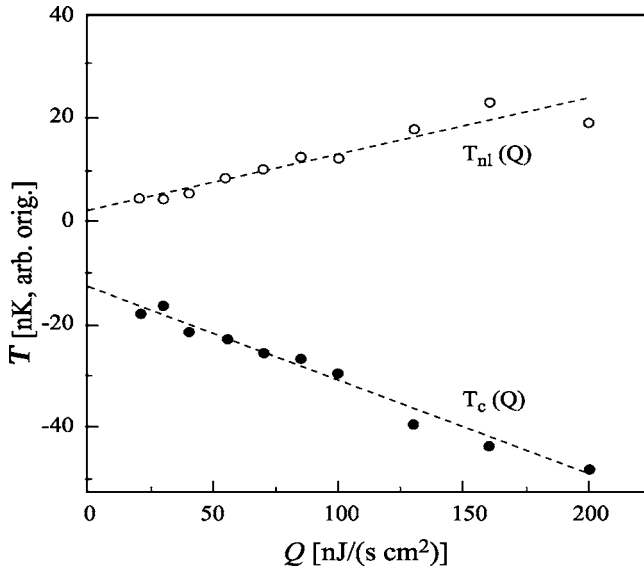
FIG. 24. $T_{\mathrm{nl}}(Q)$ and $T_c(Q)$ displayed as a function of Q on linear scales. Notice that a gap $T_{\mathrm{nl}}(Q \to 0) - T_c(Q \to 0) = 15 \pm 2$ nK exists in the static limit. This is thought to be a gravity effect, as discussed in the text. Adapted from Duncan *et al.*, 2000.

it is impossible to observe critical phenomena within 15 nK of the superfluid transition, since severe gravity rounding will dominate in this region. This observation is consistent with the rounding of the thermal resistivity data displayed in Fig. 23. Although we have adequate temperature measurement capability to resolve a change in reduced temperature at the level of $-10^{-2} \delta t$, the microgravity environment is essential to observe the true critical behavior for $t \lesssim 2\delta t$.

The above limit on the divergence of the correlation length has been observed indirectly on Earth (Duncan *et al.*, 2000). Figure 24 displays the temperatures $T_{\mathrm{nl}}(Q)$ and $T_c(Q)$, as defined above and displayed in reduced temperature format in Fig. 22, but on linear scales. We would have expected that $T_{\mathrm{nl}}(Q) \to T_c(Q) \to T_\lambda$ in the limit that $Q \to 0$, but Fig. 24 shows that the actual situation is not this simple. Instead, a gap of 15 ± 2 nK is observed in $T_{\mathrm{nl}}(Q) - T_c(Q)$ as $Q \to 0$, which is interpreted to be due to the pressure-induced difference in the superfluid transition temperature across the Earth-based limit of the correlation length ξ_g (Haussmann, 1999a). Once again this result is consistent with the Q-independent rounding of the thermal resistivity data displayed in Fig. 23, and the prediction for ξ_g discussed above.

The width of the interface is of order ξ, as discussed above. A very simple argument may be applied to predict the nature of this interfacial thickness, and hence of the correlation length, as the system is driven away from equilibrium by a heat flux Q. The reduced temperature variation across the nonlinear region is $t_{\mathrm{nl}}(Q) \equiv \Delta T_{\mathrm{nl}}/T_\lambda$, so $t_{\mathrm{nl}}(Q) = (Q\xi_0/\kappa_0 T_\lambda)^{1/(1+\nu-x)} = (Q/Q_0)^{1/(1+\nu-x)}$, where $Q_0 \approx 200$ W cm^{-2}, x is defined as the effective exponent of the thermal conductivity in this section only, and $1/(1+\nu-x) = 0.82$. This is in good agreement with experimen-

tal results if the temperature width of the nonlinear region is interpreted as twice the experimental measurements of the depression of the superfluid transition temperature by a heat flux $T_{\mathrm{DAS}}(Q)$ of Duncan *et al.* (1988), where $Q_{0,\mathrm{DAS}} = 568 \pm 200$ W cm^{-2} and the exponent $1/(1+\nu-x)_{\mathrm{DAS}} = 0.81 \pm 0.01$.

We can now estimate the Q-dependent correlation length $\xi(Q)$ and hence the Q dependence of the interfacial thickness, using the value of $t(Q)$ inferred in the analysis above: $\xi[t(Q)] = \xi_0[(Q/Q_0)^{1/(1+\nu-x)}]^{-\nu} \approx 2.2 \times 10^{-8}$ cm$[Q/(200 \text{ W cm}^{-2})]^{-0.55}$. Hence the dynamic correlation length, the interfacial thickness, and the range of critical fluctuations are all expected to decrease from their static values as $Q^{-0.55}$ as the heat flux is increased in the absence of gravity.

It is interesting to note that the static He I/He II interface is stable only under a hydrostatic pressure gradient, and the width of this static interface ξ_g, as discussed above, goes to infinity as the hydrostatic pressure gradient goes to zero. So the static interface does not exist in a weightless laboratory, and the gravitational limit on the interfacial width becomes the upper bound on $\xi[t(Q)]$ as $Q \to 0$. Weichman *et al.* (1998) found that the interface is stabilized robustly perpendicular to Q under weightless conditions, and they predicted that a surface second-sound mode must exist at the interface to couple the bulk second-sound modes in He II to the diffusive modes in He I. Such a mode has not been observed on Earth, but it may become observable in future second-sound measurements on Earth or in microgravity, such as those that are part of the planned heat capacity at constant pressure (CP) flight experiment that is described below.

The highly simplified analysis of the nonlinear region dynamics was presented above in order to provide some physical insight. This system has been analyzed rigorously by Dohm and Haussmann (1994) using their renormalization-group treatment of model F. This work predicts a Q-dependent quasiscaling of the interfacial thickness that scales as $Q^{-0.55}$, as was suggested in the simplified analysis. Furthermore, the analysis of Haussmann and Dohm (1991, 1992a) has provided detailed predictions for the extent of the nonlinear region, as displayed in Fig. 22, and the Q-dependent thermal profiles in this region for $T > T_\lambda$. This theory has led to other predictions, such as the behavior of the superfluid fraction and the specific heat of He II immediately below $T_c(Q)$ (Haussmann and Dohm, 1992c, 1994) and of the variation of $T_c(Q)$ (Haussmann and Dohm, 1992b, 1992c). These predictions refer only to the zero-gravity case, so they may be conclusively tested only in space experiments. Haussmann (1999a) has succeeded in developing a theory that includes both these dynamical effects and the effects of gravity, only for $Q \gtrsim 10^{-7}$ W cm^{-2}, where the thermal gradient across the interface is larger than the pressure-induced variation of T_λ across the interface due to Earth's gravity. In this limit, however, the interfacial thickness is too narrow to permit a direct measurement of the critical thermal pro-

file across the interface, thus once again mandating the on-orbit measurements to test these new theoretical predictions. Careful experimental tests of these theories will provide rare insight into our most advanced theories of the dynamics of continuous phase transitions.

From the extensive ground-based evidence presented above, it appears that critical phenomena may not be observed within 15 nK of T_λ due to hydrostatic limits imposed on the diverging correlation length. The DYNAMX experiment was developed to circumvent these limits and to test theoretical descriptions of continuous phase transitions. This flight experiment was designed to accurately measure the nonlinear thermal profiles across the He I/He II interface using values of Q from 10 to 100 nW cm^{-2} that would allow exploration of the phenomena discussed above (Duncan, 2000).

4. Universality experiments

Since the system's dimensionality and order parameter symmetry do not depend on position along the lambda lines, universality predicts that the critical exponents and amplitude ratios will not depend upon pressure. Of course the nonuniversal parameters, such as the amplitudes themselves, and the corrections to scaling, may vary with pressure.

A guest experiment called CP was designed to test universality using the DYNAMX flight hardware (Lipa *et al.*, 2005). The DYNAMX cell's static ($Q=0$) specific heat will be measured at various elevated pressures and over a much wider range of temperatures than in CQ to test the universality predictions while in the weightless laboratory, and thus with the sample free from the hydrostatic pressure rounding that is observed on Earth. These specific-heat measurements will be used to determine the critical exponent α and the universal amplitude ratio A^+/A^-, and to determine if these universal quantities are independent of pressure. Second-sound velocity measurements will also be made at these elevated pressures as a function of reduced temperature. These measurements will be used along with the specific-heat data to infer the superfluid density as a function of reduced temperature, as shown in Eq. (15). These data will be used to derive the critical exponent ν, which describes how the superfluid density varies with reduced temperature, as discussed earlier. These second-sound measurements can be accomplished by applying a pulse of heat to one of the endplates while the cell is maintained at a set-point temperature within the superfluid phase. This heat pulse will then propagate away from the pulsed endplate and pass each of the sidewall thermometers, and be reflected a number of times from the cell ends. The speed of this second-sound propagation will be inferred from the time of flight required for multiple passes of the sidewall thermometer probes that are located approximately 5, 6, and 7 mm from the most distant cell endplate. The DYNAMX sidewall thermometers have demonstrated a time constant of about 50 ms near T_λ, which is adequate to measure the speed of second sound accurately up to a second-sound velocity of about 10 cm s^{-1}, permitting measurements of the velocity for $|t|<10^{-5}$. In addition to the universality measurements, the CP data will provide the first observation of second-sound propagation in a homogeneous superfluid free from the bias of a steady pressure gradient created by Earth's gravity. This should permit the study of other nonuniversal phenomena, such as nonlinear second-sound propagation (Goldner *et al.*, 1993), and possibly a new second-sound surface mode at the He I/He II interface (Weichman *et al.*, 1998).

VI. TRICRITICAL POINT

As discussed above, some thermophysical properties of systems near their critical point may be predicted based upon the number of components n of their order parameter and the spatial dimension d (Stanley, 1971). Every physical system falls into a distinct universality class, which depends primarily on d and n for the system. The $O(1)$ and $O(2)$ classes considered above have an upper critical dimension $d_u=4$ for all n, so in three dimensions $d<d_u$.

Calculation of the static properties when $d<d_u$ requires approximation techniques within the RG calculations, such as an expansion in $\varepsilon=d_u-d$ in field-theoretic renormalization-group methods, for example, those employed near the superfluid transition (Dohm, 1991). Some (but relatively few) physical systems fall into universality classes where $d\geq d_u$, where mean-field calculations provide exact predictions for the critical exponents and amplitude ratios. When $d=d_u$, corrections to scaling may be calculated using a RG technique, and they are logarithmic (Sarbach and Fisher, 1978), and hence very weak. If the ϕ^4 model discussed above is extended with higher even-order powers of ϕ, and if the coefficients of these higher-order terms are appropriately tuned, then special multicritical points are predicted with $d_u<4$. In particular, the simplest one is the tricritical point with $d_u=3$, which is realized physically in liquid ^{3}He-^{4}He mixtures at the point where the lambda line intersects with the mixture's phase separation line, as described below.

The term tricritical point was introduced by Griffiths (1970a) to describe the thermophysics where the lambda line intersects with two other lines of critical points. For helium mixtures this occurs where the lambda line meets the first-order ^{3}He-^{4}He mixture phase separation line. Physically, this point does not appear to be the intersection of three second-order lines, but in the appropriate parameter space it actually is such a point. Figure 25 shows a three-dimensional plot, where one axis is temperature and another is the chemical potential difference $\Delta\mu=\mu_3-\mu_4$, where μ_3 and μ_4 are the chemical potentials of the ^{3}He and ^{4}He, respectively. The third dimension is η, which is the field variable that is conjugate to the superfluid order parameter, and is not experimentally accessible. Hence, only the T-$\Delta\mu$ plane is experimentally accessible, and the sheets labeled B and B' in Fig. 25 exist only at nonzero values of η and terminate in the dashed lines. The solid line is the continuation of
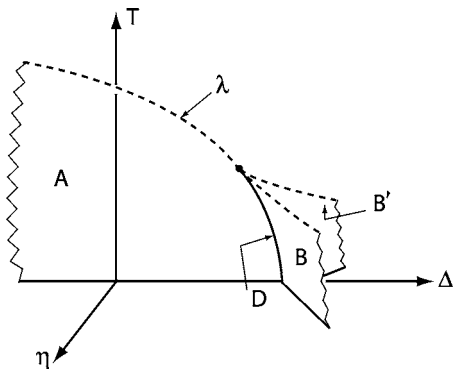
FIG. 25. Superfluid phase transition in ^{3}He-^{4}He mixtures. The bifurcation of this phase diagram occurs at the tricritical point. Adapted from Griffiths, 1970a.

the lambda line in the mixture, which becomes first order below the tricritical point. Hence, the tricritical point does exist at the intersection of three lines of critical points, but lines outside of the T-$\Delta\mu$ plane cannot be realized experimentally except right at the tricritical point, where all three lines intersect. Actual experimental data that map out the phase diagram near the tricritical point are displayed in Fig. 26 (Leiderer and Bosch, 1980). The data in Fig. 26 are plotted against the ^{3}He concentration difference from tricritical, which sets the chemical potential difference as described above. Here the experimentalists measured small changes in the index of refraction between the ^{3}He-rich phase and ^{4}He-rich phase using a sensitive optical interferometer,
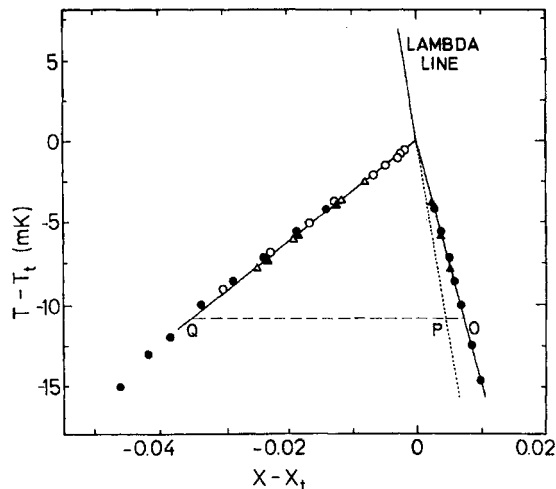
FIG. 26. Phase diagram of ^{3}He-^{4}He mixtures near the tricritical point as inferred from data by Leiderer and Bosch (1980). X is the ^{3}He concentration, X_t is the tricritical point concentration, and T_t is the tricritical point temperature. The triangles represent data taken at SVP, while the circles represent data taken at 22.6 bars. Open circles represent data taken by detecting small deflections of a laser beam corresponding to changes in the index of refraction at the phase separation interface. The solid circles represent data taken using an interferometer as described in detail by the authors. Adapted from Leiderer and Bosch, 1980.

and extrapolated back to the line where these two phases first emerged as a function of concentration and temperature. The intersection of this curve with the lambda line defines the tricritical point experimentally. For more information on this, and on the predicted scaling relations near the tricritical point, see Griffiths (1970a). Sarbach and Fisher (1978) also provide an excellent theoretical review of the tricritical point.

The ^{3}He-^{4}He mixture tricritical point has been studied experimentally since 1967, as discussed below. It occurs at $T_t = 0.8698 \pm 0.0001$ K and at a ^{3}He mole fraction of $62.7 \pm 0.1\%$ (Garcia and Chan, 2002). Here, the second-order line of critical points, corresponding to the superfluid transition in the homogeneous mixture above the tricritical point, intersects with the first-order phase boundary, where the homogeneous ^{3}He-^{4}He mixture splits into two distinct phases of differing ^{3}He concentrations.

While there are exact predictions for the exponents in tricritical systems, there exist very little data due to sample stratification under Earth's gravity. Measurements of the thermophysical properties of ^{3}He-^{4}He mixtures in the low-gravity environment of Earth's orbit promise to provide the first data set, free from systematic errors induced by gravity, of a system within this universality class. Such an experiment, called "Experiment along Co-existence near Tricriticality" (EXACT), has been developed for flight aboard the ISS (Larson, 2000).

The intersection of the lambda line with the ^{4}He-^{3}He mixture phase separation curve was mapped by Graf *et al.* (1967). Light-scattering measurements identified this intersection as a tricritical point (Leiderer *et al.*, 1974). Many static properties of mixtures have been measured near the tricritical point, and these have been reviewed by Ahlers (1976) and by Ryschkewitsch and Meyer (1979), who also discussed relaxation time measurements. A more comprehensive study of diffusive relaxation processes in mixtures, including near the tricritical point, has been reported by Behringer and Meyer (1982). There have also been extensive experimental studies of the dynamics near the tricritical point. Acoustic attenuation measurements by Roe *et al.* (1977) have determined the mass diffusion constant, which tends to zero near the tricritical point, consistent with predictions by Siggia and Nelson (1977). The thermal diffusion ratio and its scaling have been measured in this region as well (Ruppeiner *et al.*, 1980). Second-sound measurements have been made by Ahlers and Greywall (1972) near the tricritical point, and shear viscosity measurements in this region have been reported by Howald *et al.* (1992).

The EXACT experiment (Larson, 2000) was designed to measure second-sound propagation in microgravity to avoid stratification of the ^{3}He-^{4}He mixture under the Earth's gravitational acceleration. Measurements of the second-sound velocity as a function of temperature would permit a more precise determination of the critical exponent ζ, which is the critical exponent of the order parameter which corresponds to the superfluid frac-

tion. Earth-based measurements have been made to $t \sim 4 \times 10^{-4}$ (Leiderer and Bosch, 1980). Measurements closer to criticality may only be made accurately on orbit where sample inhomogeneities associated with the stratification of the ^{3}He concentration gradient along gravity are absent. The EXACT experiment was designed to measure the second-sound velocity as a function of concentration and temperature in ^{3}He-^{4}He mixtures near the tricritical point to $t \sim 5 \times 10^{-6}$ (Larson *et al.*, 2000). From these measurements, the superfluid density could be inferred from the data, and the critical behavior of the superfluid density could be determined experimentally. The EXACT experiment could also measure the shape of the coexistence curve and the lambda line as a function of temperature and concentration (Larson *et al.*, 2000; Nash *et al.*, 2003).

VII. FINITE-SIZE EFFECTS—LAMBDA TRANSITION IN ^{4}He

When ordinary matter is confined by boundaries in one or more dimensions to the length scale over which its local properties are correlated, its global properties are found to change. In metals and insulators the length scale involved is very small, but in superconductors, systems near critical points, superfluid ^{3}He, and semiconductors, the scale can be tens of nanometers or more. For example, in the semiconducting material $Ga_xAl_{1-x}As$, the correlation length of the electronic wave function can be as large as 0.1 μm (Dobson, 1995). With recent advances in nanofabrication techniques, the behavior of materials at small length scales is becoming a topic of technological importance. Outside the quantum world, the effects of interest are commonly modeled using mean-field theories, except near critical points, where more sophisticated methods are needed. With these confinement effects typically occurring in very small systems, it is difficult to separate them experimentally from perturbations due to interactions with the confinement structure itself. Fortunately, there are some situations where intrinsic effects are greatly magnified allowing detailed experimental measurements, free of artifacts, which can be compared with theoretical models. The case of most interest here is the lambda transition of helium, although the general phenomenon is common to all critical points. As described earlier, in the field of critical phenomena, the correlation length ξ describes the characteristic length scale over which an order parameter can vary. Far from the lambda transition, ξ is of the order of angstroms, making boundary effects difficult to observe, but very close to the transition, ξ can be much larger. This allows the confinement behavior of helium to be examined under nearly ideal conditions. In addition to the order parameter, other properties such as the specific heat, the thermal conductivity, and the free energy (Casimir force) are modified by the finite-size effect. Near the lambda point, the measurable quantity related to the order parameter is the superfluid density. However, no devices have yet been developed to probe the variation of ρ_s or any other property near a surface. Instead, the temperature variation of thermodynamic properties averaged over a sample contained within a confining geometry is typically measured.

Early models of finite-size effects near the critical point were developed by Fisher and co-workers, who described the scaling approach and emphasized the importance of ξ as the relevant length scale. The universality of finite-size scaling functions was first introduced by Privman and Fisher (1984). An introduction to the field has been given by Fisher (1971) and comprehensive reviews of the concepts by Barber (1983), Binder (1983), and Privman (1990). Quantitative estimates of the behavior near the lambda point have been obtained by RG and Monte Carlo techniques. This work led to predictions for the departure from the bulk behavior for the specific heat and the superfluid density in the affected region. The scaling behavior expected on general grounds was also verified. The RG theory of finite-size effects near the lambda transition was reviewed by Dohm (1993). Quantitative predictions were made by Schmolke *et al.* (1990), Sutter and Dohm (1994), and Schultka and Manousakis (1995a, 1995b), and are discussed below. More recently, Chen and Dohm (1999b, 2002) have found that the effect of finite cutoffs in lattice models and field theories cannot always be neglected, leading to a breakdown of finite-size scaling in the regime $L \gg \xi$, where L is the confining dimension. The same type of nonuniversal and nonscaling finite-size effect was found to exist in the presence of van der Waals forces for the case of periodic boundary conditions (Dantchev and Rudnick, 2001) as well as for the relevant case of Dirichlet boundary conditions in the region $L \gg \xi$ (Chen and Dohm, 2002, 2003). Recently, noncubic anisotropy has been predicted as a new source of nonuniversality of finite-size effects (Chen and Dohm, 2004). Within the $O(2)$ universality class this effect may occur in anisotropic XY lattice models, but not in liquid ^{4}He, which is intrinsically isotropic.

It is important to note that the finite-size behavior described here is within the context of second-order transitions. This means that interesting phenomena, such as the detailed behavior over a wide temperature range of a two-dimensional system obtained by thinning down the related three-dimensional system, are not completely accessible. We can only observe this behavior in the small range of temperatures where ξ is sufficiently large to produce a dominant effect, unperturbed by the substrate. Also, the models used are typically only applicable in the asymptotic region close to the transition where fluctuation effects dominate the behavior. Thus only certain aspects of the full finite-size phenomenon can be studied with critical point experiments. Other types of measurements can of course access other aspects, such as the details of the Kosterlitz-Thouless transition in 2D systems (Kosterlitz and Thouless, 1973).

Early experimental results have been reviewed by Gasparini and Rhee (1992). These authors concluded that the expected scaling behavior for the specific heat and superfluid density did not occur. However, more re-

cent work has shown improved behavior at least for the specific heat with planar confinement. We concentrate on this work in the following section, since some of the results were obtained in microgravity.

A. Finite-size specific heat

Detailed theoretical predictions for finite-size behavior in the case of the lambda transition are not yet fully developed, due to computational difficulties below the transition. Nevertheless, significant progress has been made. Schmolke *et al.* (1990) predicted the effect of confinement in terms of a geometry-dependent function $f_1(x)$ calculated using RG techniques. In this model, the heat capacity C can be written in the form

$$C(t,L) - C(t_0, \infty) = L^{\alpha/\nu} f_1(x), \qquad (16)$$

where $t_0 = (\xi_0^+/L)^{1/\nu}$ and $x = tL^{1/\nu}$ (not to be confused with the exponent x, used elsewhere). Here we follow the convention that L is the parallel-plate separation or the pore diameter measured in angstroms (although we otherwise quote sizes in microns), thus x has the dimension (angstrom)$^{1/\nu}$. In order to simplify the calculations, Schmolke *et al.* (1990) calculated the curve $f_1(x)$ separately above and below T_λ.

Further from the transition, a bulk-plus-surface model can be introduced, which treats the first-order confinement effect as a simple surface effect, with the full confinement leading to deviations as T_λ is approached. Above the transition, the predictions of Schmolke *et al.* (1990) can be written in terms of a function $f_2(x)$ defined by

$$C(t,L) - C(t, \infty) = -L^{\alpha/\nu} f_2(x). \qquad (17)$$

The surface term dominates the behavior of f_2 for $x > 100$, which corresponds to the region far from the transition. Similar behavior is expected below the transition, but so far no detailed prediction appears to exist. Knowledge of the surface specific-heat term allows a straightforward estimate of the free-energy departure from bulk in the region where it is small. In principle, it should be the same for all geometries where the approximation holds, to the extent that the boundary condition on helium is constant. Krech and Dietrich (1992) have performed calculations based on the ε expansion, but the results appear to be rather unstable at $d=3$ (Sutter and Dohm, 1994). Through the transition region the most detailed prediction is based on Monte Carlo calculations by Schultka and Manousakis (1995b). Their results also showed the importance of realistic boundary conditions on the detailed shape of the curve. Ferrell and Bhattacharjee (2000) developed an approximate model that is useful above the specific-heat maximum.

In the late 1970s, Chen and Gasparini (1978) reported specific-heat measurements of helium films and cylinders near the lambda point that indicated an unexpected scaling behavior with ξ/L. They concluded that the optimum value of the exponent characterizing the scaling of their data was close to 0.56, rather than 0.67 expected

from theoretical arguments based on the divergence of ξ. This observation was a serious problem for the development of confinement theory in general. The possibility was raised that fractal surface effects may be responsible for the difficulties, but a strong case was not made (Gasparini and Mhlanga, 1986). Additional analysis of the film data cast some doubt on the original conclusion and showed that the peak locations were consistent with the theoretical scaling exponent (Wacker and Dohm, 1994). In general, most of these early results now appear to be either of low accuracy, in rough agreement with traditional scaling, or too far removed from the critical region to be useful for detailed analysis. More recent submicron planar geometry results are in good agreement with scaling above the bulk superfluid transition, but some difficulties remain at the transition and below (Mehta and Gasparini, 1997; Kimball *et al.*, 2000). We note that below the bulk transition the experimental difficulties increase due to the presence of superfluid in the upper parts of the cells used, and the resulting nonlinear dynamics of the measurement technique. Data from most samples below the finite-size peak were abandoned because of the problems encountered (Mehta *et al.*, 1999). However, the general shape of the peak agrees quite well with Monte Carlo calculations (Schultka and Manousakis, 1995b, 1998) for both planar and pore systems with Dirichlet boundary conditions (Lipa *et al.*, 2001). This gives us hope that the remaining problems are of an experimental nature and will ultimately be resolved in favor of finite-size scaling. We will revisit some of the submicron measurements below.

1. Microgravity measurements

We now briefly describe the microgravity experiment called CHeX that was designed to give new, high-precision specific-heat data for helium confined to a 2D planar geometry with a characteristic length scale of 57 μm (Lipa *et al.*, 2000). On this scale, surface effects related to van der Waals forces and fractal geometry should be completely negligible, allowing a very clean measurement of the intrinsic behavior as helium crosses over from bulk to the 2D state. The results should therefore provide a high-quality reference curve against which other experiments can be compared. In addition, the results allow comparisons with theory well within the asymptotic region where the theoretical models apply, and significantly extend the range of the length scale available for scaling tests. The CHeX experiment was performed on the Space Shuttle mission STS-87 to reduce the effect of gravity on helium, which masks the finite-size effect, and the measurement technique was between equilibrium states, avoiding problems with dynamic methods.

To perform measurements on helium with ξ in the range of tens of microns it is necessary to work at a reduced temperature $t \sim 10^{-8}$. A high-quality experiment spanning such a small temperature interval clearly puts severe demands on thermometry. The paramagnetic salt thermometry described earlier was used in the experi-
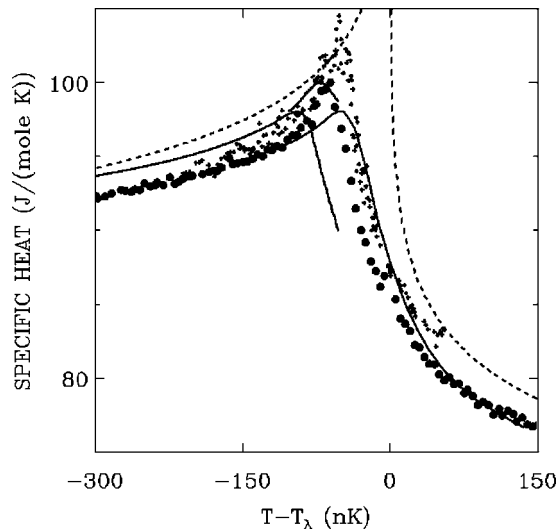
FIG. 27. Finite-size specific-heat measurements close to the lambda transition with a 57 μm confining geometry obtained in microgravity (Lipa *et al.*, 2000), •; results of Monte Carlo simulations (Schultka and Manousakis, 1995b), +; bulk curve scaled to fit the data far from the transition, - - -; predictions of Schmolke *et al.* (1990), −. From Lipa *et al.*, 2000.

ment with modifications to reduce excess noise from the charged particle flux. This resulted in improved measurements with a thermometer noise only slightly exceeding the value measured on the ground (Qin *et al.*, 1996). The calorimeter was designed to serve two main purposes: to maintain 60% of the sample in a confined state, and to provide the thermal coupling between helium and the thermometers. Helium was confined in the gaps between uniformly etched (100) silicon wafers nominally 110 μm thick and 3.8 cm in diameter. One side of each wafer was etched to a depth of 57 μm, leaving 30 small spacers in a gridlike pattern.

The specific-heat data close to the transition are shown in Fig. 27. Also shown for comparison are the results of Monte Carlo simulations (Schultka and Manousakis, 1995b) and the predictions of Schmolke *et al.* (1990). It appears that the models are fairly representative of the measurements, but the effect of confinement is somewhat underestimated, with the experimental curve generally showing greater deviations from the bulk. A similar effect is visible in the submicron data (Kimball *et al.*, 2000). Ahlers (1999) has compared some preliminary 57 μm data with the 0.2113 μm data of Mehta *et al.* (1999) in the inner region and demonstrated quite impressive agreement with scaling. This comparison is reproduced in Fig. 28. The upper solid curves in the figure are the bulk specific heat from Eq. (11) and the lower curves are a smoothed model of the 57 μm data scaled according to Eq. (16) with exponents ν =0.6705 and α=−0.0127. It can be seen that at this level of testing there is no reason to seriously doubt proper scaling behavior over a very wide range of length scales. In addition, the f_2 plot based on Eq. (17) above T_λ does not show any significant problems that exceed possible experimental error. This can be seen in Fig. 29, where
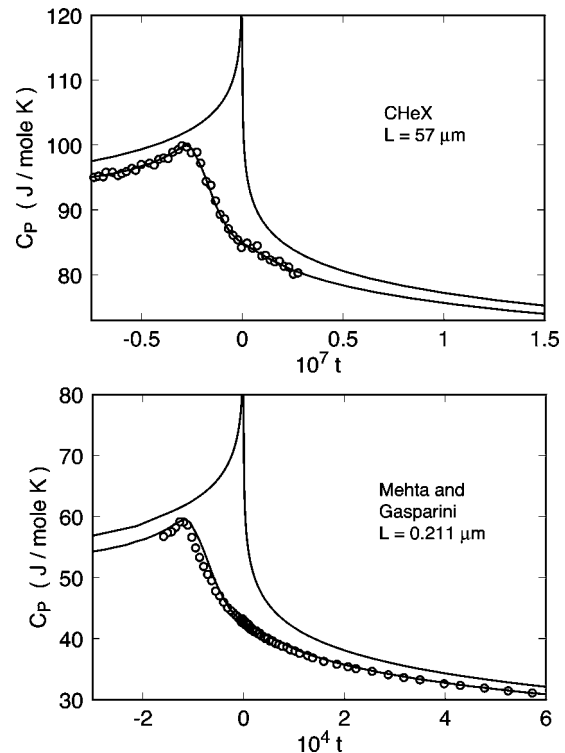
FIG. 28. Comparison of finite-size specific-heat results for L =57 μm obtained in microgravity (Lipa *et al.*, 2000) (top panel), with the measurements by Mehta and Gasparini (1997) for L=0.211 μm (lower panel). In each case, the upper curve is the bulk specific heat. The smooth curve through the microgravity data was used to estimate the specific heat for L =0.211 μm, using finite-size scaling and a correlation-length exponent ν=0.6705, and yielded the solid curve through the 0.211 μm data. Note that the horizontal scales differ by a factor of 4000. From Ahlers, 1999.

we plot the 57 μm data in this region. For $x>100$, the plot shows the surface specific heat above the transition scaled as in Eq. (11) for comparison with the theoretical function f_2 calculated by Schmolke *et al.* (1990), with no
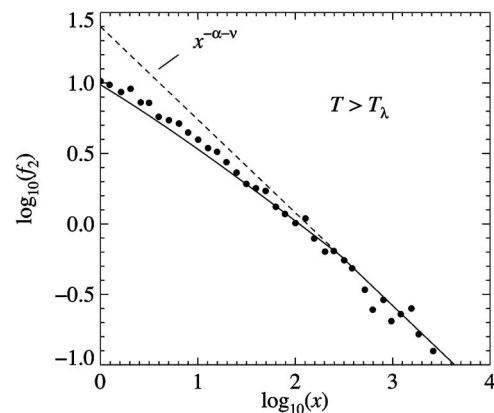
FIG. 29. Scaled surface specific-heat results above the transition obtained with a 57 μm plate separation in microgravity. Solid curve, function $f_2(x)$ of Schmolke *et al.* (1990); broken curve, extrapolated surface specific-heat contribution. From Lipa *et al.*, 2000.
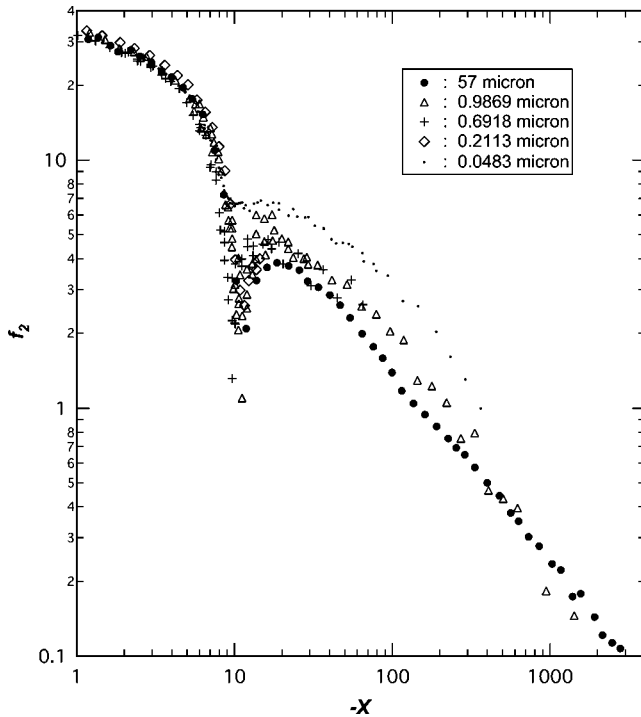
FIG. 30. Deviations of the confined helium specific heat from the bulk, scaled to give $f_2(x)$ below the transition, for planar geometry. The 57 μm data were obtained in microgravity (Lipa *et al.*, 2000); 0.9869 μm data are from Kimball *et al.* (2000); 0.6918, 0.2113, and 0.0483 μm data are from Mehta *et al.* (1999).

adjustable parameters. Over the range shown, the match is very good. For $x > 3000$, the scatter in the data becomes large. The wide range and high accuracy of the 57 μm data give us an opportunity to obtain an estimate of the surface specific-heat exponent $\alpha_s = \nu + \alpha$ with relatively low uncertainty. The result obtained in the range $100 < x < 2000$ was $\alpha_s = 0.65 \pm 0.2$, which compares well with the predicted value of 0.658. Below T_λ, some residual problems exist, as mentioned earlier. In Fig. 30, we plot the parameter f_2 derived from the 57 μm results, the 0.9869 μm results of Kimball *et al.* (2000), and the 0.6918, 0.2113, and 0.0483 μm sets of data recommended by Mehta *et al.* (1999). It can be seen even below T_λ that there is quite good agreement between the results for $0.2 < L < 57$ μm, which covers a factor of 270 in length scaling. On the other hand, the 0.0483 μm data show a clear lack of scaling for $x < -10$. We note that for this case the peak of the specific heat falls at $t \sim -10^{-3}$, beyond which finite-size scaling may break down due to nonasymptotic corrections. However, it is also possible that there is an as-yet unrecognized experimental artifact in these data, in addition to those found in measurements with other cells (Mehta *et al.*, 1999). Also, the behavior in the region near $x \sim -10$ corresponding to the onset of superfluidity on cooling is in some doubt with the data from thinner films showing a somewhat more rounded peak than expected [see Fig. 11 of Kimball *et al.* (2000)]. Until the anomalous results are confirmed by
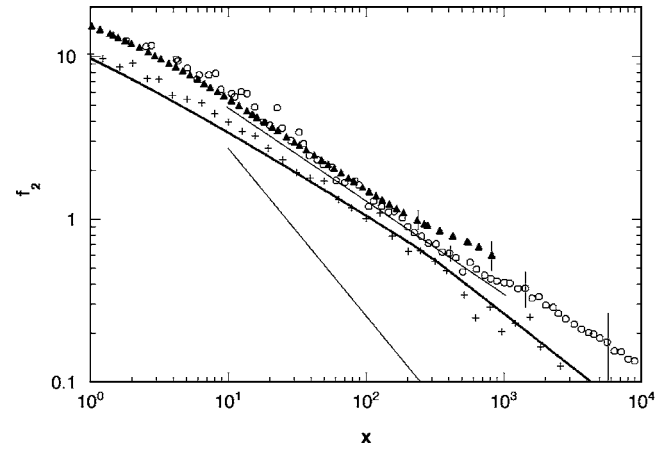
FIG. 31. Deviations of the confined helium specific heat from the bulk, scaled to give $f_2(x)$ above the transition. Open circles, 8 μm pores; filled triangles, 0.26 μm pores; +, 57 μm planar geometry. Solid curve, model of Schmolke *et al.* (1990); sloped straight lines indicate the range of results of Mehta *et al.* (1999). From Lipa *et al.*, 2001.

other methods, it seems reasonable to put them in the suggestive but not definitive category. A reasonable conclusion appears to be that acceptable scaling holds for films thicker than 0.2 μm but thinner films may show deviations. The 57 μm results appear to be the most useful for comparison with theory below the transition, involving measurements between easily defined equilibrium thermodynamic states. A power-law fit to the 57 μm data in Fig. 30 over the range $-2000 < x < -100$ gave $\alpha_s = 0.64 \pm 0.05$, again in good agreement with theory (Lipa *et al.*, 2000).

Ground measurements have also been made on helium confined to a range of substrates with pore geometries. The early work of Chen and Gasparini studied helium in the pores of Nucleopore filters of diameters 0.03–0.2 μm. Measurements on 0.26 μm Anopore and 8 μm microchannel plates were reported by Lipa *et al.* (2001). Recently some measurements on 1-μm-square channels have also been reported (Kimball *et al.*, 2004). The 1 and 8 μm substrates provide extremely uniform confining dimensions for helium with which to observe finite-size effects. Surprisingly, the 8 μm results do not compare very well with other measurements in the region of the peak. On the other hand, the Anopore and 1 μm results are in good agreement with Monte Carlo predictions (Schultka and Manousakis, 1998).

In the region where deviations from bulk are small, f_2 again reduces to a simple surface specific-heat term that is expected to be the same for 1D and 2D confinement, after allowance is made for the difference in the surface area-to-volume ratio for the two cases. The behavior of f_2 over the range of interest is shown in Fig. 31 for the Anopore, 8 μm, and 57 μm data sets. For comparison, we also show predictions of Schmolke *et al.* (1990) for the 2D confinement case. It can be seen that at large x the pore data are approximately a factor of 2 higher than the predicted curve, as expected from the surface
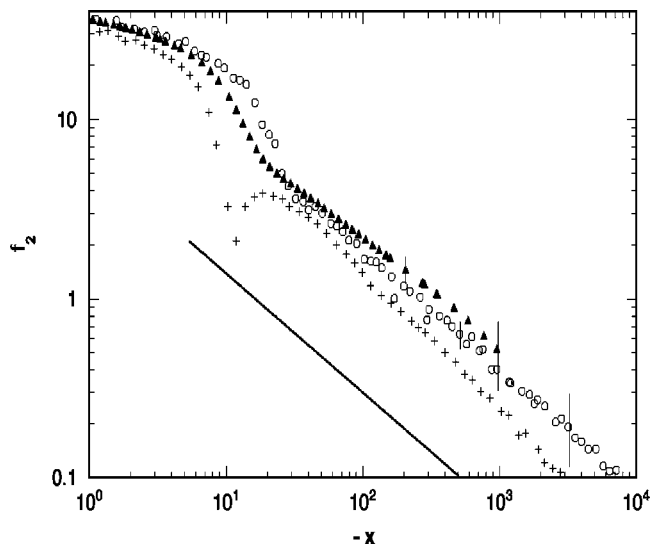
FIG. 32. Plot of f_2 versus x below the transition. Open circles, 8 μm pores; filled triangles, 0.26 μm pores; +, 57 μm planar geometry. Line shows the low-order perturbative result of Mohr and Dohm (2000). From Lipa *et al.*, 2001.

FIG. 33. Comparison of finite-size specific-heat data scaled to give $f_1(x)$ for pores: open circles, 8 μm; filled triangles, 0.26 μm; ×, open triangles, +, 800, 1000, and 2000 Å data of Chen and Gasparini (1978); squares, model of Schultka and Manousakis (1998, 1995b). From Lipa *et al.*, 2001.

area-to-volume ratio. The general behavior appears to be very similar to the predicted curve even in the region $x < 100$, where higher-order contributions beyond the surface term become significant. The two lines in the region $10 < x < 1000$ show the approximate limits of the planar geometry results of Mehta *et al.* (1999).

The corresponding plot for below the transition is shown in Fig. 32. Clear differences between the pore and planar geometry results can be seen near $x \sim -10$. Below the transition, no detailed prediction is available for the full range for any dimensionality, but the ratio of the surface terms on the two sides has been estimated by renormalization techniques. The low-order perturbation theory result derived by Mohr and Dohm (2000) for planar geometry is shown by the line in the figure. The authors do not consider this result a reliable prediction and further work in this area is very desirable. On the other hand, the Monte Carlo results of Manousakis (1995b, 1998) are in good agreement with the two types of data shown in Fig. 32, as indicated by Figs. 9 and 10 of Lipa *et al.* (2001).

We find that the ratio R_s of the surface specific heat on the two sides of the transition varies somewhat as a function of x. Over the range $30 < |x| < 200$, we find $R_s = 1.29 \pm 0.1$ for the 8 μm data and 1.42 ± 0.03 for 0.26 μm. Further from the transition R_s appears to approach unity in both cases, but here the uncertainties in the surface terms rapidly increase, making the ratio measurement unreliable. These results can be compared with the prediction of Bhattacharyya and Bhattacharjee (2000), who find $R_s = 2.06$ on the basis of approximate RG arguments. It is possible that some of the discrepancies on the low-temperature side are associated with the longer correlation length there, as compared to the value a similar distance above the transition. Hohenberg *et al.* (1976) find that the ratio of the correlation lengths below and above the transition is $\xi_0^-/\xi_0^+ \approx 2.7$ for helium, al-

though the definition on the two sides is somewhat different, due to the infinite range of the superfluid correlation function. Since the region $x < 0$ also includes the finite-size peak, the measurements can be compared with the results of Schultka and Manousakis (1995b) converted to f_2. The level of agreement was found to be encouraging in both the pore and planar geometry cases (Lipa *et al.*, 2001). Additional contributions to the finite-size effect from edges have been reported (Kimball *et al.*, 2004), although these are not expected to be significant for the range covered here. These authors also report the result $R_s = 1.46 \pm 0.1$, in reasonable agreement with the values quoted earlier.
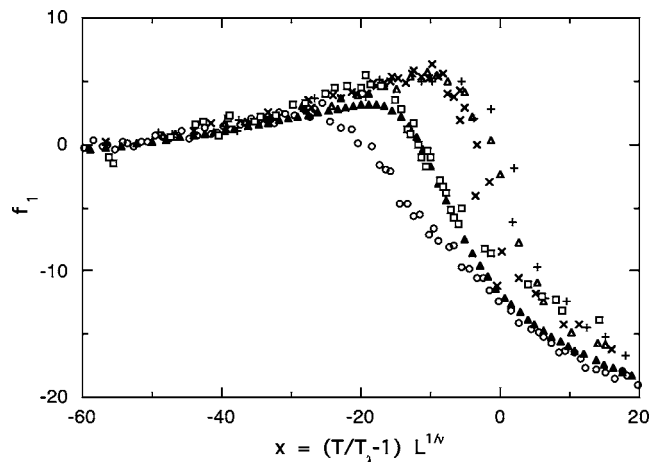
In Fig. 33, we show the results for f_1 derived from the experiments on pores. For comparison, we also show the results of Monte Carlo calculations performed with a boundary condition simulating a node in the superfluid density at the walls. It can be seen that there is good agreement between the Monte Carlo results and Anopore measurements, but only fair agreement for the other samples. This result is surprising since the 8 μm substrate appears to be much closer to an ideal material than Anopore. Overall, from Fig. 33 it is hard to claim a good collapse of the data at small x. It will be interesting to review these results when more detailed estimates of the effects described by Chen and Dohm (1999b, 2002, 2003) become available, after extension of their theory to the region below T_λ. Additional specific-heat measurements may soon become available for 1 and 2 μm pores (Ahlers, 2006). Other aspects of finite-size scaling involve the height and location of the peak and the value of $C(t=0)$ as functions of the confining dimension. In Fig. 34, we show results for the shift of the specific-heat maximum relative to the bulk as a function of pore diameter and compare them with the Chen-Gasparini data reanalyzed by Wacker and Dohm (1994). It can be seen that the results fall on two roughly parallel lines. If we require $\Delta T_m = aL^{1/\nu}$, then the Anopore and 8 μm
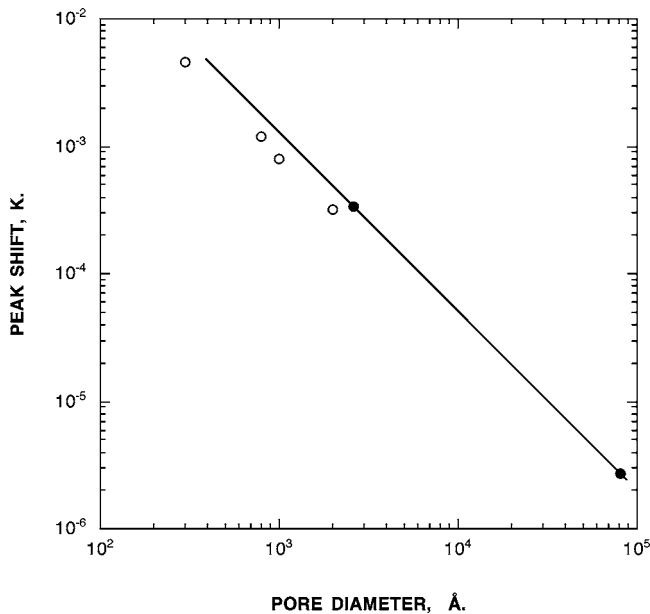
FIG. 34. Shift of finite-size specific-heat peak versus pore size. Open circles, Chen and Gasparini (1978); filled circles, Lipa *et al.* (2001). From Lipa *et al.*, 2001.

data indicate $\nu=0.716$. The deviation from the expected value, $\nu=0.6704$, is a reflection of the lack of collapse of the f_1 plots in Fig. 33. It can be seen that the results from the Chen and Gasparini experiment appear to be offset from those of Lipa *et al.* (2001) on a roughly parallel curve consistent with $\nu=0.6704$. We note that the pore sizes in the Chen and Gasparini experiment were not measured, although an estimate suggests they were 10–20 % smaller than the nominal values quoted (Gasparini *et al.*, 1981). To reconcile the two sets of results, the pores would need to be ∼35% larger than assumed, which seems well outside the expected error. It is possible that the boundary condition for helium differs for different substrates, causing an apparent lack of scaling.

In summary, it appears that most current theoretical predictions for the specific heat in planar and cylindrical geometries are in approximate agreement with experiment over a wide range of length scales. However, near the heat-capacity peaks there is some evidence for rounding that does not scale correctly. More measurements are needed to resolve these lingering issues. Overall, the results provide a remarkable degree of confirmation of finite-size scaling for the specific heat near the lambda point. Interesting finite-size effects on the free energy (Casimir effect) have also been predicted (Krech and Dietrich, 1991, 1992) and detected (Garcia and Chan, 1999, 2002). In this case, van der Waals forces are predicted to cause nonscaling finite-size effects for $L \gg \xi$ (Chen and Dohm, 2002, 2003).

A flight experiment, CHeX-2, was proposed to measure the confinement effect in very uniform 50 μm pores, to expand the range of scaling tests and provide additional information on the surface specific heat in the asymptotic region. This experiment would reuse some of the equipment returned from the 57 μm experiment de-

scribed above. Improved thermometry would allow about a factor of 2 reduction in the noise of the measurements. The main components of the flight calorimeter for this experiment have been fabricated.

B. Superfluid density

To date, no finite-size superfluid density measurements have been proposed for microgravity, but for completeness we mention ground experiments in this area. Data in the critical region have been obtained by a number of groups. The most useful for the present discussion are from Rhee *et al.* (1989) for planar geometry. Films in the range 0.106–3.9 μm were studied using torsion oscillator techniques. Deviations of the superfluid density from bulk behavior showed two regimes, a small-departure regime with a weak temperature dependence and a region with a more abrupt falloff, close to the bulk transition. The latter region was identified as a crossover region to 2D behavior, dominated by the Kosterlitz-Thouless transition (Kosterlitz and Thouless, 1973). Data from the former region were analyzed for scaling behavior and the expected power-law behavior was not found. The departures from bulk showed the expected L^{-1} amplitude behavior but the temperature dependence was stronger than indicated by the variation of the correlation length. This effect was most noticeable in the 2.8 and 3.9 μm data sets. As yet there appears to be no explanation for this anomaly. Gasparini and Rhee (1992) have reviewed the results of this and related experiments in detail. A possibly related lack of scaling has been reported by Schultka and Manousakis (1997), who found a lack of L scaling in Monte Carlo computations of the superfluid density in films.

C. Finite-size thermal conductivity

At present, theoretical methods are not sufficiently advanced to provide detailed predictions of the finite-size effect on the thermal conductivity $\kappa(t,L)$ of helium near the lambda point. Nevertheless, some useful results have been obtained. Bhattacharjee (1996) performed an approximate calculation equivalent to a self-consistent single-loop model and derived a scaling function for $\kappa(t,L)$ similar to that suggested by Kahn and Ahlers (1995). A one-loop calculation of $\kappa(t,L)$ has been performed by Töpler and Dohm (2003) for the region above and at the transition. These calculations used the model-F Hamiltonian (Halperin *et al.*, 1976a) with corrections to scaling, and Dirichlet boundary conditions at the surface. Both the quantities $1-\kappa(t,L)/\kappa(t,\infty)$ for $\xi \ll L$ and $\kappa(0,L)$ were calculated. Significant progress has also been made with Monte Carlo calculations of transport properties. Krech and Landau (1999) studied the spin dynamics of the *XY* model (*E*) for a cubic geometry with periodic boundary conditions. They obtained a scaling function $\kappa(0,L) \sim L^{2-z}$, where z is a dynamic exponent ($z \approx 1.38$). This result appears to be consistent with the function derived by Töpler and

Dohm (2003), however, strictly speaking, it belongs to a separate universality class (Hohenberg and Halperin, 1977). Nho and Manousakis (2001) have determined the shape of the scaling function $\kappa(t, L)$ for a barlike geometry with open boundary conditions, but not its absolute value. A phenomenological approach to the calculation of the thermal resistivity $R(t, L) = \kappa(t, L)^{-1}$ was developed by Ferrell and Mukhin (2000, 2001). These authors calculated dissipation in a superfluid confined to a cylindrical geometry by considering the phase slip associated with the migration of vortices in the superfluid, caused by the heat current. Their results give the resistivity well below the bulk T_λ where the coherence length is significantly smaller than the cylinder radius.

Ahlers (1999) has pointed out that finite-size effects for transport properties are richer than those for equilibrium properties because the heat current breaks the rotational symmetry of the sample. Thus one should expect different behavior when current flows in different directions relative to the confinement geometry, implying that there could be as many as three different universal scaling functions involved. These correspond to (i) a parallel-plate geometry with the current in the plane, (ii) a parallel-plate geometry with the current perpendicular to the plane, and (iii) a cylindrical geometry with the current along the cylinder axis. For relatively thick spacings, (ii) is dominated by the boundary resistance and has been investigated in ground-based experiments below the bulk T_λ.

Approximating the thermal conductivity as $\kappa(t, \infty) \sim \kappa_0 t^{-x}$ for $t > 0$, Ahlers (1999) has proposed a scaling law involving $R(t, L)$. By analogy to static finite-size scaling, he obtained the dynamic scaling function

$$F(X) = (L/\xi_0)^{x/\nu}[R(t, L)/R_0], \qquad (18)$$

where $X = (L/\xi_0)^{1/\nu} t$ and $R_0 = \kappa_0^{-1}$. Regardless of the geometry, we expect the relationship between $R(t, L)$ and $R(t, \infty)$ to be given by a function of L/ξ only. Ahlers (1999) also obtained a difference function

$$G(X) = (L/\xi_0)^{x/\nu}[R(t, L) - R(t, \infty)]/R_0. \qquad (19)$$

Above T_λ, the function $G(X)$ is more sensitive to the finite-size effect since the bulk resistivity is subtracted, while below T_λ, $G(X) = F(X)$. Ahlers (1999) also obtained

$$R(0, L) = R_0 F(0)(L/\xi_0)^{-x/\nu} \qquad (20)$$

for the resistivity at T_λ. However, it is not entirely clear how one would derive the same result from the low-temperature side, or even how $F(X)$ should be defined. Based on the static scaling analogy, the functions $F(X)$ and $G(X)$ are expected to be universal, implying that (for a given geometry) they do not depend on L and P, but the uncertainty in the form of their continuation to negative t implies that some caution is prudent at this stage. Also, the exponential behavior of $R(t, L)$ observed below T_λ suggests that the physical phenomena which dominate the finite-size effects on the two sides of the transition might be different (Ahlers, 1999). In addi-
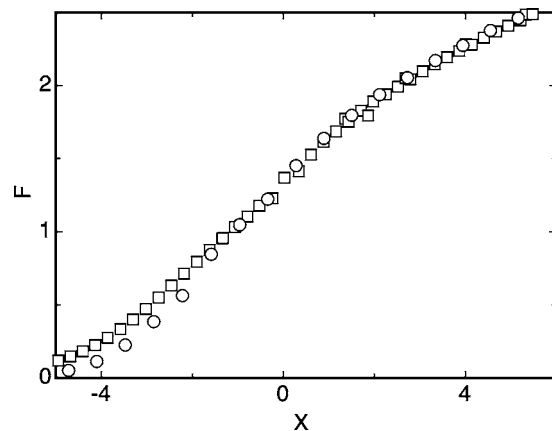
FIG. 35. The scaling function $F(X)$ for pores of 1 μm diameter (circles) and 2 μm diameter (squares) in the transition region at SVP. From Murphy *et al.*, 2003.

tion, the power-law representation of the thermal conductivity is only approximate, so ideal scaling behavior cannot be expected with the present level of understanding.

Thermal conductivity measurements of confined helium have been made by Kahn and Ahlers at the SVP. Their sample was contained in the long, narrow tubes of a glass microchannel array and thus represents the cylindrical geometry with axial heat flow. The tube diameter L was 2 μm. Their results showed that $R(t, L)$ in the cylindrical geometry remains finite at T_λ, and decays exponentially as T is reduced below T_λ. Additional results have been reported by Murphy *et al.* (2003), who used 1- and 2-μm-diam pores and covered the range of pressures from the SVP up to 28 bars in the latter case.

Data for R in the finite-size-affected region of t are shown in Fig. 3 of Murphy *et al.* (2003). Above T_λ, the finite-size effect on R was found to extend to quite large values of t. This is characteristic of the surface contribution to finite-size effects as seen in static properties. Below T_λ, $R(t, L)$ approaches zero rather more rapidly. Kahn and Ahlers fit their data for $R(t, L)$ with $t < 0$ to the exponential function $R/R_0 = \exp(t/t_0)$ and found $t_0 \sim 1.1 \times 10^{-6}$. Murphy *et al.* (2003) reported similar results for their data sets. They found that both R_0 and t_0 were approximately independent of pressure, suggesting that universality breaks down in this region, with the thermal conductivity becoming independent of P. However, it should be remembered that we do not yet know exactly how universality should manifest itself in this region. In the region near $t = 0$, the thermal resistivity was found to scale approximately as in Eq. (20). This agrees qualitatively with the prediction of Töpler and Dohm (2003), although a somewhat different dependence on L was observed. In the region above T_λ, scaling and universality were found to apply reasonably well. Figure 35 shows the function $F(X)$ for the two sizes of pores in the transition region (Murphy *et al.*, 2003). Differences in the curves may be due to a breakdown of scaling.

1. Microgravity experiment

The significance of the results to date would be substantially enhanced by equivalent results over a much wider range of confinement sizes. Some measurements would be worthwhile on smaller systems, but the full range of behavior seen above the transition would soon extend beyond the critical region, a problem already encountered with the measurement of static properties. This makes it difficult to compare the results with an asymptotic theory. Thus one is led to extending the length scale to relatively large values. However, for $L \geq 15~\mu$m the effect of Earth's gravity perturbs the measurements and experiments are feasible only in microgravity. This problem has been analyzed by Ahlers (1999), who showed that gravity effects are most serious in the region just below the transition. The upper limit on the size is set by the available thermometer resolution of about 10^{-10} K because as L increases, the phenomena of interest occur progressively closer to the bulk transition. Scaling the data shown in Fig. 35 to larger lengths suggests that quantitative measurements for L up to 100 μm should be possible. Residual acceleration levels of $<10^{-4}g$ rms in space are expected to be unimportant.

An experiment called BEST (Boundary Effects on the Superfluid Transition) has been designed to explore the cases of cylindrical geometry with a pore diameter of 100 μm and rectangular plate geometry with $L = 50~\mu$m at pressures from the SVP to 29 bars in zero gravity (Ahlers, 2000; Lammerzahl *et al.*, 2004). The apparatus will also contain a bulk helium cell for reference and additional high-resolution measurements. High-resolution thermometry similar to that described earlier will be capable of reaching a resolution of 8×10^{-10} K/Hz$^{1/2}$ and measurements will be made using the two-terminal technique in which the temperature rise across the cell is monitored as a function of the applied heat current. The design of the cells is similar to that described by Murphy *et al.* (2003) except for the use of a thicker sample plate. The apparatus will also have a superconducting pressure gauge (Edwards *et al.*, 1996) to allow measurements to be performed along isobars.

VIII. SUMMARY

We have presented an overview of the developments in critical phenomena that have occurred since the review of Moldover *et al.* (1979) with an emphasis on the situation in low-gravity conditions. It has become clear that low gravity can provide significantly improved results for testing the theory, and some experiments have demonstrated this. The relevance of performing these types of experiments has thus been clearly shown. However, in spite of over 25 years of effort, the scientific community has only just begun to reap the advantages of the space environment.

In the $O(1)$ universality class, the divergence of the constant-volume specific heat in SF_6 was successfully measured in the asymptotic region to $t = 10^{-6}$. The specific-heat exponent and asymptotic critical amplitude ratio obtained from this measurement agreed with theoretical predictions. Also, the viscosity divergence and the effects of viscoelasticity near the critical point of xenon were studied extensively in two microgravity experiments. In addition, the unexpected critical speeding up of the equilibrium time constant (piston effect) near a liquid-gas critical point observed on the ground and in early rocket experiments was studied extensively in several microgravity experiments. Many unusual features of this piston effect were observed and explained in these microgravity studies with convection suppressed. The MISTE and COEX experiments are planned to take advantage of the results obtained from these previous studies in order to perform simultaneous thermodynamic measurements throughout the liquid-gas critical region.

In parallel with the flight experimental activities described in this review, there have been many new studies in ground-based laboratories. Some of these ongoing experiments could lead to future microgravity studies. In the $O(1)$ class, there have been theoretical studies of finite-size effects (Chen and Dohm, 1999a, 1999b; Dantchev, 2001; Dantchev and Rudnick, 2001), but experimental validation has been very difficult due to the gravity effect. The interpretation of the Yang-Yang relation derived many years ago (Yang and Yang, 1964) has been reconsidered theoretically and experimentally in recent years (Fisher and Orkoulas, 2000; Orkoulas *et al.*, 2000); however, both impurity and gravity effects have significantly hampered experimental studies (Wyczalkowska *et al.*, 2002; Anisimov *et al.*, 2004). A sensitive technique for measuring the bulk viscosity of xenon near its critical point has recently been developed (Gillis *et al.*, 2004, 2005), but the gravitational stratification will interfere with the data analysis very near the transition. There have also been new attempts to reduce the gravity effect on the ground by using a steady heat flow technique that produces a density gradient opposite to that of gravity. Magnetic levitation techniques employing diamagnetic fluid systems have also been used to reduce gravity effects (Lipa, 2004; Beysens *et al.*, 2005).

In the $O(2)$ universality class, there have been two successful flight experiments, LPE and CHeX, that measured the specific heat near the ^{4}He lambda point. These studies were able to make measurements to within $t = 10^{-9}$ of the transition in a homogeneous sample. The LPE experiment provided the most accurate determination of any critical exponent to date and challenged the theoretical community to improve the quality of existing theoretical predictions. These experiments have opened up the possibility of performing studies of other properties very close to the lambda transition and for measurements with correlation lengths of 50 μm or more, regimes inaccessible on the ground.

Further measurements of static properties are of course possible, allowing improved testing of universality along the lambda lines. Also, very high-precision measurements could put improved bounds on models that invoke logarithmic corrections to standard scaling.

TABLE IX. Summary of important previous microgravity experiments and experiments that were or may be planned for future space flights.

Platform/ Experiment	Description	Date flown	Section discussed
TEXUS			
Nos. 11 and 13	$O(1)$, Mixture, phase separation	1988	III.A and IV.G
No. 25	$O(1)$, CO_2, piston effect	1990	III.A and IV.G
FREE FLYER			
EURECA-I	$O(1)$, SF_6, Critical adsorption	1992	IV.G
SHUTTLE			
D-1/HOLOP	$O(1)$, SF_6, thermal equilibrium	1985	IV.B
D-1/HPT	$O(1)$, SF_6, C_V	1985	IV.B
LPE	$O(2)$, ^{4}He, C_P	1992	V.A
IML-1/CPF	$O(1)$, SF_6, Mixture, nucleation, and growth	1992	III.B and IV.G
D-2/HPT-HYDRA	$O(1)$, SF_6, Piston effect, C_V	1993	IV.B and IV.G
IML-2/CPF	$O(1)$, SF_6, Piston effect, electrostriction	1994	III.B, IV.A, and IV.G
USMP-2/ZENO	$O(1)$, Xe, Turbidity	1994	IV.E
USMP-3/ZENO-2	$O(1)$, Xe, Turbidity	1996	IV.E
CHeX	$O(2)$, ^{4}He, C_P, Finite size (planar)	1997	VII.A
CVX	$O(1)$, Xe, Viscosity	1997	IV.F
CVX-2	$O(1)$, Xe, Viscosity	2003	IV.F
MIR			
ALICE-2	$O(1)$, SF_6, Two-phase fluid, thermal equilibrium	1999	IV.G
ALICE-2	$O(1)$, SF_6 & CO_2, Critical boiling	1999	IV.G
ISS			
BEST	$O(2)$, ^{4}He, κ, Finite size	Future	VII.B
CHeX-2	$O(2)$, ^{4}He C_P, Finite size (pores)	Future	VII.A
COEX	$O(1)$, ^{3}He, Coexistence curve	Future	IV.D
CP	$O(2)$, ^{4}He, C_P	Future	V.D
CQ	$O(2)$, ^{4}He, $C_V(Q)$	Future	V.B
DYNAMX	$O(2)$, ^{4}He, $\kappa(Q)$	Future	V.D
EXACT	$O(1)/O(2)$, Tricritical, ^{3}He-^{4}He mixture	Future	VI
MISTE	$O(1)$, ^{3}He, C_V, κ_T, PVT	Future	IV.B and C
SUE	$O(2)$, ^{4}He, Superfluid density	Future	V.C
DECLIC/ALI/HTI	$O(1)$, CO_2, SF_6, and Xe, Critical boiling, piston effect, critical fluctuations	Future	IV.G and Summary
FSL	$O(1)$, TBD	Future	Summary

More finite-size measurements in well-defined geometries could also be performed, for example, with cylindrical confinement. Recent measurements (Kimball *et al.*, 2004) showing possible edge and corner confinement effects in well-defined geometries could also benefit from the space environment where long correlation lengths allow the use of larger-scale confining systems. It is also possible that the properties of boundary layers could be investigated using first- and second-sound propagation in narrow channels, and in thermal gradient measurements across the critical component of the thermal boundary resistance. Beyond static critical and finite-size phenomena, heat-transport measurements have been planned near the He I/He II fluid interface as part of DYNAMX, and future measurements of critical viscosity near this interface may be conducted as well. The BEST experiment would measure finite-size effects in heat transport in cylindrical and slab geometries near the superfluid transition. The tricritical point at the intersection of the phase separation and lambda lines in ^{3}He-^{4}He mixtures represents an interesting system where the predictions for the critical exponents and amplitude ratios are exactly calculable without the use of sophisticated theoretical techniques to obtain perturbative corrections. The EXACT microgravity experiment (Larson, 2000) has been designed to obtain specific-heat and second-sound measurements near the tricritical

point, thus permitting the critical exponents of the superfluid fraction and the specific heat to be obtained in this system. Other measurements, such as second-sound propagation into the interface layer and the possible detection of interface-related second-sound modes (Weichman *et al.*, 1998), are best suited for microgravity. Magnetic levitation devices have also been developed to reduce the effect of gravity on liquid helium for studies of the $O(2)$ universality class, and some data have been obtained (Liu, Larson, and Israelsson, 2000). At present, this technique is somewhat limited but it could provide valuable Earth-based data regarding the experimental definition of future low-gravity experiments. If suitable bolometers working at high magnetic fields could be developed, some progress toward the second-sound-related experiments mentioned above could be made. Table IX provides a summary of previous microgravity flight experiments and those that were or are planned for future space flights.

There have also been some problems in the critical phenomena experiments in microgravity to date. Because of the cost and time involved in preparing these flight experiments, generally researchers have only had one flight opportunity to successfully perform their investigation. Complicated experiments typically encounter many technical problems during their development, and extensive ground-based testing is usually performed before an experiment is flown in space. However, the effects of the space environment on Earth-orbiting experiments cannot always be anticipated. The research community is awaiting the day when there will be many flight opportunities so that experiments can be performed in low gravity and returned to Earth quickly. A shorter turnaround time would clear the backlog of proposed experiments and permit more reflights if necessary, resulting in an enhanced scientific benefit. In parallel, it is also necessary to reduce the cost of the experiments, perhaps by reducing the penalty for failure.

As shown in Table IX, worldwide, a substantial number of microgravity studies have been performed to date. ESA is developing facilities and experiments for future flights on the ISS. There are several critical phenomena experiments planned for the DECLIC facility (Cambon *et al.*, 2004). Initial ISS studies in the ALICE-Like Insert (ALI) to the DECLIC facility should allow for direct observation of the boiling crisis and critical density fluctuations in near-ambient fluids (CO_2, SF_6, and Xe). The High Temperature Insert (HTI) is dedicated to the study of the piston effect and the coupling between hydrodynamics and chemical reactions in the highly compressible supercritical region of water. The FSL facility is also planned to be integrated into the Columbus module that is expected to be installed in the ISS in the 2007–2008 time frame. While there are no critical phenomena experiments initially planned for FSL, this facility is capable of performing these types of studies in the future.

As to the question of the correctness with the current paradigm on critical phenomena, it seems fair to say that the predictions of the RG theory have been reasonably well validated. Nevertheless, the theory is based on some "seemingly innocuous" assumptions that will stand or fall based on more sophisticated experiments.

REFERENCES

Adriaans, M. J., T. C. P. Chui, M. Ndesandjo, D. R. Swanson, and J. A. Lipa, 1991, Physica B **169**, 455.

Adriaans, M. J., D. R. Swanson, and J. A. Lipa, 1994, Physica B **194-196**, 733.

Agayan, V. A., M. A. Anisimov, and J. V. Sengers, 2001, Phys. Rev. E **64**, 026125.

Aharony, A., 1974, Phys. Rev. B **9**, 2107.

Ahlers, G., 1968a, Phys. Rev. **171**, 275.

Ahlers, G., 1968b, Phys. Rev. Lett. **21**, 1159.

Ahlers, G., 1971, Phys. Rev. A **3**, 696.

Ahlers, G., 1973, Phys. Rev. A **8**, 530.

Ahlers, G., 1976, in *The Physics of Liquid and Solid Helium*, Vol. 1, edited by K. H. Bennemann and J. B. Ketterson (Wiley, New York), p. 85.

Ahlers, G., 1991, J. Low Temp. Phys. **84**, 173.

Ahlers, G., 1999, J. Low Temp. Phys. **115**, 143.

Ahlers, G., 2000, The Science Requirements Document for BEST, JPL Document Number D-18651.

Ahlers, G., 2006, private communication.

Ahlers, G., and R. V. Duncan, 1988, Phys. Rev. Lett. **61**, 846.

Ahlers, G., and D. Greywall, 1972, Phys. Rev. Lett. **29**, 849.

Albright, P. C., Z. Y. Chen, and J. V. Sengers, 1987, Phys. Rev. B **36**, 877.

Albright, P. C., J. V. Sengers, J. F. Nicoll, and M. Ley-Koo, 1986, Int. J. Thermophys. **7**, 75.

Amiroudine, S., J. Ouazzani, P. Carlès, and B. Zappoli, 1997, Eur. J. Mech. B/Fluids **16**, 665.

Amiroudine, S., and B. Zappoli, 2003, Phys. Rev. Lett. **90**, 105303.

Andrews, T., 1869, Philos. Trans. R. Soc. London **159**, 575.

Anisimov, M. A., 1991, *Critical Phenomena in Liquids and Liquid Crystals* (Gordon & Breach, Philadelphia).

Anisimov, M. A., E. E. Gorodetskii, V. D. Kulikov, and J. V. Sengers, 1995a, Phys. Rev. E **51**, 1199.

Anisimov, M. A., E. E. Gorodetskii, V. D. Kulikov, and J. V. Sengers, 1995b, Physica A **220**, 227.

Anisimov, M. A., S. B. Kiselev, J. V. Sengers, and S. Tang, 1992, Physica A **188**, 487.

Anisimov, M. A., F. Zhong, and M. Barmatz, 2004, J. Low

Temp. Phys. **137**, 69.

Avdeeva, G. M., and A. A. Migdal, 1972, JETP Lett. **16**, 178.

Baddar, H., G. Ahlers, K. Kuehn, and H. Fu, 2000, J. Low Temp. Phys. **119**, 1.

Bagatskii, M. I., A. V. Voronel, and V. G. Gusak, 1962, Sov. Phys. JETP **16**, 517.

Bagnuls, C., and C. Bervillier, 1984, J. Phys. (France) Lett. **45**, L95.

Bagnuls, C., and C. Bervillier, 1985, Phys. Rev. B **32**, 7209.

Bagnuls, C., and C. Bervillier, 2002a, e-print hep-th/0112209.

Bagnuls, C., and C. Bervillier, 2002b, Phys. Rev. E **65**, 066132.

Bagnuls, C., C. Bervillier, and Y. Garrabos, 1984, J. Phys. (France) Lett. **45**, L127.

Bagnuls, C., C. Bervillier, D. I. Meiron, and B. G. Nickel, 1987, Phys. Rev. B **35**, 3585.

Bagnuls, C., C. Bervillier, D. I. Meiron, and B. G. Nickel, 2002, Phys. Rev. B **65**, 149901.

Bailly, D., and B. Zappoli, 2000, Phys. Rev. E **62**, 2353.

Barber, M. N., 1983, in *Phase Transitions and Critical Phenomena*, edited by C. Domb and J. Lebowitz (Academic, New York), Vol. 8, p. 146.

Barmatz, M., 1999, The Science Requirements Document for MISTE, JPL Document Number D-17083.

Barmatz, M., I. Hahn, and F. Zhong, 1998, J. Low Temp. Phys. **113**, 891.

Barmatz, M., I. Hahn, and F. Zhong, 2001, in *Proceedings of the International Space Station Utilization 2001 Conference*, American Institute of Aeronautics and Astronautics, paper no. AIAA-2001-4933.

Barmatz, M., I. Hahn, F. Zhong, M. A. Anisimov, and V. A. Agayan, 2000, J. Low Temp. Phys. **121**, 633.

Barmatz, M., P. C. Hohenberg, and A. Kornblit, 1975, Phys. Rev. B **12**, 1947.

Barmatz, M., F. Zhong, and I. Hahn, 2000, Physica B **284**, 206.

Barmatz, M., F. Zhong, and I. Hahn, 2003 in *Proceedings of the 2002 NASA/JPL Workshop on Fundamental Physics in Microgravity*, JPL Publication 01-10, p. 86.

Barmatz, M., F. Zhong, and A. Shih, 2004, Int. J. Thermophys. **25**, 1667.

Barmatz, M., F. Zhong, and A. Shih, 2005, Int. J. Thermophys. **26**, 921.

Bartscher, C., and J. Straub, 2002, Int. J. Thermophys. **23**, 77.

Batchelor, G. K., 1970, *The Theory of Homogeneous Turbulence* (Cambridge University Press, New York).

Behringer, R. P., and H. Meyer, 1982, J. Low Temp. Phys. **46**, 407.

Behringer, R. P., A. Onuki, and H. Meyer, 1990, J. Low Temp. Phys. **81**, 71.

Berg, R. F., 1993, Phys. Rev. E **48**, 1799.

Berg, R. F., 1995, Rev. Sci. Instrum. **66**, 4665.

Berg, R. F., 2004, J. Rheol. **48**, 1365.

Berg, R. F., and M. R. Moldover, 1990, J. Chem. Phys. **93**, 1926.

Berg, R. F., M. R. Moldover, and G. A. Zimmerli, 1999a, Phys. Rev. Lett. **82**, 920.

Berg, R. F., M. R. Moldover, and G. A. Zimmerli, 1999b, Phys. Rev. E **60**, 4079.

Berg, R. F., G. A. Zimmerli, and M. R. Moldover, 1998, Int. J. Thermophys. **19**, 481.

Bervillier, C., 1986, Phys. Rev. B **34**, 8141.

Beysens, D., D. Chatain, P. Evesque, and Y. Garrabos, 2005, Phys. Rev. Lett. **95**, 034502.

Beysens, D., and Y. Garrabos, 2001, Acta Astronaut. **48**, 629.

Beysens, D., Y. Garrabos, V. S. Nikolayev, C. Lecoutre-Chabot, J.-P. Delville, and J. Hegseth, 2002, Europhys. Lett. **59**, 245.

Beysens, D., Y. Garrabos, R. Wunenburger, and C. Lecoutre, 2002, Physica A **314**, 427.

Beysens, D., P. Guenoun, and F. Perrot, 1988, Phys. Rev. A **38**, 4173.

Bhattacharjee, J. K., 1996, Phys. Rev. Lett. **77**, 1524.

Bhattacharjee, J. K., and R. A. Ferrell, 1983, Phys. Rev. A **27**, 1544.

Bhattacharjee, J. K., R. A. Ferrell, R. S. Basu, and J. V. Sengers, 1981, Phys. Rev. A **24**, 1469.

Bhattacharyya, S., and J. K. Bhattacharjee, 2000, Phys. Rev. B **61**, 5899.

Binder, K., 1983, in *Phase Transitions and Critical Phenomena*, edited by C. Domb and J. Lebowitz (Academic, New York), Vol. 8, p. 1.

Binney, J. J., N. J. Dowrick, A. J. Fisher, and M. E. J. Newman, 1993, *The Theory of Critical Phenomena. An Introduction to the Renormalization Group* (Clarendon, Oxford).

Bonetti, M., F. Perrot, D. Beysens, and Y. Garrabos, 1994, Phys. Rev. E **49**, R4779.

Boukari, H., M. E. Briggs, J. N. Shaumeyer, and R. W. Gammon, 1990, Phys. Rev. Lett. **65**, 2654.

Boukari, H., R. Pego, and R. W. Gammon, 1995, Phys. Rev. E **52**, 1614.

Boukari, H., J. N. Shaumeyer, M. E. Briggs, and R. W. Gammon, 1990, Phys. Rev. A **41**, 2260.

Brout, R., 1965, *Phase Transitions* (Benjamin, New York).

Brown, G. R., and H. Meyer, 1972, Phys. Rev. A **6**, 364.

Buckingham, M. J., C. Edwards, and J. A. Lipa, 1973, Rev. Sci. Instrum. **44**, 1167.

Buckingham, M. J., and W. M. Fairbank, 1961, *Progress in Low Temperature Physics* (North-Holland, Amsterdam), Vol. 3, p. 80.

Buckingham, M. J., and J. D. Gunton, 1969, Phys. Rev. **178**, 848.

Cagniard de la Tour, C., 1822, Ann. Chim. Phys. **21**, 127, 178.

Cambon, G., B. Zappoli, S. Barde, F. Duclos, R. Lauver, R. Marcout, G. Raymond, D. Beysens, Y. Garrabos, C. Lecoutre, B. Billia, N. Bergeon, and N. Mangelinck, 2004, *55th International Astronautical Congress*, paper IAC-IAF/IAA-04-J.5.03.

Cambon, G., B. Zappoli, R. Marcourt, Y. Garrabos, F. Cansell, D. Beysens, B. Billia, and H. Jamgotchian, 1997, Acta Astronaut. **41**, 447.

Campostrini, M., M. Hasenbusch, A. Pelissetto, P. Rossi, and E. Vicari, 2001, Phys. Rev. B **63**, 214503.

Campostrini, M., A. Pelissetto, P. Rossi, and E. Vicari, 2002, Phys. Rev. E **65**, 066127.

Cannell, D. S., 1975, Phys. Rev. A **12**, 225.

Cardy, J. L, 1996, *Scaling and Renormalization in Statistical Physics* (Cambridge University Press, Cambridge).

Carlès, P., 1998, Phys. Fluids **10**, 2164.

Carlès, P., 2000, Physica D **147**, 36.

Carlès, P., and K. Dadzie, 2005, Phys. Rev. E **71**, 066310.

Carlès, P., F. Zhong, M. Weilert, and M. Barmatz, 2005, Phys. Rev. E **71**, 041201.

Chang, M.-C., and A. Houghton, 1980, Phys. Rev. B **21**, 1881.

Chen, J. H., M. E. Fisher, and B. G. Nickel, 1982, Phys. Rev. Lett. **48**, 630.

Chen, T. P., and F. M. Gasparini, 1978, Phys. Rev. Lett. **40**, 331.

Chen, X. S., and V. Dohm, 1999a, Eur. Phys. J. B **7**, 183.

Chen, X. S., and V. Dohm, 1999b, Eur. Phys. J. B **10**, 687.

Chen, X. S., and V. Dohm, 2000, Eur. Phys. J. B **15**, 283.

Chen, X. S., and V. Dohm, 2002, Phys. Rev. E **66**, 016102.

Chen, X. S., and V. Dohm, 2003, Physica B **329**, 202.

Chen, X. S., and V. Dohm, 2004, Phys. Rev. E **70**, 056136.

Chen, Z. Y., A. Abbaci, S. Tang, and J. V. Sengers, 1990, Phys. Rev. A **42**, 4470.

Chen, Z. Y., P. C. Albright, and J. V. Sengers, 1990, Phys. Rev. A **41**, 3161.

Chui, T. C. P., D. L. Goodstein, A. W. Harder, and R. Mukhopadhyay, 1996, Phys. Rev. Lett. **77**, 1793.

Chui, T. C. P., D. R. Swanson, M. J. Adriaans, J. A. Nissen, and J. A. Lipa, 1992, Phys. Rev. Lett. **76**, 944.

Coopersmith, M. H., 1968a, Phys. Rev. **167**, 478.

Coopersmith, M. H., 1968b, Phys. Rev. Lett. **20**, 432.

Cowan, M., J. Rudnick, and M. Barmatz, 1996, Phys. Rev. E **53**, 4490.

Dahl, D., and M. R. Moldover, 1972, Phys. Rev. A **6**, 1915.

Dantchev, D., 2001, Eur. Phys. J. B **23**, 211.

Dantchev, D., and J. Rudnick, 2001, Eur. Phys. J. B **21**, 251.

Day, P. K., W. A. Moeur, S. McCready, D. Sergatskov, F-C. Liu, and R. V. Duncan, 1998, Phys. Rev. Lett. **81**, 2474.

de Bruijn, R., R. J. J. van Diest, T. D. Karapantsios, A. C. Michels, W. A. Wakeham, and J. P. M. Trusler, 1997, Physica A **242**, 119.

de Gennes, P. G., and J. Prost, 1993, *The Physics of Liquid Crystals*, 2nd ed. (Oxford University Press, Oxford).

Dingus, M., F. Zhong, and H. Meyer, 1986, J. Low Temp. Phys. **65**, 185.

Dobson, J. F., 1995, in *Density Functional Theory*, edited by E. Gross and R. Dreizler, NATO Advanced Study Institute Series B, Vol. 337 (Plenum, New York), p. 397.

Dohm, V., 1985a, Z. Phys. B: Condens. Matter **60**, 61.

Dohm, V., 1985b, Z. Phys. B: Condens. Matter **61**, 193.

Dohm, V., 1987, J. Low Temp. Phys. **69**, 51.

Dohm, V., 1991, Phys. Rev. B **44**, 2697.

Dohm, V., 1993, Phys. Scr., T **49**, 46.

Dohm, V., 2006, Phys. Rev. B **73**, 092503.

Dohm, V., and R. Folk, 1980, Z. Phys. B: Condens. Matter **40**, 79.

Dohm, V., and R. Folk, 1981, Phys. Rev. Lett. **46**, 349.

Dohm, V., and R. Haussmann, 1994, Physica B **197**, 215.

Domb, C., 1996, *The Critical Point: A Historical Introduction to the Modern Theory of Critical Phenomena* (Taylor and Francis, London).

Duncan, R. V., 2000, The Science Requirements Document for DYNAMX, JPL Document No. D-18698.

Duncan, R. V., G. Ahlers, and V. Steinberg, 1987, Phys. Rev. Lett. **58**, 377.

Duncan, R. V., G. Ahlers, and V. Steinberg, 1988, Phys. Rev. Lett. **60**, 1522.

Duncan, R. V., P. K. Day, S. McCready, W. A. Moeur, F-C. Liu, and D. Sergatskov, 1998, J. Low Temp. Phys. **113**, 861.

Duncan, R. V., D. A. Sergatskov, A. V. Babkin, S. T. P. Boyd, R. C. Nelson, P. K. Day, J. Dooley, and D. Elliott, 2001, in *Proceedings of the 2nd Pan Pacific Basin Workshop on Microgravity Science*, edited by N. Ramachandran and M. Lee (Institute of Aeronautics and Astronautics, Pasadena, CA).

Duncan, R. V., D. A. Sergatskov, S. T. P. Boyd, S. S. McCready, T. D. McCarson, A. V. Babkin, P. K. Day, F-C. Liu, and D. Elliott, 2000, J. Low Temp. Phys. **119**, 265.

Edwards, C., J. A. Lipa, and M. J. Buckingham, 1968, Phys. Rev. Lett. **20**, 496.

Edwards, C., L. Marhenke, and J. A. Lipa, 1996, Czech. J. Phys. **46**, Suppl. S5, 2755.

El Khouri, L., and P. Carlès, 2002, Phys. Rev. E **66**, 066309.

Eyal, G., M. Moshe, S. Nishigaki, and J. Zinn-Justin, 1996, Nucl. Phys. B **470**, 369.

Ferrell, R. A., and J. K. Bhattacharjee, 2000, J. Low Temp. Phys. **119**, 283.

Ferrell, R. A., and H. Hao, 1993, Physica A **197**, 23.

Ferrell, R. A., N. Menyhard, H. Schmidt, F. Schwabl, and P. Szepfalusy, 1967, Phys. Rev. Lett. **18**, 891.

Ferrell, R. A., N. Menyhard, H. Schmidt, F. Schwabl, and P. Szepfalusy, 1968a, Phys. Lett. **24A**, 493.

Ferrell, R. A., N. Menyhard, H. Schmidt, F. Schwabl, and P. Szepfalusy, 1968b, Ann. Phys. (N.Y.) **47**, 565.

Ferrell, R. A., and S. I. Mukhin, 2000, J. Low Temp. Phys. **119**, 277.

Ferrell, R. A., and S. I. Mukhin, 2001, Int. J. Thermophys. **22**, 1411.

Fisher, M. E., 1964, Int. J. Thermophys. **7C**, 1.

Fisher, M. E., 1966, Phys. Rev. Lett. **16**, 11.

Fisher, M. E., 1969, Phys. Rev. **180**, 594.

Fisher, M. E., 1971, in *Proceedings of the International School of Physics "Enrico Fermi," Course LI*, edited by M. S. Green (Academic, New York), p. 1.

Fisher, M. E., 1974, Rev. Mod. Phys. **46**, 597.

Fisher, M. E., 1998, Rev. Mod. Phys. **70**, 653.

Fisher, M. E., and P. G. de Gennes, 1978, C. R. Seances Acad. Sci., Ser. B **287**, 207.

Fisher, M. E., and G. Orkoulas, 2000, Phys. Rev. Lett. **85**, 696.

Fisher, M. E., and S.-Y. Zinn, 1998, J. Phys. A **31**, L629.

Fröhlich, T., P. Guenoun, M. Bonetti, F. Perrot, D. Beysens, Y. Garrobos, B. Le Neindre, and P. Bravais, 1996, Phys. Rev. E **54**, 1544.

Furukawa, A., and A. Onuki, 2002, Phys. Rev. E **66**, 016302.

Gammon, R. W., 1987, in *Critical Fluid Light Scattering*, in *The Nation's Future Material Needs*, edited by T. Lynch, J. Persh, T. Wolf, and N. Rupert (Soc. Adv. Mater. Process Eng., Covina, CA) *Proceedings of the 19th International Technical Conference of the Society for the Advancement of Material and Process Engineering* (SAMPE).

Gammon, R. W., 1998, *Zeno: A Critical-Fluid Light Scattering Experiment*, Final Technical Report, Contract NAS3-25370.

Gammon, R. W., J. N. Shaumeyer, M. E. Briggs, H. Boukari, D. Gent, and R. A. Wilkinson, 1996, *Highlights of the Zeno Results from the USMP-2 Mission, Second United States Microgravity Payload: One Year Report*, NASA Technical Memorandum 4737 (NASA, Marshall Space Flight Center), p. 5.

Garcia, R., and M. H. W. Chan, 1999, Phys. Rev. Lett. **83**, 1187.

Garcia, R., and M. H. W. Chan, 2002, Phys. Rev. Lett. **88**, 086101.

Garrabos, Y., 1986, J. Phys. (Paris) **47**, 197.

Garrabos, Y., M. Bonetti, D. Beysens, F. Perrot, T. Fröhlich, P. Carlès, and B. Zappoli, 1998, Phys. Rev. E **57**, 5665.

Garrabos, Y., C. Chabot, R. Wunenburger, J.-P. Delville, and D. Beysens, 1999, J. Chim. Phys. Phys.-Chim. Biol. **96**, 1066.

Garrabos, Y., A. Dejoan, C. Lecoutre-Chabot, D. Beysens, V. Nikolayev, and R. Wunwnburger, 2001, J. Phys. IV France **11**, Pr6-23.

Garrabos, Y., C. Lecoutre-Chabot, J. Hegseth, V. S. Nikolayev, D. Beysens, and J.-P. Delville, 2001, Phys. Rev. E **64**, 051602.

Garrabos, Y., B. Le Neindre, P. Guenoun, B. Khalil, and D. Beysens, 1992, Europhys. Lett. **19**, 491.

Garrabos, Y., B. Le Neindre, P. Guenoun, F. Perrot, and D. Beysens, 1993, Microgravity Sci. Technol. **6**, 110.

Garrabos, Y., B. Le Neindre, R. Wunenburger, C. Lecourte-Chabot, and D. Beysens, 2002, Int. J. Thermophys. **23**, 997.

Gasparini, F. M., T. P. Chen, and B. Bhattacharyya, 1981, Phys. Rev. B **23**, 5797.

Gasparini, F. M., and A. A. Gaeta, 1978, Phys. Rev. B **17**, 1466.

Gasparini, F. M., and S. Mhlanga, 1986, Phys. Rev. B **33**, 5066.

Gasparini, F. M., and M. R. Moldover, 1975, Phys. Rev. B **12**, 93.

Gasparini, F. M., and I. Rhee, 1992, Prog. Low Temp. Phys. **13**, 1.

George, M. J., and J. J. Rehr, 1984, Phys. Rev. Lett. **53**, 2063.

Gerber, P. R., 1975, J. Phys. A **8**, 67.

Gillis, K. A., I. I. Shinder, and M. R. Moldover, 2004, Phys. Rev. E **70**, 021201.

Gillis, K. A., I. I. Shinder, and M. R. Moldover, 2005, Phys. Rev. E **72**, 051201.

Gitterman, M., and V. Steinberg, 1970, J. Appl. Math. Mech. **34**, 305.

Goldner, L. S., N. Mulders, and G. Ahlers, 1993, J. Low Temp. Phys. **93**, 131.

Goodstein, D. L., 2002, The Science Requirements Document for CQ, JPL Document No. D-23026.

Gorter, C. J., and J. H. Mellink, 1949, Physica (Amsterdam) **5**, 285.

Gouy, G., 1892, C. R. Hebd. Seances Acad. Sci. **115**, 720.

Graf, E. H., D. M. Lee, and J. D. Reppy, 1967, Phys. Rev. Lett. **19**, 417.

Green, C. J., D. A. Sergatskov, and R. V. Duncan, 2005, J. Low Temp. Phys. **138**, 871.

Greywall, D., and G. Ahlers, 1973, Phys. Rev. A **7**, 2145.

Griffiths, R. B., 1965a, Phys. Rev. Lett. **14**, 623.

Griffiths, R. B., 1965b, J. Chem. Phys. **43**, 1958.

Griffiths, R. B., 1967, Phys. Rev. **158**, 176.

Griffiths, R. B., 1970a, Phys. Rev. Lett. **24**, 715.

Griffiths, R. B., 1970b, Phys. Rev. Lett. **24**, 1479.

Griffiths, R. B., and J. C. Wheeler, 1970, Phys. Rev. A **2**, 1047.

Guenoun, P., R. Gastaud, F. Perrot, and D. Beysens, 1987, Phys. Rev. A **36**, 4876.

Guenoun, P., B. Khalil, D. Beysens, Y. Garrabos, F. Kammoun, B. Le Neindre, and B. Zappoli, 1993, Phys. Rev. E **47**, 1531.

Guggenheim, E. A., 1945, J. Chem. Phys. **13**, 253.

Guida, R., and J. Zinn-Justin, 1997, Nucl. Phys. B **489**, 626.

Guida, R., and J. Zinn-Justin, 1998, J. Phys. A **31**, 8103, and references therein.

Gutenberg, B., and C. F. Richter, 1954, *Seismicity of the Earth and Associated Phenomena* (Princeton University Press, Princeton, NJ).

Guth, A. H., and S. Y. Pi, 1982, Phys. Rev. Lett. **49**, 1110.

Güttinger, H., and D. S. Cannell, 1981, Phys. Rev. A **24**, 3188.

Habgood, H. W., and W. G. Schneider, 1954, Can. J. Phys. **32**, 98; 1954, Can. J. Phys. **32**, 164.

Hahn, I., 2002, The Science Requirements Document for COEX, JPL Document No. D-23024.

Hahn, I., M. Weilert, F. Zhong, and M. Barmatz, 2004, J. Low Temp. Phys. **137**, 579.

Hahn, I., F. Zhong, M. Barmatz, R. Haussmann, and J. Rudnick, 2001, Phys. Rev. E **63**, 055104(R).

Halperin, B. I., P. C. Hohenberg, and S. Ma, 1972, Phys. Rev. Lett. **29**, 1548.

Halperin, B. I., P. C. Hohenberg, and E. D. Siggia, 1974, Phys. Rev. Lett. **32**, 1289.

Halperin, B. I., P. C. Hohenberg, and E. D. Siggia, 1976, Phys. Rev. B **13**, 1299.

Hao, H., R. A. Ferrell, and J. K. Bhattacharjee, 2005, Phys. Rev. E **71**, 021201.

Harter, A. W., R. A. M. Lee, A. Chatto, X. Wu, T. C. P. Chui, and D. L. Goodstein, 2000, Phys. Rev. Lett. **84**, 2195.

Hasenbusch, M., 2001, Int. J. Mod. Phys. C **12**, 911.

Hasenbusch, M., and T. Török, 1999, J. Phys. A **32**, 6361.

Haupt, A., 1997, Ph.D. thesis (Technische Universität München).

Haupt, A., and J. Straub, 1999, Phys. Rev. E **59**, 1795.

Haussmann, R., 1999a, J. Low Temp. Phys. **114**, 1.

Haussmann, R., 1999b, Phys. Rev. B **60**, 12349.

Haussmann, R., and V. Dohm, 1991, Phys. Rev. Lett. **67**, 3404.

Haussmann, R., and V. Dohm, 1992a, Z. Phys. B: Condens. Matter **87**, 229.

Haussmann, R., and V. Dohm, 1992b, J. Low Temp. Phys. **89**, 445.

Haussmann, R., and V. Dohm, 1992c, Phys. Rev. B **46**, 6361.

Haussmann, R., and V. Dohm, 1994, Phys. Rev. Lett. **72**, 3060.

Haussmann, R., and V. Dohm, 1996, Czech. J. Phys. **46**, Suppl. S1, 171.

Hegseth, J., Y. Garrabos, V. S. Nikolayev, C. Lecoutre-Chabot, R. Wunenburger, and D. Beysens, 2002, Int. J. Thermophys. **23**, 89.

Hegseth, J., A. Oprisan, Y. Garrabos, V. S. Nikolayev, C. Lecoutre-Chabot, and D. Beysens, 2005, Phys. Rev. E **72**, 031602.

Heller, P., 1967, Rep. Prog. Phys. **30**, 731.

Hess, G. B., 1978, Phys. Rev. Lett. **40**, 1191.

Ho, J. T., and J. D. Litster, 1970, Phys. Rev. B **2**, 4523.

Hocken, R. J., and M. R. Moldover, 1976, Phys. Rev. Lett. **37**, 29.

Hohenberg, P. C, A. Aharony, B. J. Halperin, and E. D. Siggia, 1976, Phys. Rev. B **13**, 2986.

Hohenberg, P. C., and M. Barmatz, 1972, Phys. Rev. A **6**, 289.

Hohenberg, P. C., and B. I. Halperin, 1977, Rev. Mod. Phys. **49**, 435.

Houessou, C., P. Guenoun, R. Gastaud, F. Perrot, and D. Beysens, 1985, Phys. Rev. A **32**, 1818.

Howald, C., X. Qin, H. S. Nham, and H. Meyer, 1992, J. Low Temp. Phys. **86**, 375.

Ikier, C., H. Klein, and D. Woermann, 1996a, Ber. Bunsenges. Phys. Chem. **100**, 1308.

Ikier, C., H. Klein, and D. Woermann, 1996b, J. Colloid Interface Sci. **178**, 368.

Ikushima, A., and G. Terui, 1973, J. Low Temp. Phys. **10**, 397.

Itzykson, C., and J. M. DrouHe, 1989, *Statistical Field Theory* (Cambridge University Press, Cambridge).

Jackiw, R., 1972, Phys. Today **25**, 23.

Jasch, F., and H. Kleinert, 2001, J. Math. Phys. **42**, 52.

Jones, B. J. T., V. J. Martinez, E. Saar, and V. Trimble, 2004, Rev. Mod. Phys. **76**, 1211.

Josephson, B. D., 1967, Proc. Phys. Soc. **88**, 1053.

Kadanoff, L. P., 1966, Physica (Amsterdam) **2**, 263.

Kadanoff, L. P., 1971, in *Critical Phenomena, Proceedings of the Enrico Fermi International School of Physics, Course LI*, edited by M. S. Green (Academic, New York), p. 100.

Kadanoff, L. P., 1976, in *Phase Transitions and Critical Phenomena*, edited by C. Domb and M. S. Green (Academic, New York), Vol. 5A, Chap. 1.

Kadanoff, L. P., W. Götze, D. Hamblen, R. Hecht, E. A. S. Lewis, V. V. Palciauskas, M. Rayl, J. Swift, D. Aspnes, and J.

Kane, 1967, Rev. Mod. Phys. **39**, 395.

Kahn, A. M., and G. Ahlers, 1995, Phys. Rev. Lett. **74**, 944.

Kaupuzs, J., 2001, Ann. Phys. (Leipzig) **10**, 299.

Kaupuzs, J., 2005, Eur. Phys. J. B **45**, 459.

Kerrisk, J., and W. E. Keller, 1967, Bull. Am. Phys. Soc. **12**, 550.

Kerrisk, J., and W. E. Keller, 1969, Phys. Rev. **177**, 341.

Kimball, M. O., S. Mehta, and F. M. Gasparini, 2000, J. Low Temp. Phys. **121**, 29.

Kimball, M. O., K. P. Mooney, and F. M. Gasparini, 2004, Phys. Rev. Lett. **92**, 115301.

Klein, H., and B. Feuerbacher, 1987, Phys. Lett. A **123**, 183.

Klein, H., G. Schmitz, and D. Woermann, 1991, Phys. Rev. A **43**, 4562.

Kleinert, H., 1999, Phys. Rev. D **60**, 085001.

Kleinert, H., and V. Schulte-Frohlinde, 2001, *Critical Properties of φ^4 Theories* (World Scientific, Singapore).

Kleinert, H., and B. Van den Bossche, 2001, Phys. Rev. E **63**, 056113.

Kleinert, H., and V. I. Yukalov, 2005, Phys. Rev. E **71**, 026131.

Klemme, B. J., M. J. Adriaans, P. K. Day, D. A. Sergatskov, T. L. Aselage, and R. V. Duncan, 1999, J. Low Temp. Phys. **116**, 133.

Kobayashi, H., T. Takenouchi, M. Ishikawa, K. Honda, J. Kawai, M. Matsumoto, M. Sorai, M. Ohnishi, S. Yoshihara, M. Sakurai, and Y. Miura, 2004, in *Advances in the Astronautical Sciences*, Vol. 117, *Space Activities and Cooperation Contributing to all Pacific Basin Countries, 10th International Conference of Pacific Basin Societies*, edited by Peter M. Bainum, Li Furong, and Takashi Nakajima, pp. 809 and 810.

Kolmogorov, A. N., 1941, C. R. Acad. Sci. URSS **30**, 301.

Kosterlitz, J. M., and D. J. Thouless, 1973, J. Phys. C **6**, 1181.

Krech, M., and S. Dietrich, 1991, Phys. Rev. Lett. **66**, 345.

Krech, M., and S. Dietrich, 1992, Phys. Rev. A **46**, 1922.

Krech, M., and D. P. Landau, 1999, Phys. Rev. B **60**, 3375.

Kuehn, K., S. Mehta, H. Fu, E. Genio, D. Murphy, F-C Liu, Y. Liu, and G. Ahlers, 2002, Phys. Rev. Lett. **88**, 095702-1.

Lammerzahl, C., G. Ahlers, N. Ashby, M. Barmatz, P. L. Biermann, H. Dittus, V. Dohm, R. Duncan, K. Gibble, J. Lipa, N. Lockerbie, N. Mulders, and C. Salomon, 2004, Gen. Relativ. Gravit. **36**, 615.

Landau, L D., 1937, Phys. Z. Sowjetunion **11**, 26.

Lange, B. O., 1964, AIAA J. **2**, 1590.

Larin, S. A., M. Mönnigmann, M. Strösser, and V. Dohm, 1998, Phys. Rev. B **58**, 3394.

Larson, M., 2000, The Science Requirements Document for EXACT, JPL No. D-18589.

Larson, M., A. Croonquist, G. J. Dick, and Y. M. Liu, 2003, Physica B **329**, 1588.

Larson, M., J. Panek, A. Nash, and N. Mulders, 2000, J. Low Temp. Phys. **121**, 653.

Lee, R. A. M., A. Chatto, D. A. Sergatskov, A. V. Babkin, S. T. P. Boyd, A. M. Churilov, T. D. McCarson, T. C. P. Chui, P. K. Day, R. V. Duncan, and D. L. Goodstein, 2004, J. Low Temp. Phys. **134**, 495.

Lee, R. A. M., R. V. Duncan, A. W. Harter, A. Chatto, T. C. P. Chui, P. K. Day, and D. L. Goodstein, 2002, IEEE Aerospace Conference, Paper 2.0103, pp. 1–31.

Lee, T. D., and C. N. Yang, 1952, Phys. Rev. **87**, 410.

Le Guillou, J. C., and J. Zinn-Justin, 1987, J. Phys. (Paris) **48**, 19.

Leiderer, P., and W. Bosch, 1980, Phys. Rev. Lett. **45**, 727.

Leiderer, P., D. R. Watts, and W. W. Webb, 1974, Phys. Rev. Lett. **33**, 483.

Levelt Sengers, J. M. H., 1975, in *Experimental Thermodynamics*, edited by B. le Neindre and B. Vodar (Butterworths, London), Vol. 2, Chap. 14.

Levelt Sengers, A., R. Hocken, and J. V. Sengers, 1977, Phys. Today **30** (12), 42.

Lifshitz, I. M., and V. V. Slyosov, 1961, J. Phys. Chem. Solids **19**, 35.

Lipa, J., 2003, The Science Requirements Document for SUMO, Stanford Document No. SUMO-001.STR.

Lipa, J., 2004, NASA/CP 2004-213205, Vol. 2, p. 262.

Lipa, J. A., and T. C. P. Chui, 1983, Phys. Rev. Lett. **51**, 2291.

Lipa, J. A., T. C. P. Chui, J. A. Nissen, and D. R. Swanson, 1992, Temp.: Its Meas. Control Sci. Ind. **6**, 949.

Lipa, J. A., M. Coleman, and D. A. Strieker, 2001, J. Low Temp. Phys. **124**, 443.

Lipa, J. A., C. Edwards, and M. J. Buckingham, 1970, Phys. Rev. Lett. **25**, 1086.

Lipa, J. A., C. Edwards, and M. J. Buckingham, 1977, Phys. Rev. A **15**, 778.

Lipa, J. A., B. C. Leslie, and T. C. Wallstrom, 1981, Physica B & C **107**, 331.

Lipa, J. A., and Q. Li, 1996, Czech. J. Phys. **46**, 185.

Lipa, J. A., J. A. Nissen, D. A. Strieker, D. R. Swanson, and T. C. P. Chui, 2003, Phys. Rev. B **68**, 174518.

Lipa, J., D. R. Swanson, J. A. Nissen, T. C. P. Chui, and U. Israelsson, 1996, Phys. Rev. Lett. **76**, 944.

Lipa, J., D. R. Swanson, J. A. Nissen, Z. K. Geng, P. R. Williamson, D. A. Strieker, T. C. P. Chui, U. Israelsson, and M. Larson, 2000, Phys. Rev. Lett. **84**, 4894.

Lipa, J. A., S. Wang, J. A. Nissen, and D. Avaloff, 2005, Adv. Space Res. **36**, 119.

Liu, F.-C., M. J. Adriaans, and U. Israelsson, 2000, Physica B **284**, 2055.

Liu, F.-C., and G. Ahlers, 1994, Physica B **194-196**, 597.

Liu, Y., M. Larson, and U. Israelsson, 2000, Physica B **284-288**, 55.

Lorentzen, H. L, 1953, Acta Chem. Scand. (1947-1973) **7**, 1335.

Luijten, E., and H. Meyer, 2000, Phys. Rev. E **62**, 3257.

Ma, S.-K., 1976, *Modern Theory of Critical Phenomena* (Benjamin/Cummings, Reading, MA).

Marcout, R., F. F. Zwilling, J. M. Laherrere, Y. Garrabos, and D. Beysens, 1995, IAF-94-J2-1100.

Mehta, S., and F. M. Gasparini, 1997, Phys. Rev. Lett. **78**, 2596.

Mehta, S., M. O. Kimball, and F. M. Gasparini, 1999, J. Low Temp. Phys. **114**, 467.

Melnikovsky, L. A., 2005, J. Low Temp. Phys. **138**, 61.

Meyer, H., 2001, in *Proceedings of the 2001 NASA/JPL Workshop on Fundamental Physics in Microgravity*, NASA Document D-21522, pp. 5–33.

Meyer, H., and F. Zhong, 2004, C. R. Mec. **332**, 327.

Meyer-Ortmanns, H., 1996, Rev. Mod. Phys. **68**, 473.

Michels, A., and J. Strijland, 1952, Physica (Amsterdam) **18**, 613.

Mikeska, H. J., 1969, Phys. Rev. **179**, 166.

Miura, Y., K. Honda, J. Kawai, M. Matsumoto, M. Sakurai, S. Yoshihara, M. Ohnishi, H. Kobayashi, T. Takenouchi, and M. Ishikawa, 2004, 2nd International Symposium on Physical Sciences in Space, Toronto (in press).

Moeur, W. A., P. K. Day, F-C. Liu, S. T. P. Boyd, M. J. Adriaans, and R. V. Duncan, 1997, Phys. Rev. Lett. **78**, 2421.

Mohr, U., and V. Dohm, 2000, Physica B **284-288**, 43.

Moldover, M. R., 1969, Phys. Rev. **182**, 342.

Moldover, M. R., 1982, in *Phase Transitions: Cargese 1980*, edited by M. Levy, J. C. Le Guillou, and J. Zinn-Justin (Plenum, New York), p. 63.

Moldover, M. R., R. J. Hocken, R. W. Gammon, and J. V. Sengers, 1976, *Overviews and Justifications for Low Gravity Experiments on Phase Transition and Critical Phenomena in Fluids*, NBS Technical Note 925 (U.S. GPO, Washington, D.C.).

Moldover, M. R., and W. A. Little, 1965, Phys. Rev. Lett. **15**, 54.

Moldover, M. R., J. V. Sengers, R. W. Gammon, and R. J. Hocken, 1979, Rev. Mod. Phys. **51**, 79.

Mueller, K. H., G. Ahlers, and F. Pobell, 1976, Phys. Rev. B **14**, 2096.

Murphy, D., E. Genio, G. Ahlers, F. Liu, and Y. Liu, 2003, Phys. Rev. Lett. **90**, 025301.

Murphy, D., and H. Meyer, 1996, J. Low Temp. Phys. **105**, 185.

Nash, A., M. Larson, J. Panek, and N. Mulders, 2003, Physica B **329**, 160.

Nelson, R. C., D. A. Sergatskov, and R. V. Duncan, 2002, J. Low Temp. Phys. **127**, 173.

Nho, K., and E. Manousakis, 2001, Phys. Rev. B **64**, 144513.

Nicoll, J. F., and P. C. Albright, 1985, Phys. Rev. B **31**, 4576.

Nikolayev, V. S., D. Beysens, and P. Guenoun, 1996, Phys. Rev. Lett. **76**, 3144.

Nikolayev, V. S., A Dejoan, Y. Garrabos, and D. Beysens, 2003, Phys. Rev. E **67**, 061202.

Nissen, J. A., D. R. Swanson, Z. K. Geng, K. Kim, P. Day, and J. A. Lipa, 2000, Physica B **284-288**, 51.

Nitsche, K., and J. Straub, 1986, Naturwiss. **73**, 370.

Nitsche, K., and J. Straub, 1987, *Proceedings of the Sixth European Symposium on Material Sciences under Microgravity Conditions*, Bordeaux, France (European Space Agency, Paris), Vol. SP-256, p. 109.

Nitsche, K., J. Straub, and R. Lange, 1984, *Ergebnisse des TEXUS 8-Experimentes Phasenumwandlung*. Scientific Report Aeronautics and Astronautics, BMFT.

Onsager, L., 1944, Phys. Rev. **65**, 117.

Onuki, A., 1983, J. Low Temp. Phys. **50**, 433.

Onuki, A., 1984, J. Low Temp. Phys. **55**, 309.

Onuki, A., and R. A. Ferrell, 1990, Physica A **164**, 245.

Onuki, A., H. Hao, and R. A. Ferrell, 1990, Phys. Rev. A **41**, 2256.

Orkoulas, G., M. E. Fisher, and C. Üstün, 2000, J. Chem. Phys. **113**, 7530.

Oxtoby, D. W., 1975, J. Chem. Phys. **62**, 1463.

Panofsky, W. K. H., and M. Phillips, 1955, *Classical Electricity and Magnetism* (Addison-Wesley, Cambridge, MA), p. 101.

Parisi, G., 1973, J. Stat. Phys. **23**, 49.

Parisi, G., 1988, *Statistical Field Theory* (Addison-Wesley, New York).

Patashinskii, A. Z., and V. L. Pokroviskii, 1979, *Fluctuation Theory of Phase Transitions* (Pergamon, Oxford).

Pelissetto, A., and E. Vicari, 2002, Phys. Rep. **368**, 549.

Peebles, P. J. E., 1980, *The Large-Scale. Structure of the Universe* (Princeton University Press, Princeton, NJ).

Perrot, F., D. Beysen, Y. Garrabos, T. Fröhlich, P. Guenoun, M. Bonetti, and P. Bravais, 1999, Phys. Rev. E **59**, 3079.

Perrot, F., P. Guenoun, T. Baumberger, D. Beysen, Y. Garrabos, and B. Le Neindre, 1994, Phys. Rev. Lett. **73**, 688.

Pestak, M. W., and M. H. W. Chan, 1984, Phys. Rev. B **30**, 274.

Pittman, C., L. Cohen, and H. Meyer, 1982, J. Low Temp. Phys. **46**, 115.

Pittman, C., T. Doiron, and H. Meyer, 1979, Phys. Rev. B **20**, 3678.

Privman, V., 1990, in *Finite-Size Scaling and Numerical Simulations of Statistical Systems*, edited by V. Privman (World Scientific, Singapore), p. 1.

Privman, V., and M. E. Fisher, 1984, Phys. Rev. B **30**, 322.

Privman, V., P. C. Hohenberg, and A. Aharony, 1991, *in Phase Transitions and Critical Phenomena*, edited by C. Domb and J. Lebowitz (Academic, New York), Vol. 14, p. 1.

Qin, X., J. A. Nissen, D. R. Swanson, P. R. Williamson, D. A. Strieker, J. A. Lipa, T. C. P. Chui, and U. E. Israelsson, 1996, Cryogenics **36**, 781.

Rhee, I., F. M. Gasparini, and D. J. Bishop, 1989, Phys. Rev. Lett. **63**, 410.

Roe, D. B., G. Ruppeiner, and H. Meyer, 1977, J. Low Temp. Phys. **27**, 747.

Rudnick, J., M. Barmatz, and F. Zhong, 2003, Physica B **329**, 110.

Ruppeiner, G., M. Ryschkewitsch, and H. Meyer, 1980, J. Low Temp. Phys. **41**, 179.

Rushbrooke, G. S., 1963, J. Chem. Phys. **39**, 842.

Ryschkewitsch, M., and H. Meyer, 1979, J. Low Temp. Phys. **35**, 103.

Sarbach, S., and M. E. Fisher, 1978, Phys. Rev. B **18**, 2350.

Schloms, R., and V. Dohm, 1987, Europhys. Lett. **3**, 413.

Schloms, R., and V. Dohm, 1989, Nucl. Phys. B **328**, 639.

Schloms, R., and V. Dohm, 1990, Phys. Rev. B **42**, 6142.

Schmidt, C., 1988, Cryogenics **28**, 585.

Schmolke, R., A. Wacker, V. Dohm, and D. Frank, 1990, Physica B **165&166**, 575.

Schultka, N., and E. Manousakis, 1995a, Phys. Rev. B **52**, 7528.

Schultka, N., and E. Manousakis, 1995b, Phys. Rev. Lett. **75**, 2710.

Schultka, N., and E. Manousakis, 1997, J. Low Temp. Phys. **109**, 733.

Schultka, N., and E. Manousakis, 1998, J. Low Temp. Phys. **111**, 783.

Sengers, J. V., 1974, Physica (Amsterdam) **73**, 73.

Sengers, J. V., 1985, Int. J. Thermophys. **6**, 203.

Sergatskov, D. A., A. V. Babkin, S. T. P. Boyd, R. A. M. Lee, and R. V. Duncan, 2004, J. Low Temp. Phys. **134**, 517.

Sigga, E. D., B. I. Halperin, and P. C. Hohenberg, 1976, Phys. Rev. B **13**, 2110.

Siggia, E. D., and D. R. Nelson, 1977, Phys. Rev. B **15**, 1427.

Singsaas, A., and G. Ahlers, 1984, Phys. Rev. B **30**, 5103.

Stanley, H. E., 1971, *Introduction to Phase Transitions and Critical Phenomena* (Oxford University Press, New York).

Stauffer, D., M. Ferer, and M. Wortis, 1972, Phys. Rev. Lett. **29**, 345.

Straub, J., and L. Eicher, 1995, Phys. Rev. Lett. **75**, 1554.

Straub, J., L. Eicher, and A. Haupt, 1995a, Phys. Rev. E **51**, 5556.

Straub, J., L. Eicher, and A. Haupt, 1995b, Int. J. Thermophys. **16**, 1051.

Straub, J., A. Haupt, and L. Eicher, 1995, Int. J. Thermophys. **16**, 1033.

Straub, J., A. Haupt, and K. Nitsche, 1993, Fluid Phase Equilib. **88**, 123.

Straub, J., and K. Nitsche, 1993, Fluid Phase Equilib. **88**, 183.

Strösser, M., and V. Dohm, 2003, Phys. Rev. E **67**, 056115.

Strösser, M., S. A. Larin, and V. Dohm, 1999, Nucl. Phys. B **540**, 654.

Strösser, M., M. Mönnigmann, and V. Dohm, 2000, Physica B

284-288, 41.

Sutter, P., and V. Dohm, 1994, Physica B **194-196**, 613.

Swanson, D. R., T. C. P. Chui, and J. A. Lipa, 1992, Phys. Rev. B **46**, 9043.

Takada, T., and T. Watanabe, 1980, J. Low Temp. Phys. **41**, 221.

Tarn, W. Y., and G. Ahlers, 1985, Phys. Rev. B **32**, 5932.

Tam, W. Y., and G. Ahlers, 1986, Phys. Rev. B **33**, 183.

Thommes, M., and G. H. Findenegg, 1995, Adv. Space Res. **16**, 83.

Thommes, M., G. H. Findenegg, and H. Lewandowski, 1994, Ber. Bunsenges. Phys. Chem. **98**, 477.

Thommes, M., G. H. Findenegg, and M. Schoen, 1995, Langmuir **11**, 2137.

Tisza, L. C., 1948, in *Phase Transformation in Solids*, edited by R. Smoluchowsky, J. E. Mayer, and W, A. Weyl (Wiley, New York).

Tobochnik, J., 2001, Am. J. Phys. **69**, 255.

Töpler, M., and V. Dohm, 2003, Physica B **329-333**, 200.

van der Waals, J. D., 1873, Doctoral dissertation (University of Leiden).

Vladimirov, A. A., D. I. Kazakov, and O. V. Tarasov, 1979, Zh. Eksp. Teor. Fiz. **77**, 1035 [Sov. Phys. JETP **50**, 521 (1979)].

Voronel, A. V., Yu. R. Chashkin, V. A. Popov, and V. G. Simkin, 1964, Sov. Phys. JETP **18**, 568.

Voronel, A. V., and M. S. Gitterman, 1965, Sov. Phys. JETP **21**, 958.

Voronel, A. V., V. G. Gorbunova, Yu. R. Chashkin, and V. V. Shchekochikhina, 1966, Sov. Phys. JETP **23**, 597.

Voronel, A. V., V. G. Snigirev, and Yu. R. Chashkin, 1965, Sov. Phys. JETP **21**, 653.

Wacker, A., and V. Dohm, 1994, Physica B **194-196**, 611.

Wallace, D. J., and R., P. K. Zia, 1974, J. Phys. C **7**, 3480.

Watson, P. G., 1969, J. Phys. C **2**, 1883.

Wegner, F. J., 1972, Phys. Rev. B **5**, 4529.

Wegner, F., 1976, in *Phase Transitions and Critical Phenomena*, edited by C. Domb and M. S. Green (Academic, New York), Vol. 6, p. 7.

Weichman, P. B., D. L. Goodstein, and A. W. Harter, 2003, Rev. Mod. Phys. **73**, 1.

Weichman, P. B., and J. Miller, 2000, J. Low Temp. Phys. **119**, 155.

Weichman, P. B., A. Prasad, R. Mukhopadhyay, and J. Miller, 1998, Phys. Rev. Lett. **80**, 4923.

Weilert, M., I. Hahn, M. Barmatz, D. Higham, and G. Frodsham, 2002, Cryogenics **41**, 813.

Welander, P., M. Barmatz, and I. Hahn, 2000, IEEE Trans. Instrum. Meas. **49**, 253.

Welander, P., and I. Hahn, 2001, Rev. Sci. Instrum. **72**, 3600.

Widom, B., 1964, J. Chem. Phys. **41**, 74.

Widom, B., 1965a, J. Chem. Phys. **43**, 3892.

Widom, B., 1965b, J. Chem. Phys. **43**, 3898.

Wilkinson, R. A., G. A. Zimmerli, H. Hao, M. R. Moldover, R. F. Berg, W. L. Johnson, R. A. Ferrell, and R. W. Gammon, 1998, Phys. Rev. E **57**, 436.

Williams, G. A., 1993, J. Low Temp. Phys. **93**, 1079.

Wilson, K. G., 1971a, Phys. Rev. B **4**, 3174.

Wilson, K. G., 1971b, Phys. Rev. B **4**, 3184.

Wilson, K. G., and M. E. Fisher, 1972, Phys. Rev. Lett. **28**, 240.

Wilson, K. G., and J. Kogut, 1974, Phys. Rep. **12**, 75.

Wunenburger, R., Y. Garrabos, C. Lecoutre-Chabot, D. Beysens, and J. Hegseth, 2000, Phys. Rev. Lett. **84**, 4100.

Wunenburger, R., Y. Garrabos, C. Lecoutre-Chabot, D. Beysens, J. Hegseth, F. Zhong, and M. Barmatz, 2002, Int. J. Thermophys. **23**, 103.

Wyczalkowska, A. K, M. A. Anisimov, and J. V. Sengers, 2002, J. Chem. Phys. **116**, 4202.

Yang, C. N., and C. P. Yang, 1964, Phys. Rev. Lett. **13**, 303.

Yukalov, V. I., and S. Gluzman, 1998, Phys. Rev. E **58**, 1359.

Zappoli, B., 1992, Phys. Fluids A **4**, 1040.

Zappoli, B., 2003, C. R. Mec. **331**, 713.

Zappoli, B., D. Bailly, Y. Garrabos, B. Le Neindre, P. Guenon, and D. Beysens, 1990, Phys. Rev. A **41**, 2264.

Zappoli, B., and P. Carlès, 1995, Eur. J. Mech. B/Fluids **14**, 41.

Zappoli, B., and P. Carlès, 1996, Physica D **89**, 381.

Zappoli, B., and A. Durand-Daubin, 1994, Phys. Fluids **6**, 1929.

Zappoli, B., R. Kuhl, J. Robey, and A. Ivanov, 2003, Acta Astronaut. **53**, 963.

Zhong, F., and M. Barmatz, 2004, Phys. Rev. E **70**, 066105.

Zhong, F., M. Barmatz, and I. Hahn, 2003, Phys. Rev. E **67**, 021106.

Zhong, F., and H. Meyer, 1993, J. American Society of Mechanical Engineers, *Fluid Mechanics Phenomena in Microgravity*, edited by D. A. Siginer, R. L. Thompson, and L. M. Trefethen, **AMD-174**, 139.

Zhong, F., and H. Meyer, 1995, Phys. Rev. E **51**, 3223.

Zhong, F., and H. Meyer, 1996, Phys. Rev. E **53**, 5935.

Zimmerli, G. A., R. A. Wilkinson, R. A. Ferrell, and M. R. Moldover, 1999a, Phys. Rev. Lett. **82**, 5253.

Zimmerli, G. A., R. A. Wilkinson, R. A. Ferrell, and M. R. Moldover, 1999b, Phys. Rev. E **59**, 5862.

Zinn, S.-Y., and M. E. Fisher, 1996, Physica A **226**, 168.

Zinn-Justin, J., 2002, *Quantum Field Theory and Critical Phenomena*, 4th ed. (Clarendon, Oxford).

Zinn-Justin, J., 2001, Phys. Rep. **344**, 159.

Zinn-Justin, J., 2003, private communication.